Surface Characterization of Oxides Synthesized by Successive Ionic Layer Deposition

by

Thomas I. Gilbert

A dissertation submitted in partial fulfillment
of the requirements for the degree of
Doctor of Philosophy
(Chemical Engineering)
in The University of Michigan
2010

Doctoral Committee:

Professor Johannes W. Schwank, Chair
Professor John W. Halloran
Professor Nicholas Kotov
Assistant Professor Suljo Linic

© Thomas I. Gilbert

2010

To Jesica, my source of endless joy and inspiration

Acknowledgments

This dissertation would not have been completed without the support, assistance, and advice of many wonderful people. First of all, I am extremely thankful for my research advisor and mentor, Professor Johannes Schwank. He has taught me by example how to enhance my research ability though posing the right questions, exploring the right places, and efficiently evaluating the relevant and meaningful data. I have been privileged to benefit from a diversity of experiences throughout my graduate school experience including the ability to participate in national conferences and professional societies. I attribute this diversity of education in large part to my friendship with Professor Schwank.

I would also like to thank my other thesis committee members Professor Nicholas Kotov, Professor Suljo Linic, and Professor John Halloran. Their collective advice during the proposal writing phase of this work was especially beneficial. As a committee they helped me focus the initial direction of my research toward tangible and attainable deliverables. I am very thankful for their thoughtful recommendation.

I acknowledge and express appreciation for my many friends and colleagues. I want to thank the research group of Professor Schwank (past and present) with whom I have associated at the University of Michigan. I am also grateful for the lifelong friends that I and my family have made while living in Ypsilanti. Thanks to all of the Chemical

Engineering Department staff and graduate students at the University of Michigan for their support and encouragement.

This research was funded by the U.S. Army Tank-Automotive Research, Development & Engineering Center (Cooperative agreement: W56HZV-05-2-0001). Characterization equipment vital to the success of this work was supported by NSF grants #DMR-0420785 and #DMR-0320740. I would also like to thank Dr. Valeri P. Tolstoy from St. Petersburg State University and Dr. Ghenadii Korotcenkov from the Technical University of Moldova for helpful advice and discussion.

I am tremendously grateful for the love and support of my parents, Ivan and Sue Gilbert. As their son, I was fortunate to have been taught by their examples, blessed by their sacrifice, and strengthened by their service.

I also want to thank my children Scott, Andrew, and Kimberly. They teach me valuable life lessons, inspire me to be a better person, and enable me to maintain a proper perspective. They are three of the greatest joys in my life.

Last but not least, I am forever grateful to my beautiful wife, Jesica. The love, patience, support, and encouragement she has given me during the last nine years of our marriage are without comparison. She provides me endless motivation to realize my potential. Thank you for all you do!

Preface

Catalysis has always been a nanoscale science. The activity and selectivity of heterogeneous catalysts are strongly dependent on their nanoscale physical properties including composition, morphology, and surface structure. Recent advances in the ability to characterize, model, and even synthesize nanostructured catalysts have positively impacted technological progress. The aspiration to perform “catalysis by design” is becoming an attainable objective of present research. For example, the tip of a scanning tunneling microscopy probe can be used as a molecular paintbrush to directly place individual clusters of atoms on a model planar support such that the fundamental surface interactions can be elucidated. Catalysis takes advantage of the electronic interactions between two or more different phases of materials to reduce the overall barrier of a particular chemical transformation. A fundamental understanding of the electronic interactions between different heterogeneous phases and chemistries of the catalyst and underlying support materials will enable the ability to control or predict the chemistry that occurs on a particular catalyst surface. However, transferring this nanoscale understanding from the laboratory bench top to industrial scale is challenging, particularly as it relates to bulk scale catalyst synthesis.

The inhomogeneity and surface complexity of typical supported catalyst systems make it difficult to isolate the effects of the catalyst-support interactions. Model catalysts with structural uniformity are often difficult to synthesize in bulk quantities using

conventional techniques. Bulk scale catalyst synthesis techniques, such as wet impregnation, synthesize supported catalyst nanoparticles of which only a fraction of the catalyst mass can directly be influenced by the support. Enhancing the support effects of highly loaded catalysts synthesized by wet impregnation is often difficult because catalyst dispersion tends to decrease as weight loading increases.

This dissertation focuses on a bulk scale synthesis procedure with the potential to create thin films, or rafts, of highly dispersed oxides on high surface area supports rather than supported catalyst nanoparticles. Successive ionic layer deposition (SILD), a thin film synthesis technique, was selected for its ability to produce this highly dispersed phase of supported oxides in a controlled layer-by-layer fashion at the nanometer scale over very large surface areas. The ability to selectively synthesize a dispersed catalyst phase on a high surface area support would enable a more detailed characterization of the effects of catalyst-support interactions on overall catalytic activity by decoupling dispersion from weight loading.

In its essence, SILD is a method for depositing thin films of oxide materials on a support in a layer-by-layer fashion through a series of aqueous chemical reactions. Rather than simply placing the oxide molecules on the surface, SILD adheres a thin film of molecules to the support through ionic interactions between the support and the aqueous SILD precursors. This persistent interaction between the thin oxide film as it is being deposited and the underlying support sets SILD apart from other thin film deposition techniques. As a differentiated technique, capable of achieving nanoscale control and maintaining these electronic interactions, SILD has the potential to revolutionize the way heterogeneous catalysts are designed in the future.

Table of Contents

Dedication ii

Acknowledgments iii

Preface v

List of Figures ix

List of Tables xii

List of Appendices xiii

Abstract xiv

Chapter

1. Introduction to Successive Ionic Layer Deposition (SILD) 1

   1.1 General Introduction and Motivation 1

   1.2 Historic Development of SILD 2

   1.3 Thesis Objectives and Research Overview 9

2. SILD of Zirconia 12

   2.1 Introduction 12

   2.2 Equipment, Procedures, and Materials 13

   2.3 Characterization 16

   2.4 Results & Discussion 22

   2.5 Conclusions 30

3. SILD of Alumina and Barium Oxide on a Silicon Wafer 32
3.1 Introduction 32
3.2 Equipment, Procedures, and Materials 33
3.3 Characterization 34
3.4 Results & Discussion 35
3.5 Conclusions 43
4. SILD of Barium Oxide on Fused Alumina Powder 45
4.1 Introduction 45
4.2 Equipment, Procedures, and Materials 48
4.3 Characterization 51
4.4 Control Experiment 52
4.5 Temperature Programmed Desorption Experiments 54
4.6 Results and Discussion 55
4.7 Conclusions 63
5. Conclusions and Future Recommendations 65
5.1 Conclusions 65
5.2 Future Recommendations 66
Appendices 70
Bibliography 101

List of Figures

Figure 1. Illustration of the steps in the SILD cycle 5

Figure 2. Stern's model of the electric double layer arrangement of cations and anions on the surface of a solid substrate in which the IEP of the solid is less than the pH of the aqueous solution 7

Figure 3. Diagram of the apparatus for SILD of thin films on planar supports 14

Figure 4. Photograph of the SILD apparatus for planar thin films 14

Figure 5. (a) SEM image of a polyurethane droplet on the surface of a silicon wafer used to block SILD and (b) AFM image after SILD of the edge of the polyurethane droplet only now the polyurethane has been physically delaminated and the underlying silicon wafer is shown 17

Figure 6. SEM image of three holes pre-etched into the surface of a silicon wafer by a focused ion beam (FIB) of gallium prior to the SILD of a thin film 19

Figure 7. SEM image at a 45° angle of the three holes etched in the silicon wafer surface after SILD of a multicomponent film of ceria and zirconia. 20

Figure 8. SEM images of (a) pre-etched vertical channel in the surface of a silicon wafer with another 45° angle etched into the side, (b) higher magnification of the 45° side channel surface underneath the top surface of the silicon wafer, (c) same as image 'b' after 58 SILD cycles showing precipitate in the vertical channel, (d) higher magnification of the 45° side channel 21

Figure 9: SEM images at a 45° angle of (A) a corner of a silicon wafer fragment after SILD of a ZrO_2 thin film and (B) a higher magnification of the edge of wafer fragment showing the surface roughness of the SILD film on the silicon wafer substrate 22

Figure 10. (a) AFM image of a zirconia thin film (sample A.15 from Table 2) synthesized on a silicon wafer via 45 SILD cycles (image width is 1 μm) and (b) a cross section of the thin film surface topography as indicated by the white line in the AFM image above. Another AFM image of this sample is Figure A.13 of Appendix A. 24

Figure 11. XPS spectra of a blank silicon wafer and a wafer containing a thin film of zirconia deposited using the SILD technique..25

Figure 12. XPS spectra of a SILD-synthesized zirconia thin film dried at 110ºC. Only minimal levels of potassium and nitrogen were detected in the thin film. 26

Figure 13. Histogram showing the distribution of ZrO_2 island diameters (from AFM) for three samples of 5, 10, and 50 total SILD cycles. The following SILD variables were constant: $[ZrO(NO_3)_2]$ = 0.01 M, [KOH] = 0.04 M, residence time = 30 sec. 27

Figure 14. Effect of zirconium nitrate concentration of the 1st SILD solution on the island diameter of the resultant ZrO_2 thin film. In these samples the following SILD variables were constant: number of SILD cycles = 10, [KOH] = 0.04 M, residence time = 60 sec. 28

Figure 15. Effect of SILD solution residence time on the silicon wafer on the island diameter of the resultant ZrO_2 thin film. In these samples the following SILD variables were constant: number of SILD cycles = 50, $[ZrO(NO_3)_2]$ = 0.01 M, [KOH] = 0.04 M. 29

Figure 16. Effect of the total number of SILD cycles on the island diameter of the resultant ZrO_2 thin film. In these samples the following SILD variables were constant: $[ZrO(NO_3)_2]$ = 0.01 M, [KOH] = 0.04 M, residence time = 30 sec...29

Figure 17. XPS spectra of the potassium-containing thin film synthesized by SILD 36

Figure 18. AFM image of the potassium-containing thin film synthesized by SILD........37

Figure 19. XPS peaks of (a) the SILD-deposited alumina layer before and after SILD of barium oxide and (b) the BaO nanoislands deposited on the alumina supported on a silicon wafer 40

Figure 20. AFM images of (a) blank silicon wafer, (b) alumina deposited on the blank silicon wafer, (c) 5 cycles of barium oxide deposited on the alumina, and (d) an additional 11 cycles of barium oxide, all deposited using the SILD technique 41

Figure 21. AFM images of three samples (same as Figure 20 a-c): (1) a blank silicon wafer, (2) alumina deposited via SILD on the blank silicon wafer, (3) barium oxide deposited on the alumina via SILD. AFM images (a) through (c) are identical for each of the three samples with only the z-height changing from 4 nm to 30 nm. These images highlight the difference between particles of contamination (indicated by arrows) and the alumina and barium oxide thin films. 42

Figure 22. Thermogravimetric analysis (TGA) of NO_2 released from 21.4 wt% BaO supported on γ-alumina (252 m^2/g) as the sample is heated to 800ºC at 2ºC/min. The percentage of BaO in the dispersed and bulk-like phases was reported to be 44% and 56%, respectively [49]. 46

Figure 23. Molar ratio of $Ba(NO_3)_2$ to alumina support (252 m^2/g) after NO_2 adsorption vs. the total weight loading of BaO via wet impregnation. Molar quantities of $Ba(NO_3)_2$ assigned to the bulk-like and dispersed phases were derived from integration of TGA derivative peaks from NO_2 TPD experiments [49]....................47

Figure 24. TEM image of fused alumina 49

Figure 25. XPS spectra of barium oxide synthesized by SILD on fused alumina powder....................51

Figure 26. Illustration of the three different synthesis techniques used to compare SILD to the conventional wet impregnation technique....................53

Figure 27. Weight loss of NO_2 during TPD from a BaO / fused alumina sample in which the BaO was loaded using the single step wet impregnation technique.56

Figure 28. Weight loss of NO_2 during TPD from a blank fused alumina sample 57

Figure 29. Net weight loss of NO_2 during TPD corresponding to only the BaO 57

Figure 30. Derivative NO_2 weight loss peaks comparing the BaO dispersion of samples synthesized using the SILD technique to wet impregnation samples .61

Figure 31. Bell-shaped curve represents the integral of the signature IR peaks for the characteristic wave numbers corresponding to NO_2 with respect to time. The solid line represents the TGA temperature profile during TPD at a constant ramp rate of 30ºC/min....................62

Figure 32. Illustration of the ability of SILD to synthesize highly dispersed and intimately mixed multicomponent thin films on a support 67

List of Tables

Table 1. Examples of oxide thin films synthesized by SILD 8

Table 2. Summary of SILD conditions for ZrO_2 thin film samples synthesized on silicon wafer fragments as a part of this variable study. AFM images for each sample are available in Appendix A (Figures A.1 - A.22). 23

Table 3. Summary of the SILD conditions for Al_2O_3 and BaO thin films synthesized on silicon wafer fragments as a part this study. In each case the SILD solutions contained 25% ethanol by volume and the balance DI water. 39

Table 4. Distribution of dispersed and bulk-like barium oxide in samples prepared via the SILD and wet impregnation techniques 59

List of Appendices

Appendix A. Successive Ionic Layer Deposition of Zirconia 70

Appendix B. Successive Ionic Layer Deposition of Alumina 93

Abstract

Successive ionic layer deposition (SILD) is an aqueous technique for depositing thin oxide films on a surface in a layer-by-layer fashion through a series of chemical reactions. This dissertation examines empirical aspects of the SILD technique by characterizing thin oxide films synthesized on model planar supports and then extends the SILD technique to synthesize supported oxide nanostructures on three dimensional supports of interest to catalysis.

Atomic force microscopy, x-ray photoelectron spectroscopy, and scanning electron microscopy provided insight into the SILD of zirconia, alumina, and barium oxide thin films on silicon wafers. The SILD conditions that most affected the surface morphology of the thin oxide films were the selection of aqueous metal salt precursors comprising the SILD solutions and the total number of SILD cycles.

Recent studies suggest that a highly dispersed phase of barium oxide supported on alumina interacts differently with NO_2 than a bulk-like phase of barium oxide. SILD was used to synthesize disperse nanoislands or rafts of barium oxide on larger rafts of alumina supported on a silicon wafer. The SILD method was then extended to deposit barium oxide on an alumina powder support comprised of dense 150 nm spherical crystallites fused together into 1-2 μm particles.

Equally weight loaded samples of barium oxide on the fused alumina powder were prepared by SILD and wet impregnation. The NO_2 storage behavior of the barium

oxide, evaluated by thermogravimetric analysis during NO_2 temperature programmed desorption (TPD) experiments, provided insight into the dispersion of barium oxide that resulted from each of the loading techniques. The highly dispersed barium oxide rafts synthesized by SILD on fused alumina released NO_2 at temperatures below 500ºC during TPD. By comparison, the barium oxide loaded by wet impregnation showed a higher temperature desorption feature above 500ºC indicative of bulk-like barium oxide nanoparticles. The NO_2 weight loss curves were also used to calculate the relative percentages of BaO in the dispersed phase and bulk-like phase for each loading technique.

The ability of SILD to synthesize highly disperse and uniform, conformal oxide coatings on three dimensional supports provides fundamental insight into the interactions between catalysts and supports.

Chapter 1

Introduction to Successive Ionic Layer Deposition (SILD)

1.1 General Introduction and Motivation

Successive ionic layer deposition (SILD), also known as successive ionic layer adsorption and reaction (SILAR) [1], is an aqueous method for depositing materials on a support through a series of chemical reactions. However, rather than simply physically depositing small particles or atoms randomly onto a surface, SILD utilizes interactions between ionic precursors and the support to ultimately adhere the thin film to the support surface. The SILD procedure exploits the electric double layer effect [2] to create a supported thin solid film in a layer-by-layer fashion. During each step of SILD, submonolayers of desired cations and anions are alternately and selectively adsorbed on a surface to produce SILD nanolayers with controlled composition and morphology. The simple equipment, low operating temperatures, and atmospheric pressure of the SILD process make it a comparatively low cost technology.

SILD is also becoming a technology which enables the controlled nanoscale modification of surfaces. This ability of SILD to uniformly coat materials on a three dimensional surface under ambient conditions should be of interest to the catalysis community. Heterogeneous catalysts containing structural uniformity are difficult to synthesize in bulk quantities using conventional techniques. Enhancing the electronic interactions between a catalyst and its support by increasing and maintaining the catalyst

dispersion on the support will increase the effectiveness of many catalytic systems. On most supports, post deposition drying and calcination lead to the agglomeration of the dispersed catalyst phases into less active and more bulk-like catalyst particles [3,4]. Tailoring the catalyst synthesis procedure such that high dispersion on a support is maintained before, during, and after the reaction would be enormously beneficial for many catalyst systems. Because SILD adheres the thin film to the support through electronic interactions between the support and the aqueous precursors, SILD may prove to become a powerful method for uniformly depositing oxide materials on a support such that they remain stable even at elevated temperatures.

1.2 Historic Development of SILD

In aqueous thin film synthesis, the term 'aqueous' signifies that water is the solvent containing the precursors used to form the thin solid film. There are four main techniques for producing thin solid films from aqueous methods:

1. Chemical Bath Deposition (CBD)
2. Liquid-Phase Deposition (LPD)
3. Electroless Deposition (ED)
4. Successive Ionic Layer Deposition (SILD)

In CBD, an aqueous metal salt reacts with a complexing agent (i.e. ammonia, triethanolamine, tartrate) to form an ionic metal-ligand complex which is then hydrolyzed by an oxygen source (water or a base) to precipitate a metal hydroxide on a substrate. The aqueous metal salt, complexing agent, and oxygen source are all present within a single bath. Their precipitation on a substrate is initiated by externally heating the bath

[5]. Often in CBD the precipitation of the metal hydroxide as suspended crystallites also occurs in the solution, which is the case when no substrate is present. CBD had been used to produce dozens of oxide and sulfide thin films including ZnO, SnO_2, CdO, CoO, ZnS, Sn_xS, PbS, and CoS [6].

In LPD, an aqueous solution of a metal-fluoro complex is slowly hydrolyzed by adding water, boric acid, or aluminum metal. LPD, like CBD, occurs in a single bath. However, rather than being thermally initiated, homogeneous nucleation of the metal hydroxide occurs as the water or boric acid is slowly added to the LPD bath. Subsequent thin films are formed on the substrate via attraction and attachment of colloidal particles. LPD has predominantly been used to produce silica thin films [6].

In ED, the oxidation state of the aqueous metal cation changes to an insoluble state via the participation of the substrate surface and a catalyst initiator. If the substrate is not catalytic to the deposition process it must first be activated or sensitized to the deposition. ED, like CBD and LPD, is a single bath technique [6]. SILD is different from these three aqueous techniques because the thin film is produced on a surface through sequential exposure to separate baths of cationic and anionic solutions. Of the aqueous techniques, SILD provides the option of tuning and controlling the greatest quantity of variables, enabling the production of a variety of thin films for a greater number of potential applications.

Iler is often credited as the first to recognize that thin films were able to be deposited on a support in a layer-by-layer fashion from colloidal and aqueous precursors [7]. Twenty years later Nicolau and Tolstoy independently secured patents on the

synthesis of ZnS and MnO_2 thin films through the stepwise adsorption of aqueous precursors [8,9].

Although variations in SILD technique have been developed over the last 25 years, the general step wise procedure remains the same. The procedure for the SILD of oxide thin films has been described previously [10,11,12,13] and generalized using silicon wafer supports as follows. First, the silicon wafer is cleaned by rinsing it alternately three times with acetone and DI water. Then, the silicon wafer is placed in the spin coater and 2 ml of the 1st SILD solution containing a dilute concentration of the desired aqueous metal salt is applied onto the wafer surface. With each application of the SILD solutions, a period of contact time is allowed for the solution to interact with the wafer sample surface prior to spinning off the excess solution. Next, the rinse SILD solution is applied twice to remove the residual aqueous metal complexes from the surface. Then, the 2nd SILD solution, containing the desired hydroxyl species, is applied followed by another two applications of the rinse SILD solution. These six SILD steps (cationic species, hydroxyl species, and four rinses) are repeated in sequence for the desired number of SILD cycles. The sample is then dried in air to 110°C for 24 hours and heated to 450°C for 6 hours to completely oxidize the SILD-synthesized metal hydroxide thin film. An oversimplified representation of SILD procedure is shown in Figure 1. Please note that the water molecules are not present in this illustration and it is not intended to fully represent the mechanism of aqueous metal complexes interacting with hydrated surfaces.

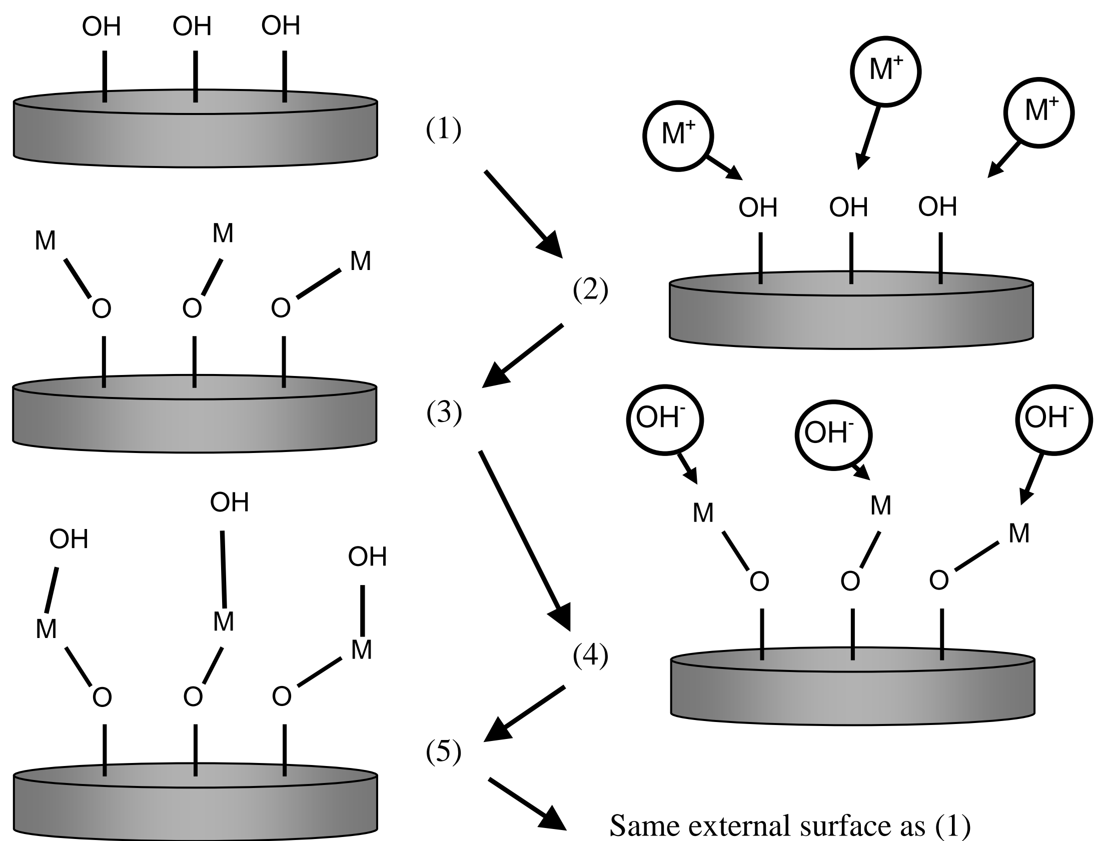

Figure 1. Illustration of the steps in the SILD cycle

Although the complete mechanism for SILD is not yet fully understood, there are several features of the overall mechanism that are generally accepted though not yet experimentally verified. However, before describing the currently accepted SILD mechanism, the concept of a surface's isoelectric point needs explanation.

The solid oxide surface has a net positive or negative charge when placed in contact with an aqueous solution. This surface charge results from either the dissociation of water at the oxide surface or the hydrolysis of the oxide to form $M^{+}OH^{-}$ groups. Regardless, a charge develops on the oxide surface that is dependent on the pH of the surrounding aqueous environment. There also exists a point of zero net charge, also

commonly referred to as the isoelectric point (IEP), where the surface exhibits a neutral net electric charge. Thus, if the pH of the aqueous solution is greater than the oxide's IEP, the surface has a net negative charge, and if the solution pH is less than IEP of the surface, its net charge is positive. [14].

The common theory for the SILD mechanism begins with Stern's model of an electrical double layer that is formed between an aqueous ionic solution and an oxide surface. An illustration of Stern's model for a positively charged surface is shown in Figure 2. The inner Helmholtz plane (IHP) contains the aqueous species of opposite charge to the oxide surface. However, the aqueous cationic species is not a single ion but rather a larger ionic complex of multiple atoms, hydroxyl bridges, and water molecules. It is unclear whether atomic species or larger complexes exist in the inner Helmholtz plane. The answer to this question may be dependent on the surface and aqueous species chemistry. There is also the outer Helmholtz plane (OHP) containing aqueous counter ions. Finally, the region beyond the OHP is defined as the diffusion layer [6].

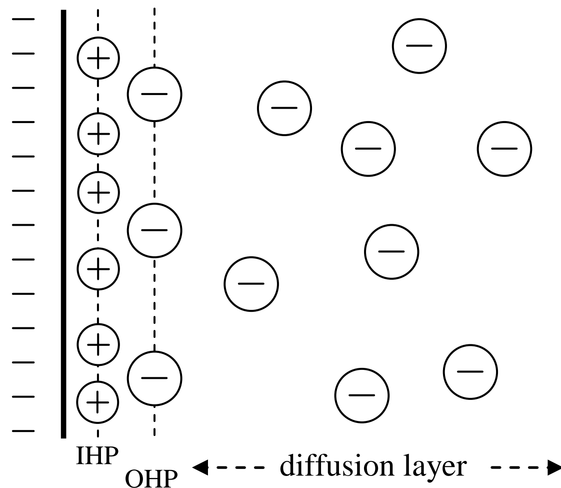

Figure 2. Stern's model of the electric double layer arrangement of cations and anions on the surface of a solid substrate in which the IEP of the solid is less than the pH of the aqueous solution

In SILD, when a substrate is first exposed to the aqueous metal salt solution, specific adsorption of the cations (or cationic species, hereafter referred to as simply cations) occurs in the IHP if the solution's pH is above the substrate's IEP. The anion of the metal salt solution also adsorbs in the OHP during this SILD step. The first rinsing step most likely removes excess cations from the diffusion layer of Stern's model, with the last rinsing step likewise removing excess anions. When the SILD surface is exposed to the second SILD solution, the anions are assumed to be attracted to the adsorbed cations in the IHP. However, these anions must replace the undesired anions of the first SILD solution already occupying the OHP. This full mechanism in not completely understood, but the second SILD solution appears to be necessary in reforming the net negative surface charge in preparation for the next cationic layer.

There are also uncertainties regarding the physical characteristics of SILD film growth. In the 1990's Resch and co-workers studied physical aspects of the SILD growth

mechanism using an Atomic Force Microscope liquid cell as a flow-through reactor. They determined that the growth mechanism was strongly dependent on the substrate material. They observed three-dimensional cluster growth on atomically flat mica, two-dimensional layer growth followed by layer-plus-island growth on glass, and island then layer growth on GaAs [15,16,17].

Specific application advantages and procedural notes related to SILD have been described by Tolstoy and others [10,11,12,13]. The SILD technique has predominantly been used to synthesize thin films of numerous oxides and sulfides on a variety of two dimensional supports. For example, photocatalytically active TiO_2 thin films were deposited on silicon wafers through SILD and subsequent thermal treatment [18]. Many other oxides, crystalline and amorphous, have been formed using the SILD method (Table 1). Layers of multiple oxide compounds have also been synthesized using SILD [19].

Oxide	Support	Reference
ZrO_2	Si	[20]
CoO / Co_3O_4	SnO_2	[19]
MnO_2	Si, SnO_2	[19,21]
CeO_2	Si	[22]
$FeOOH$ / Fe_2O_3	Si, SiO_2, SnO_2	[19,23]
NiO	Si, Quartz, SnO_2	[19,24]
CuO	Glass, SnO_2	[12,19]
ZnO	Glass, Quartz, Mica, Si, SiO_2, PVC	[25,26,27,28,29,30,31,32]
Tl_2O_3	Si, Quartz	[33]
SnO_2	Si	[34]

Table 1. Examples of oxide thin films synthesized by SILD

In SILD there are many synthesis conditions or variables which affect the chemical and physical properties of the deposited thin film. The following list highlights several of these controllable synthesis variables.

- Support preparation procedure (temperature, rinsing or cleaning agents)
- Solvent for the SILD solutions
- Concentrations of cationic and anionic precursors in the SILD solutions
- SILD solution pH
- Chemical additives to the SILD solutions
- Residence time or contact time between the SILD solutions and the support
- Rinsing residence time and frequency
- Temperatures of the SILD and rinse solutions
- Post-SILD drying conditions (temperature, time, drying environment)
- The ratio of cycles of the different cationic species (multicomponent thin films)

1.3 Thesis Objectives and Research Overview

The first objective of this study was to better understand which of all the controllable variables in the SILD technique are the most important in the practical synthesis of novel oxides nanostructures of interest to catalysis. Once the fundamental conditions necessary to control the synthesis of highly dispersed oxides via SILD were understood on two dimensional surfaces, the second objective was to extend SILD to porous three dimensional structures. Confirmation that the highly dispersed thin films synthesized by SILD (1) have indeed been formed on three dimensional support structures and (2) are fundamentally more stable than materials deposited by

conventional techniques was endeavored through the study of NO_2 adsorption on alumina supported barium oxide as an appropriate target application.

Once the SILD technique becomes better understood it can be tailored to new applications. Some of the specific questions concerning the SILD process that are addressed in this dissertation include:

- Which SILD variables are the most important in influencing the thin film growth? Are these variables controllable or system dependent?
- What effect does the concentration or pH of the SILD solutions have on the surface morphology of SILD films?
- How do other chemical additives to the aqueous SILD solutions affect the SILD film growth?
- How do the initial changes in surface morphology and surface chemistry affect the deposition that occurs during subsequent SILD cycles?
- How effectively can the undesirable ions or impurities in the SILD solutions be prevented from intermingling with growing SILD films?
- To what extent is SILD on three dimensional structures similar to SILD on two dimensional wafers?
- How does the SILD of thin films on three dimensional structures compare to other techniques for loading oxides, such as wet impregnation?

The dissertation itself is divided into the three sections. First, the SILD of zirconia on silicon wafers is analyzed. Insights into the sensitivity of zirconia deposition on the controllable SILD variables are presented. Second, the SILD of alumina and

barium oxide on silicon wafers is likewise analyzed with the additional emphasis on understanding how to manage the SILD of a multicomponent thin film. Third, the SILD of a highly dispersed phase of barium oxide on fused alumina powder is discussed. This work is one of the first attempts to extend SILD from its role as a two dimensional thin film deposition technique toward becoming a three dimensional conformal coating technique of interest for catalyst synthesis. The final chapter summarizes the results of this dissertation and offers suggestions for future areas of research.

Chapter 2

SILD of Zirconia

2.1 Introduction

Zirconium oxide has as high refractive index and high transparency in the visible and near-infrared region making it practical for use in optical devices [35]. Zirconia thin films are currently also used for protective coatings [36,37], sensors [38,39], electrochemical devices [40] and other applications [41]. Zirconia-based metal oxides, including yttria-stabilized zirconia and ceria-zirconia, are also used in solid oxide fuel cells [42,43] and as supports for catalysts [44,45]. Due to its use in multiple consumer products including fuel cells and catalysts, zirconia was selected as the thin film material of choice for this study of the successive ionic layer deposition (SILD) technique.

The intent of this chapter is to present insights into the SILD of zirconia thin films on model silicon wafer supports. This can then be applied more generally to the synthesis of other thin oxide films using the SILD technique. Several SILD parameters or conditions were experimentally varied to determine which conditions most significantly affect the early stages of zirconia thin film deposition. Characterization of the supported zirconia thin films by spectroscopy and microscopy provided insight into the effects of the SILD conditions and also confirmed the utility of SILD as a nanoscale technique to create ultra-thin conformal coatings on oxide surfaces.

2.2 Equipment, Procedures, and Materials

The SILD apparatus used for the deposition of ZrO_2 on silicon wafers consisted of an Automate Scientific ValveBank 8 liquid perfusion system in combination with a Laurell WS-400B-6NPP/LITE spin coater (Figure 3 and Figure 4). Polished n-type (100) silicon wafers were used as supports for the SILD experiments in the spin coater apparatus. Prior to SILD, the supports were cut to one inch squares, cleaned in acetone, and heated overnight at 110°C in air.

Aqueous SILD solutions were prepared from $ZrO(NO_3)_2$ and KOH salts (Sigma-Aldrich) dissolved in DI water. The pH of the 1st SILD solution was between 2.0 and 3.0 for concentrations of $ZrO(NO_3)_2$ ranging from 0.04 to 0.005 M, respectively. The pH of the 2nd SILD solution of 0.01 M KOH was 11.0, whereas a pH of 12.5 was observed for the 0.04 M KOH SILD solution. The tetramer $[Zr_4(OH)_8(H_2O)_{16}]^{8+}$ is the aqueous species expected to be present in the majority of the SILD solutions [46,47].

Ethanol was also added to the SILD solutions. Rinse solutions were prepared using equivalent DI water and ethanol ratios as the corresponding SILD solutions for each sample. Ethanol has been shown to improve the growth rate of SILD films [13]. The SILD and rinse solutions were used at ambient temperature for the deposition of zirconia thin films.

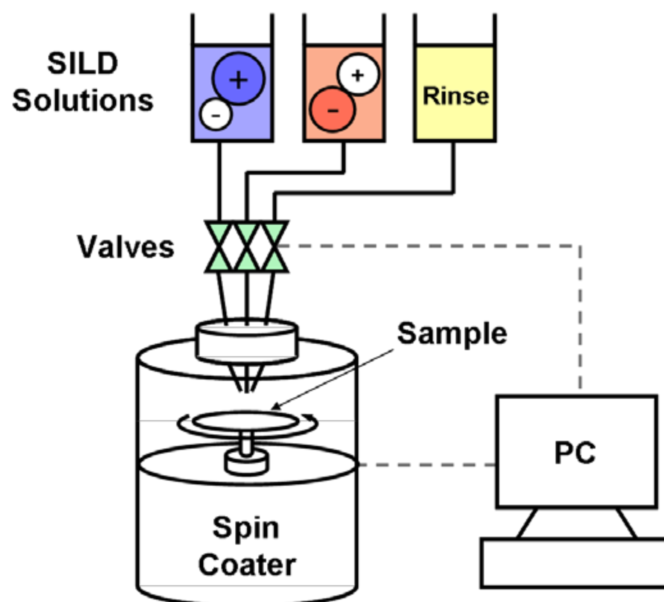

Figure 3. Diagram of the apparatus for SILD of thin films on planar supports

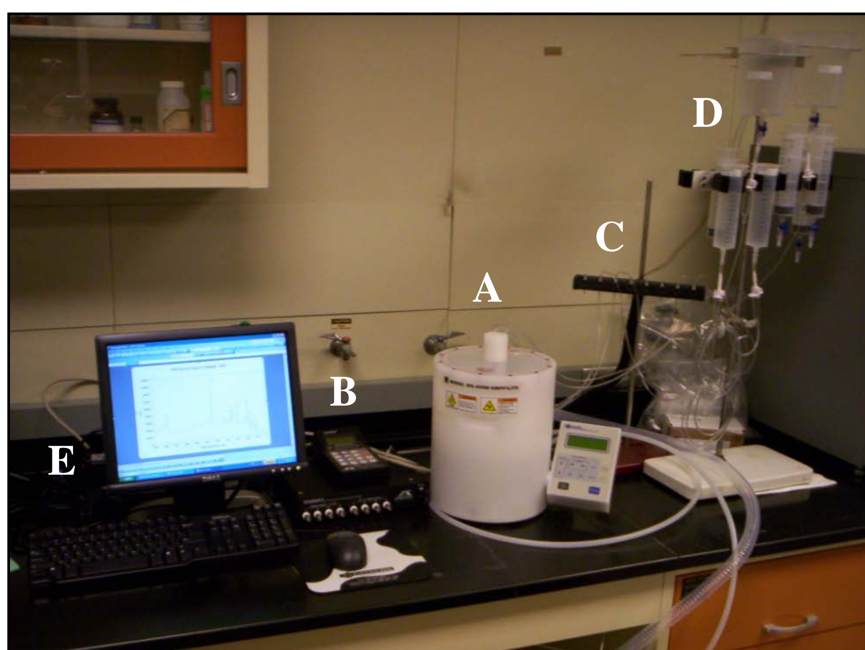

A - Laurell WS-400B-6NPP/LITE spin coater
B - Automate Scientific ValveBank 8 controller
C - Automate Scientific Teflon valves
D - Reservoirs for SILD solutions
E - Computer

Figure 4. Photograph of the SILD apparatus for planar thin films

The specific procedure for the SILD of zirconia on a silicon wafer substrate is summarized as follows. First, the silicon wafer is cleaned by rinsing it alternately three times with acetone and distilled water. The silicon wafer is then placed in the spin coater and 2 ml of the 1st SILD solution containing a dilute concentration of $ZrO(NO_3)_2$ is applied. With each application of the SILD solutions, a period of contact time or residence time is allowed for the solution to interact with the support prior to spinning off the excess solution. Next, a rinse SILD solution is applied twice to remove the excess aqueous metal complexes from the substrate surface. Then, the 2nd SILD solution containing KOH is applied followed by another two applications of the rinse solution. These six SILD steps (cationic species, hydroxyl species, and four rinses) are repeated in sequence for the desired number of SILD cycles. The sample is then dried in air to 110°C for 24 hours and heated to 450°C for 6 hours to completely oxidize the SILD-synthesized metal hydroxide thin film. Up to 200 SILD cycles were performed by exposing the supported silicon wafer substrate to a controlled quantity of the aqueous SILD solutions.

Several SILD synthesis conditions were varied to determine which of all the experimental parameters most significantly affected the early stages of the thin film deposition. The variables analyzed in this chapter include:

- Zirconium nitrate concentration
- Potassium hydroxide concentration
- SILD solution residence time (or contact time between solutions and support)
- Total number of SILD cycles
- Ethanol concentration (as an additive to the SILD solutions)

2.3 Characterization

The ZrO_2 thin film samples were characterized using Atomic Force Microscopy (AFM), X-ray Photoelectron Spectroscopy (XPS), and Scanning Electron Microscopy (SEM) at the University of Michigan Electron Microbeam Analysis Laboratory (EMAL). AFM is a high-resolution type of scanning probe microscopy in which a cantilever with a nanosharp tip is deflected as it scans over a sample surface. XPS is a quantitative spectroscopic technique used to analyze the surface chemistry of a material. SEM is an imaging technique that scans a sample surface with a high-energy electron beam and produces detectable signals containing information about the sample's surface topography, composition, and other properties.

Surface image plots of the ZrO_2 thin films supported on silicon wafer fragments were obtained from a NanoScope IIIa atomic force microscope in tapping mode using SPM cantilevers acquired from Pacific Nanotechnology. A Kratos Axis Ultra XPS instrument with an Al Kα x-ray source and a charge neutralizing flood gun was used to identify the elemental composition on the surface of the thin films. In XPS, line positions were corrected relative to a carbon 1s position of 284.5 eV. XPS was also useful in confirming that undesired ions (nitrate and potassium) in the SILD solutions were not being incorporated in the SILD nanolayers. Electron microscopy was performed at EMAL using either a FEI Nova Nanolab Dualbeam FIB / SEM with a Schottky FEG or a Philips XL30 FEG.

To quantify the thickness of the ZrO_2 nanofilms synthesized by SILD on silicon wafer supports, the following method was developed. A small drop of polyurethane was placed on the wafers prior to the SILD of zirconia. The dried polyurethane was

impermeable to the SILD solutions and yet able to fully delaminate from the silicon wafer upon completion of the SILD synthesis procedure. To measure the average thickness of the SILD-deposited thin films, an edge was located using AFM where SILD had been blocked by the dried polyurethane droplet. The AFM software then calculated the average step height or average SILD nanofilm thickness by comparing the difference in height between the surface of the SILD nanofilm and the surface of the underlying silicon wafer that had been blocked from SILD by the polyurethane droplet (Figure 5).

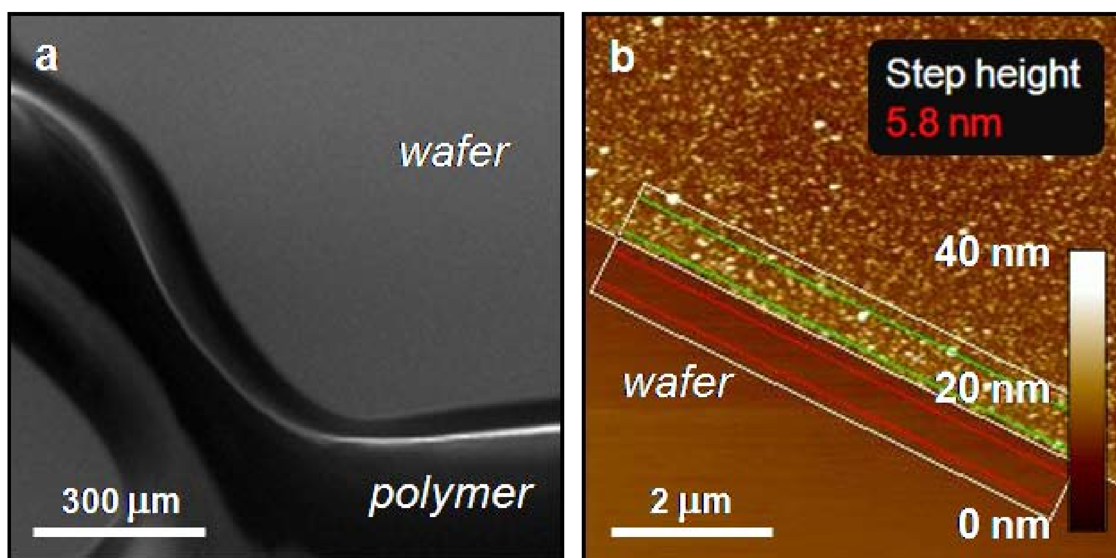

Figure 5. (a) SEM image of a polyurethane droplet on the surface of a silicon wafer used to block SILD and (b) AFM image after SILD of the edge of the polyurethane droplet only now the polyurethane has been physically delaminated and the underlying silicon wafer is shown. This also illustrates how AFM is used to calculate the average SILD film thickness as a step height measurement between the SILD layer and the underlying silicon wafer surface after the polyurethane was removed.

To demonstrate the conformal nature of the SILD technique, the following experiments were performed. The gallium focused ion beam of the FEI Nova Nanolab

was used to pre-etch holes and channels in the surface of a polished silicon wafer fragment. SEM images of the etched wafer surface were acquired prior to the SILD of ZrO_2 thin films (Figure 6). In one case, the pre-etched wafer fragment was then heated to 300ºC for 2 hours in a tube furnace with pure flowing nitrogen to remove implanted gallium ions without oxidizing the gallium on the silicon wafer surface. After thermal treatment, the wafer was cleaned in acetone and DI water and SILD of ZrO_2 was performed according to the previously described procedure. Figure 7 shows a pre-etched silicon wafer that was not subjected to heat treatment to remove gallium prior to the SILD of ZrO_2. Note the distinct gallium spheres (as determined by Energy-Dispersive X-ray Spectroscopy) located near the rims of the etched holes. Also note that inadequate rinsing during SILD leads to the co-precipitation of the zirconyl nitrate and potassium hydroxide solutions such that thin film deposition by precipitation occurs, particularly within the etched holes.

In the sample in which gallium was removed by heated the pre-etched surface to 300ºC for 2 hours, the distinct gallium spheres were not present in SEM images post-SILD of the etched region. Images (a) and (b) in Figure 8 show SEM images of the pre-etched channels in the silicon wafer surface prior to SILD. Images (c) and (d) show the same channel after 58 SILD cycles. Note the thin film that is present in the 45º channel (image d) and the inevitable coprecipitate from the two SILD solutions that was formed predominantly on the walls and in the base of the vertical channel. The fact that a SILD thin film was observed on the 45º side channel surface underneath the top surface of the silicon wafer suggests that the SILD was conformal in nature.

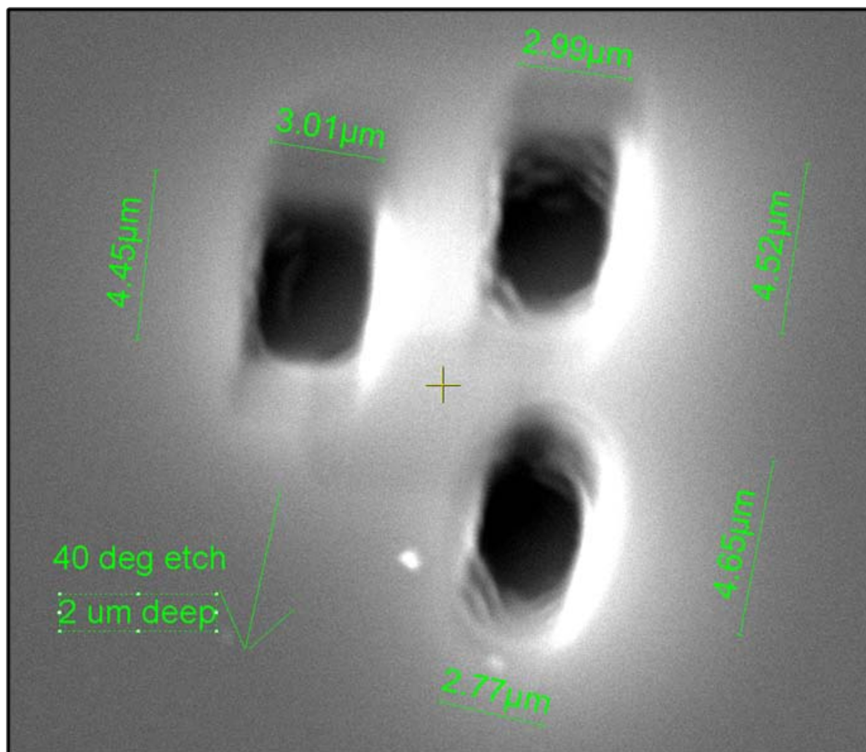

Figure 6. SEM image of three holes pre-etched into the surface of a silicon wafer by a focused ion beam (FIB) of gallium prior to the SILD of a thin film

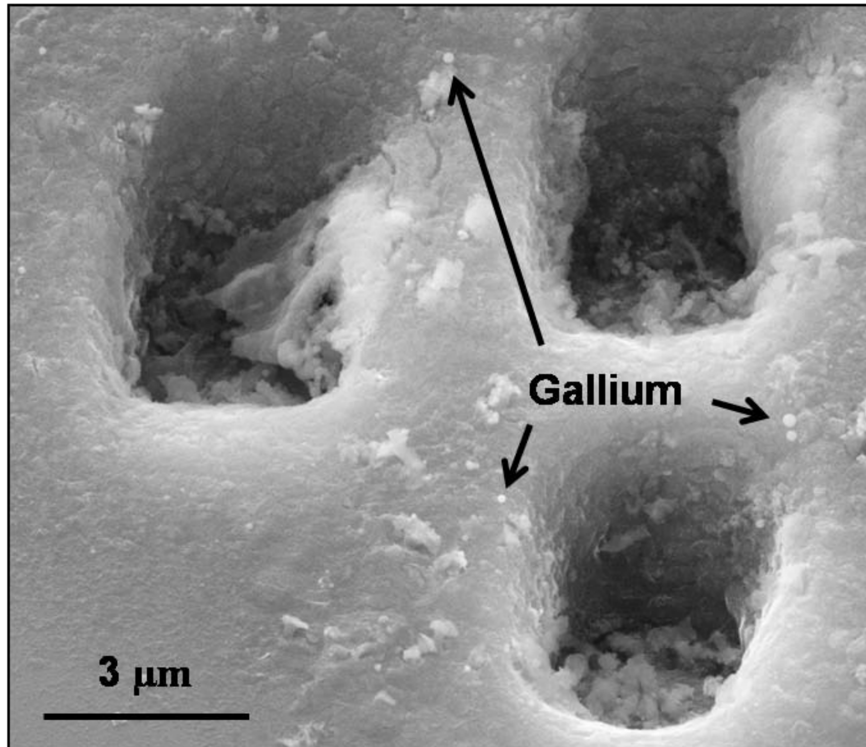

Figure 7. SEM image at a 45º angle of the three holes etched in the silicon wafer surface after SILD of a multicomponent film of ceria and zirconia. In this sample there is evidence that the gallium incorporated in the subsurface of the silicon wafer increased the growth rate of the SILD thin film.

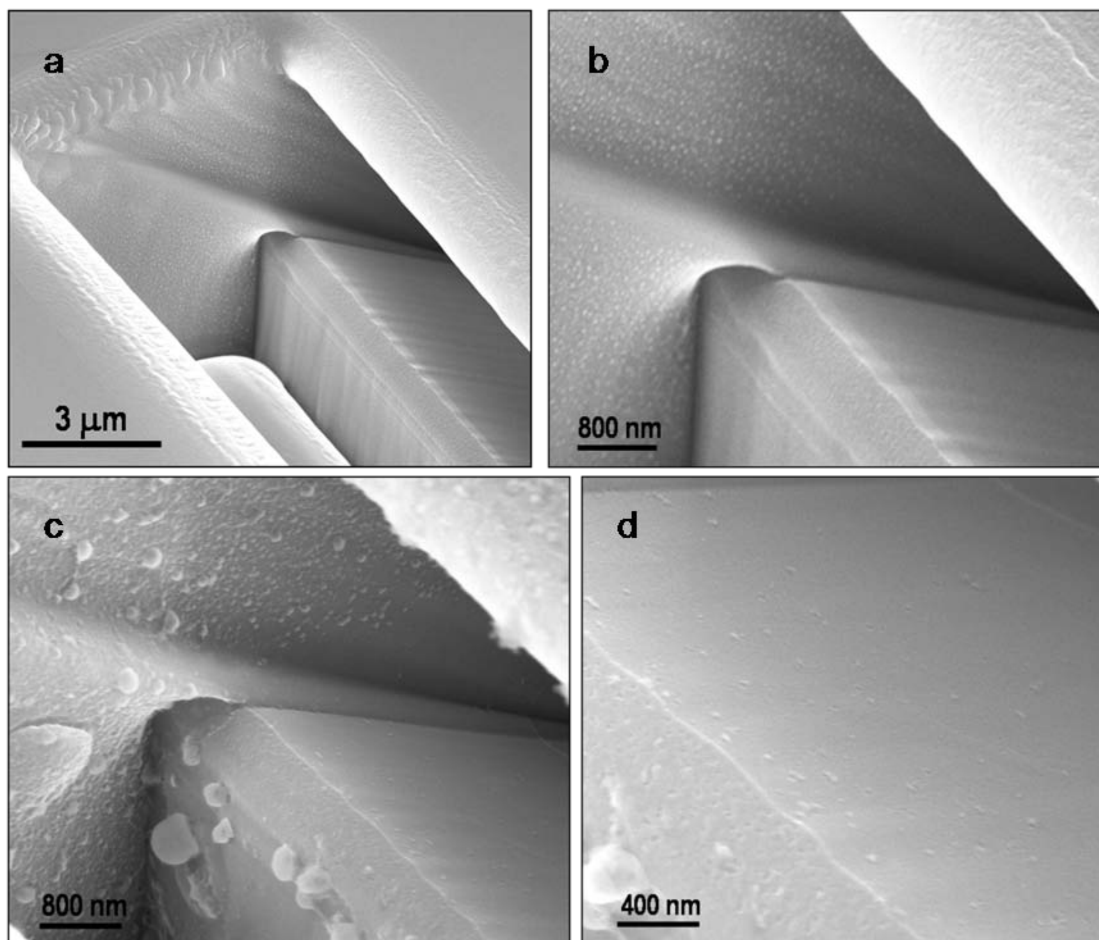

Figure 8. SEM images of (a) pre-etched vertical channel in the surface of a silicon wafer with another 45º angle etched into the side, (b) higher magnification of the 45º side channel surface underneath the top surface of the silicon wafer, (c) same as image 'b' after 58 SILD cycles showing precipitate in the vertical channel, (d) higher magnification of the 45º side channel surface

Figure 9 contains SEM images of a silicon wafer supported ZrO_2 thin film produced by 50 cycles of SILD. In the figure, image 'A' shows the edge of the sample at a 45° angle and image 'B' is a magnification of the edge of the sample. The roughness observed on the left half of the image in image (b) of Figure 9 is the thin solid film of ZrO_2 formed by SILD. This roughness was not observed on a blank silicon wafer prior to SILD of ZrO_2.

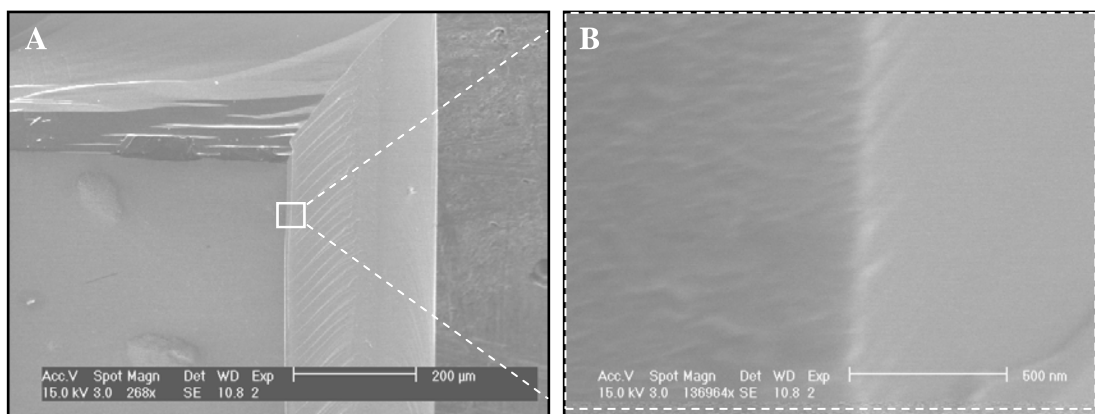

Figure 9: SEM images at a 45° angle of (A) a corner of a silicon wafer fragment after SILD of a ZrO_2 thin film and (B) a higher magnification of the edge of wafer fragment showing the surface roughness of the SILD film on the silicon wafer substrate

2.4 Results & Discussion

Table 2 summarizes the SILD experiments performed to produce ZrO_2 thin films supported on silicon wafer fragments. Appendix A contains the AFM images for the sample data set as well as additional XPS spectra. The average ZrO_2 thin film thickness was calculated using the AFM software from AFM images of step sites on several samples that were pretreated using the polyurethane droplet, SILD-blocking, technique

(refer to Figure 5). Although calculated ZrO_2 thin film thicknesses were difficult to reproduce from sample to sample using this technique, the average deposition rate (thin film thickness divided by total number of cycles) was calculated to range from 0.2 to 0.3 nm per SILD cycle over the range of SILD conditions represented by Table 2.

ZrO_2 Sample (AFM image)	$[ZrO(NO_3)_2]$ (M)	[KOH] (M)	Ethanol (vol %)	SILD cycles	Residence Time (sec)
A.1	0.005	0.04	25	10	60
A.2	0.005	0.04	25	50	60
A.3	0.01	0.01	25	10	60
A.4	0.01	0.01	25	50	60
A.5	0.01	0.04	0	10	60
A.6	0.01	0.04	0	50	60
A.7	0.01	0.04	25	5	30
A.8	0.01	0.04	25	5	60
A.9	0.01	0.04	25	5	90
A.10	0.01	0.04	25	10	30
A.11	0.01	0.04	25	10	60
A.12	0.01	0.04	25	10	90
A.13	0.01	0.04	25	45	30
A.14	0.01	0.04	25	50	30
A.15	0.01	0.04	25	50	30
A.16	0.01	0.04	25	50	60
A.17	0.01	0.04	25	50	90
A.18	0.01	0.04	25	100	5
A.19	0.01	0.04	25	150	5
A.20	0.04	0.01	0	10	60
A.21	0.04	0.01	0	50	60
A.22	0.04	0.01	25	10	60

Table 2. Summary of SILD conditions for ZrO_2 thin film samples synthesized on silicon wafer fragments as a part of this variable study. AFM images for each sample are available in Appendix A (Figures A.1 - A.22).

AFM images of the zirconia thin film samples show thin hemispherical islands or rafts up to 60 nm in diameter under certain SILD conditions. Figure 10 shows a representative AFM image and surface cross section of a zirconia thin film.

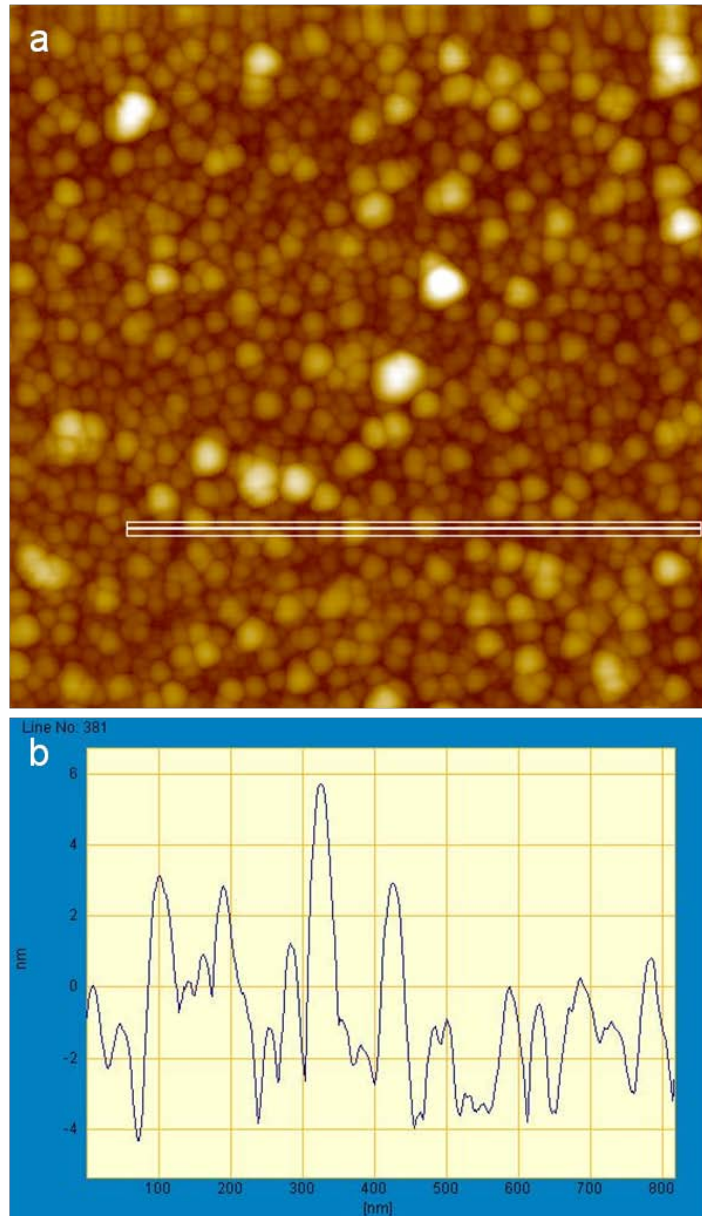

Figure 10. (a) AFM image of a zirconia thin film (sample A.15 from Table 2) synthesized on a silicon wafer via 45 SILD cycles (image width is 1 μm) and (b) a cross section of the thin film surface topography as indicated by the white line in the AFM image above. Another AFM image of this sample is Figure A.13 of Appendix A.

XPS confirmed the successful deposition of zirconia on the silicon wafer fragments for each thin film sample in Table 2 in by the presence of strong peak intensities at binding energies that correspond to the Zr 3p and Zr 3d orbitals (Figure 11). XPS also confirmed that the aqueous counter ions were not significantly incorporated into the SILD-deposited ZrO_2 thin films. XPS experiments shown in Figure 12 (focused on the binding energies corresponding to the K 2p and N 1s orbitals) were performed on the SILD-deposited ZrO_2 thin film samples prior to elevated thermal treatment (only dried to 110ºC prior to XPS). This XPS evidence in Figure 12 suggests that one can consistently minimize the level of undesirable impurities in the as-deposited SILD thin films by choosing the appropriate aqueous precursors and adequately rinsing the SILD solutions from the growing thin film during the SILD cycles.

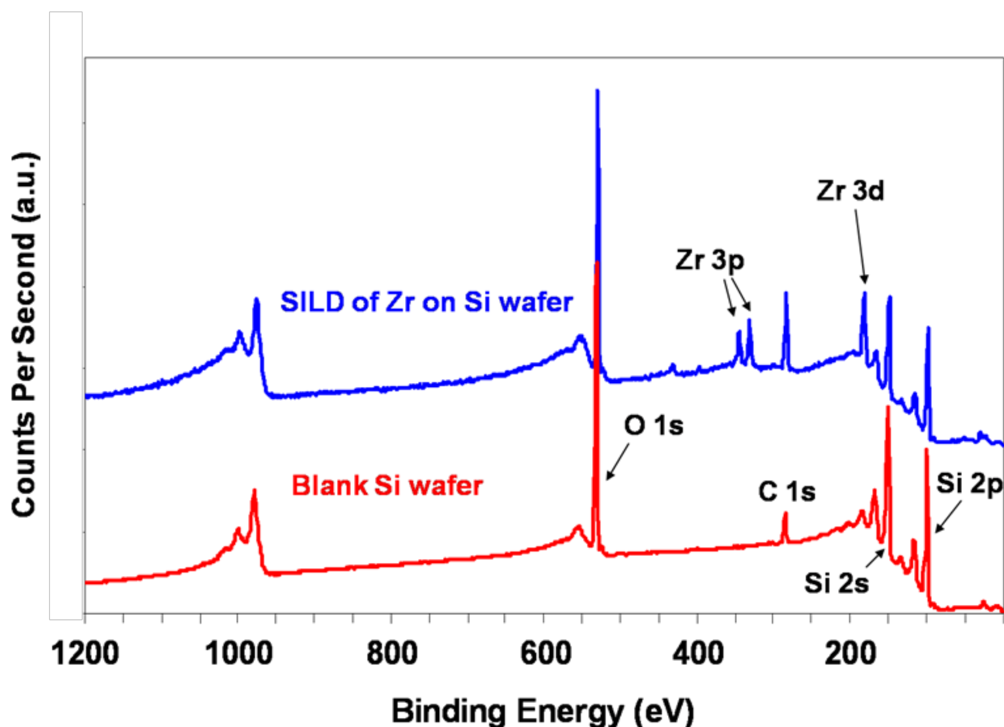

Figure 11. XPS spectra of a blank silicon wafer and a wafer containing a thin film of zirconia deposited using the SILD technique

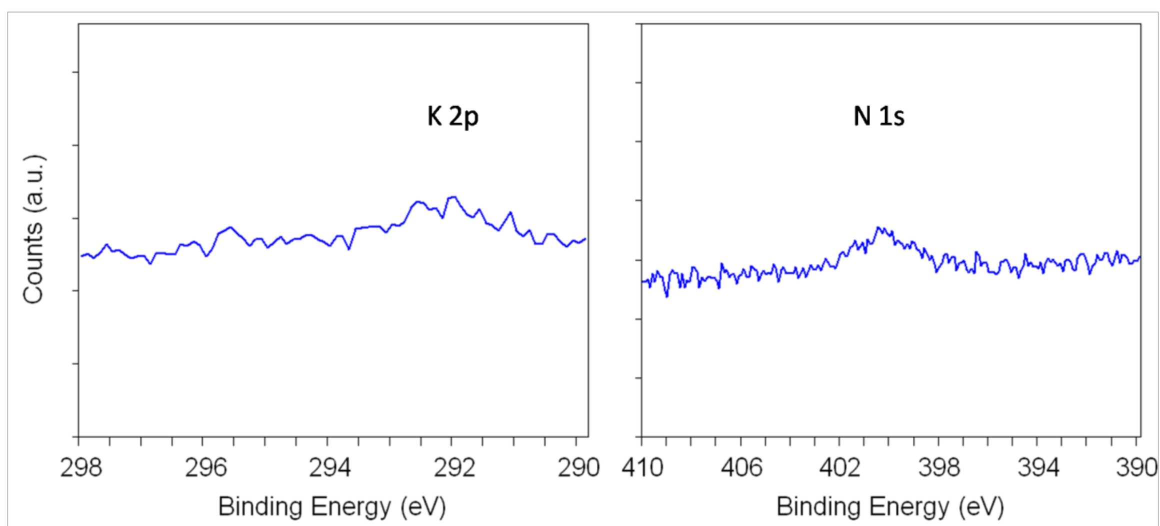

Figure 12. XPS spectra of a SILD-synthesized zirconia thin film dried at 110ºC. Only minimal levels of potassium and nitrogen were detected in the thin film.

All of the ZrO_2 thin films synthesized as a part of this dissertation were observed to grow via the island-type growth mechanism, based on the AFM images obtained for this study (Appendix A). Although not an exact measurement of dispersion, the average ZrO_2 island diameter measured by AFM can be correlated to the relative dispersion of the ZrO_2 on the support surface. For each AFM image of ZrO_2 thin films in Appendix A, a histogram of island diameters was generated (similar to data in Figure 13). Each island's diameter was the taken as the average of the longest and shortest dimensions of the feature. The feature border was defined as the point at which the gradient of color changed to the background gradient around the island. Features in the AFM images that likely represented dust or contamination were disregarded in generating the histogram of island diameters for each AFM image.

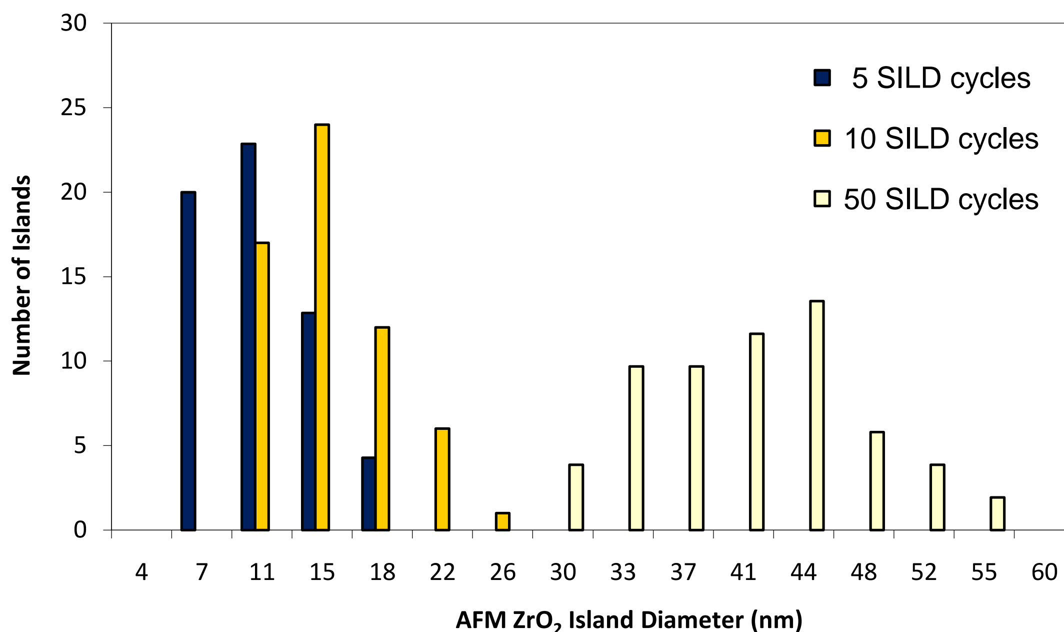

Figure 13. Histogram showing the distribution of ZrO_2 island diameters (from AFM) for three samples of 5, 10, and 50 total SILD cycles. The following SILD variables were constant: $[ZrO(NO_3)_2]$ = 0.01 M, [KOH] = 0.04 M, residence time = 30 sec.

Comparisons of average island diameters from AFM images for the set of zirconia thin film samples synthesized as outlined in Table 2 are presented in Figure 14, Figure 15, and Figure 16. The addition of 25% ethanol by volume to the SILD solutions appeared to not affect the average island diameter of the resultant zirconia thin films after 10 and 50 SILD cycles (compare Table 2 data). The zirconium nitrate concentration in the 1st SILD solution did not significantly affect the average island diameter of the resultant thin film (Figure 14). The residence time during each SILD cycle in which the solutions were in contact with the silicon wafer supports prior to performing intermediate rinsing also did not appear to affect the resultant thin film (Figure 15). However, the number of SILD cycles did affect the average island diameter of the growing ZrO_2 thin film. As the number of SILD cycles increased, the island diameter increased (Figure 16).

Not only did the average island diameter of the thin film increase, but the density of islands per unit area of the support surface also increased with an increasing number of SILD cycles. A histogram counting the frequency of nanoislands observed on AFM images of ZrO_2 thin films synthesized via 5, 10, and 50 SILD cycles was shown previously in Figure 13. This suggests not only an increase in average thin film thickness with an increasing number of SILD cycles, but also an increase in the rate of new nucleation sites for thin film growth as the number of SILD cycles increases.

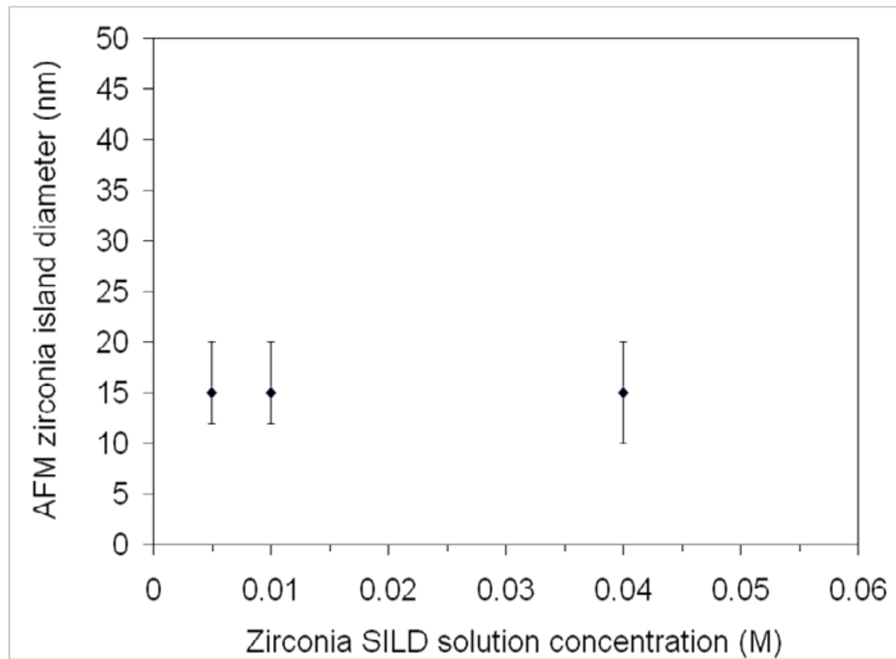

Figure 14. Effect of zirconium nitrate concentration of the 1st SILD solution on the island diameter of the resultant ZrO_2 thin film. In these samples the following SILD variables were constant: number of SILD cycles = 10, [KOH] = 0.04 M, residence time = 60 sec.

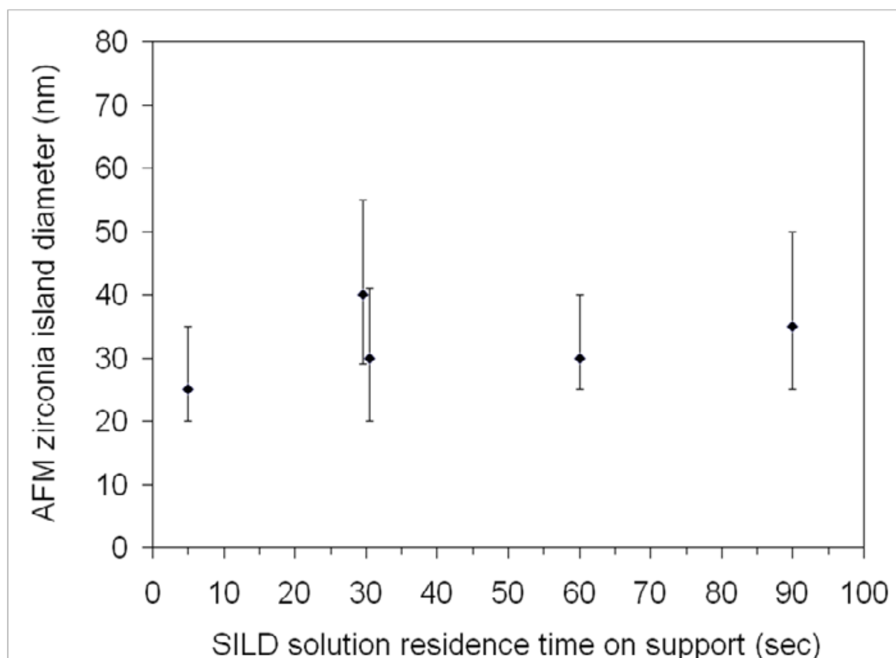

Figure 15. Effect of SILD solution residence time on the silicon wafer on the island diameter of the resultant ZrO_2 thin film. In these samples the following SILD variables were constant: number of SILD cycles = 50, $[ZrO(NO_3)_2]$ = 0.01 M, [KOH] = 0.04 M. The two data points at t = 30 seconds represent two separately synthesized thin films.

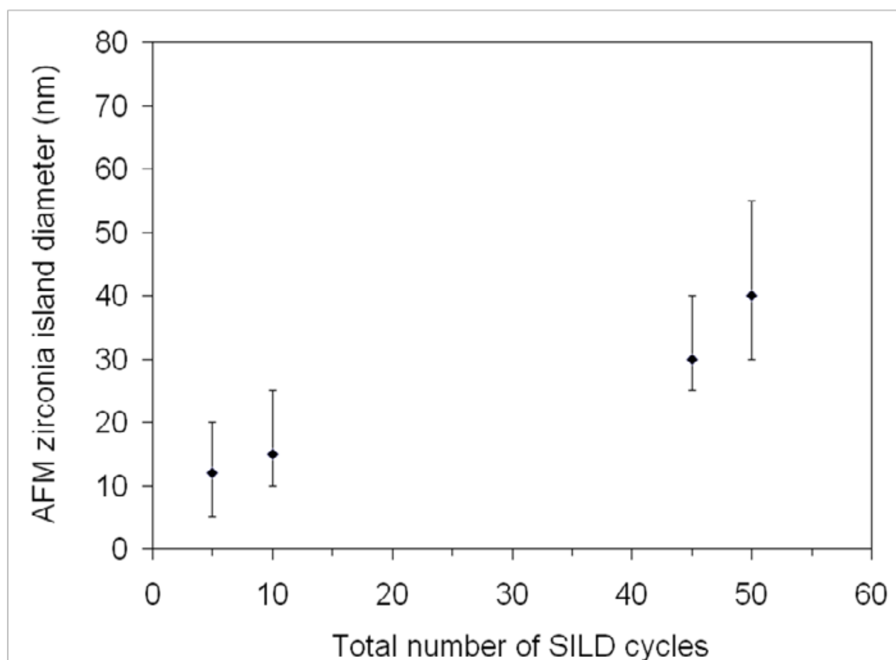

Figure 16. Effect of the total number of SILD cycles on the island diameter of the resultant ZrO_2 thin film. In these samples the following SILD variables were constant: $[ZrO(NO_3)_2]$ = 0.01 M, [KOH] = 0.04 M, residence time = 30 sec.

2.5 Conclusions

The results of this characterization study of zirconia thin film deposition on silicon wafers via the SILD technique were presented. Several insights into the SILD technique were observed. SEM images of holes and channels pre-etched in the silicon wafer surface by a focused ion beam of gallium were used to demonstrate the conformal nature of the SILD technique. This is evidence that the SILD procedure could be a technique for the conformal coating of thin films of oxide materials on three dimensional supports of interest to catalysis. In fact, three dimensional deposition on nanopowders using the SILD technique will be discussed in Chapter 4.

XPS evidence of SILD-deposited zirconia thin films suggest that one can minimize the level of undesirable impurities in the as-deposited SILD nanolayers. Minimizing the undesirable impurities in the thin films, even without subsequent high temperature thermal treatment, was achieved by selecting the appropriate aqueous precursors and adequately rinsing the SILD solutions from the growing thin film during the SILD cycles. This control over impurities sets SILD apart from the other aqueous thin film depositions techniques of chemical bath deposition, liquid-phase deposition, and electroless deposition. This has implications on the potential applicability of SILD for synthesizing higher purity thin films on temperature sensitive support structures.

AFM images and XPS spectra provided insight into the SILD synthesis conditions and their effects on the zirconia thin films deposited on silicon wafers. The most significant variable in the SILD technique that affected the final surface morphology of the zirconia thin films was the total number of SILD cycles. Whereas, the concentrations of $ZrO(NO_3)_2$, KOH, and ethanol in the SILD solutions and the residence time of the

SILD solutions on the silicon wafer samples all had less statistically significant effects on the resultant surface morphology of the zirconia thin films. Though not highlighted significantly in this chapter on zirconia thin films, the selection of aqueous metal salt precursors comprising the SILD solutions and the chemistry of the thin film also affect the final surface morphology of SILD-deposited thin oxide films. The latter effect is observed by comparing AFM images of different materials. The effect of the selection of metal salt precursors on the resultant thin film is a subtopic of Chapter 3.

Chapter 3

SILD of Alumina and Barium Oxide on a Silicon Wafer

3.1 Introduction

Several studies suggest that a highly dispersed phase of barium oxide supported on alumina reacts differently with NO_2 than a bulk-like phase of barium oxide. These studies indicate that during temperature programmed desorption (TPD) the dispersed phase of BaO releases adsorbed NO_2 around 435ºC whereas the bulk-like phase of BaO releases NO_2 at temperatures above 540ºC [48,49]. The highly dispersed BaO phase, predominant at lower BaO weight loadings on alumina, has also been identified as BaO monomers and dimers located at pentacoordinate sites of the γ-alumina support by Kwak et al (2009) [50,51]. The important role of the interface between the active phase and the support, referred to previously in this dissertation as catalyst-support interactions, has been recognized for some time. Stakheev and Kustov coauthored a 1999 review article on this subject titled "Effects of the support on the morphology and electronic properties of supported metal clusters: modern concepts and progress in 1990s" [52].

The purpose of this study is to gain a fundamental understanding of the appropriate SILD synthesis conditions that are necessary to selectively produce only the highly dispersed phase of barium oxide on a thin film of alumina. Planar silicon wafers were used as model supports for the deposition of alumina by SILD and then the deposition of BaO by SILD.

3.2 Equipment, Procedures, and Materials

The SILD apparatus used for the deposition of alumina and barium oxide on silicon wafers consisted of an Automate Scientific ValveBank 8 liquid perfusion system in combination with a Laurell WS-400B-6NPP/LITE spin coater (refer to section 2.2, Figure 3, and Figure 4). Polished n-type (100) silicon wafers were used as supports for the SILD experiments in the spin coater apparatus. Prior to SILD, the supports were cut to one inch squares, cleaned in acetone, and heated overnight at 110°C in air.

The two SILD solutions containing the desired cationic complexes were comprised of 0.01 M $Al(NO_3)_3$, pH=3.5, and 0.01 M $Ba(NO_3)_2$, pH=5.0, (Aldrich) in 25% ethanol and 75% DI water by volume. The SILD solution containing the desired hydroxyl species was comprised of 4.3% ± 0.2% NH_4OH, pH=11.0 (Sigma-Aldrich), 25% ethanol, and 70.7% water by volume. The rinse solution in the SILD of barium oxide was DI water with 25% ethanol by volume.

The general procedure for the SILD of metal oxides was described previously in chapter 1, section 1.2. The specific procedure for the SILD of an alumina thin film on a silicon wafer substrate followed by SILD of barium oxide on alumina is summarized as follows. First, the silicon wafer is cleaned again by alternately rinsing it three times with acetone and distilled water. The silicon wafer is then placed in the spin coater and 2 ml of the $Al(NO_3)_3$ SILD solution is applied. As before, with each application of the SILD solutions, a period of residence time or contact time is allowed for the support to interact with the SILD solution prior to spinning off the excess solution. The NH_4OH SILD solution is then used to rinse the surface twice before repeating the $Al(NO_3)_3$ SILD solution. The explanation for not using the typical rinsing solution is given in section 3.4.

These three SILD steps (desired cationic species followed by two rinses) are repeated in sequence for the desired number of SILD cycles. The sample is then dried in air to 110^oC for 24 hours and heated to 450^oC for 6 hours to completely oxidize the SILD-synthesized aluminum hydroxide thin film.

The SILD of barium oxide on the supported alumina was performed after the complete oxidation of the thin film at 450^oC and subsequent cooling to room temperature. The specific procedure for the SILD of barium oxide using solutions of 0.01 M $Ba(NO_3)_2$ and NH_4OH (pH of 11.0) is similar to the general six step procedure described in section 1.2. The only difference is that the basic NH_4OH solution is applied first to functionalize the alumina surface to attract the aqueous barium species in the 0.01 M $Ba(NO_3)_2$ SILD solution. The rinse solution of 25% ethanol in DI water is applied twice between the subsequent $Ba(NO_3)_2$ and NH_4OH solutions, just as outlined in the general SILD procedure.

3.3 Characterization

Surface topography images of the barium oxide nanoislands deposited on the SILD-deposited alumina rafts supported on silicon wafer fragments were obtained from a NanoScope IIIa atomic force microscope (AFM) in tapping mode using SPM cantilevers acquired from Pacific Nanotechnology. X-ray Photoelectron Spectroscopy (XPS) characterization to identify elemental composition of the multicomponent thin films was performed on a Kratos Axis Ultra using an Al Kα x-ray source and a charge neutralizing flood gun. In XPS, line positions were corrected relative to a carbon 1s position of 284.5 eV and signal peak intensity was maximized by adjusting the z-axis on the sample stage

manipulator to enable accurate qualitative comparison of signal intensity from one sample to the next. AFM and XPS characterization was performed at the University of Michigan Electron Microbeam Analysis Laboratory (EMAL).

3.4 Results & Discussion

Depositing aluminum oxide on a silicon wafer through SILD was a challenge. In the initial synthesis experiments, the SILD solutions were comprised of aqueous aluminum nitrate and potassium hydroxide (rather than ammonium hydroxide). These SILD solutions initially resulted in absolutely no alumina deposition over a wide range of SILD synthesis conditions. After several attempts, it was determined that the aqueous aluminum complexes were being completely washed off during the multiple rinsing steps of the SILD cycles. One possible reason this occurred has to do with the isoelectric point (IEP) of alumina, which is approximately 9.0. This IEP is higher than the pH of the DI water used for the rinsing steps following the adsorption of aqueous aluminum ions in the first SILD solution. The natural wetting of the silicon wafer surface with the DI water used in the rinse steps was preferable to the adsorption of aqueous aluminum species.

To succeed in depositing alumina on a silicon wafer, it was necessary to use a rinsing solution with a pH greater than the IEP of the adsorbed aluminum species to prevent it from being removed with each SILD cycle by the rinsing solution. KOH with a pH of 12.5 and NH_4OH with a pH of 11.0 were used as the rinsing solutions. Because the rinsing solution was now also hydroxylating the adsorbed aluminum complexes, the 2nd SILD solution was eliminated from the general SILD procedure. Additional rinsing steps were performed to thoroughly remove any excess coprecipitate that was formed in

the diffusion layer through the intermixing of the aluminum nitrate and the basic rinse solutions.

In the case where potassium hydroxide was used as the rinsing SILD solution, results of XPS and AFM experiments suggest that the SILD procedure deposited a layer of discrete potassium hydroxide islands on the silicon wafer surface replacing any and all adsorbed aluminum complexes (Figure 17 and Figure 18). These results suggest that the ionic strength of the aqueous potassium species is greater than the ionic strength of the aqueous aluminum species. Potassium hydroxide is known to react with carbon dioxide to produce potassium carbonate. Due to carbon contamination of all XPS samples, it is unclear whether the layer of islands observed by AFM on the wafer surface is potassium hydroxide or potassium carbonate. Whether in the hydroxide phase or the carbonate phase, this is the first recorded deposition of a potassium-containing thin film by SILD.

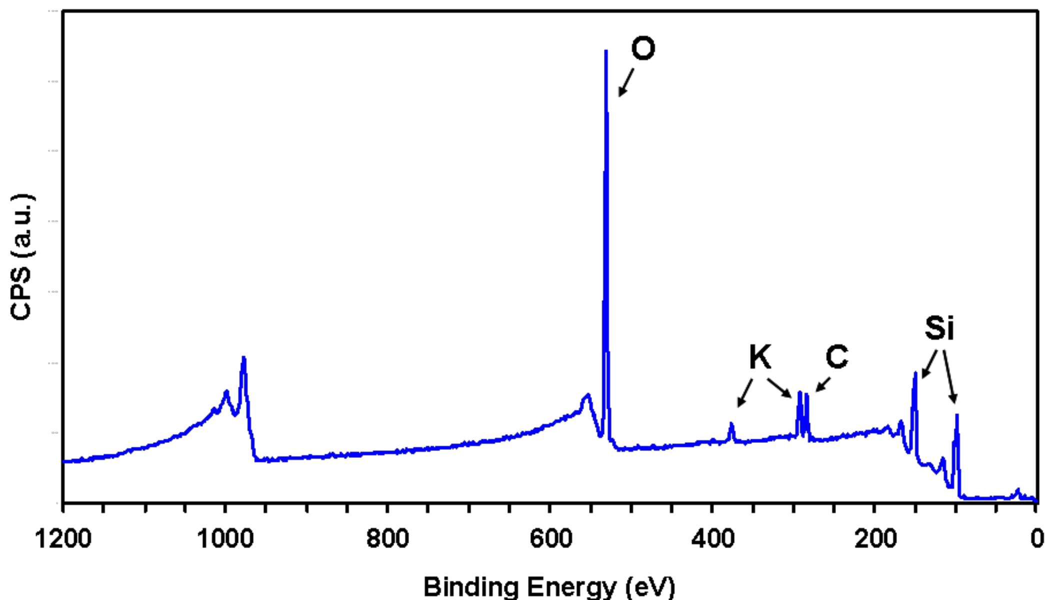

Figure 17. XPS spectra of the potassium-containing thin film synthesized by SILD

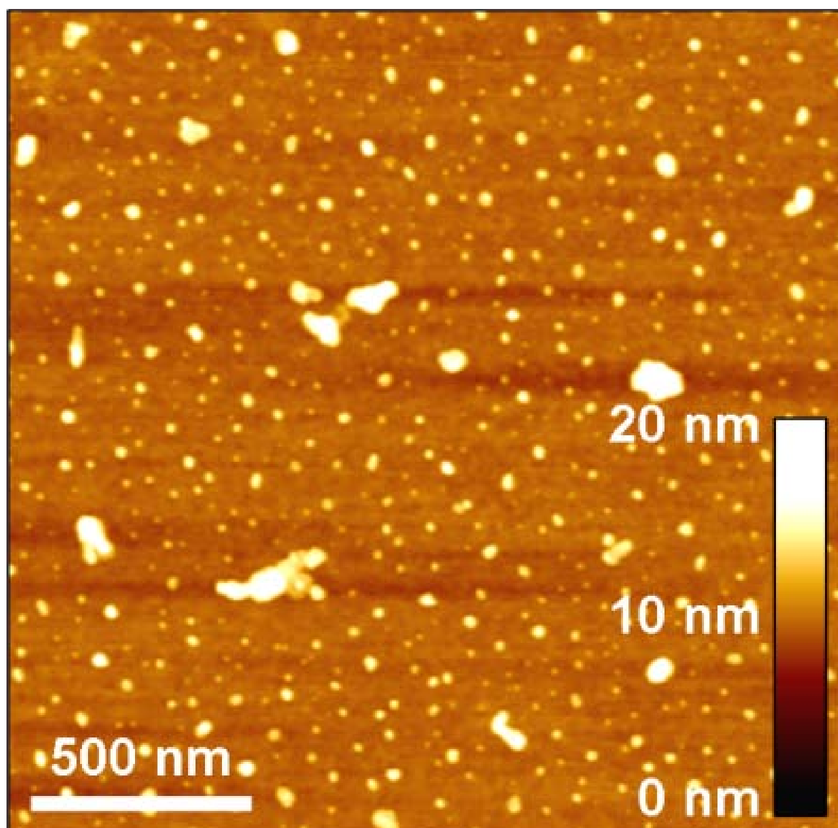

Figure 18. AFM image of the potassium-containing thin film synthesized by SILD

In the case where NH_4OH was used as the rinsing SILD solution and $Al(NO_3)_3$ as the SILD solution, a thin film of alumina or aluminum hydroxide was formed on the silicon wafer supports (conformed by later XPS results). However, the subsequent attempts to deposit BaO on the as-deposited aluminum hydroxide thin film were initially unsuccessful. The aqueous barium complexes completely removed the alumina layer that had just been formed by SILD. Like the potassium hydroxide layer that was synthesized due to an apparently greater ionic strength of the aqueous potassium species, it is likely that the ionic strength of the aqueous barium species completely removed the more weakly adsorbed alumina or aluminum hydroxide SILD nanolayer. However, after removing the wafer fragment sample from the spin coater and heating the SILD

nanolayer of aluminum hydroxide in air to 450^oC to fully oxidize it, the successful synthesis of barium oxide on the surface of the oxidized alumina thin film was accomplished.

The first step in the SILD of barium oxide on alumina also required an adaptation. The isoelectric point of alumina is higher than the 5.0 pH of the 0.01 M $Ba(NO_3)_2$. Thus, one would predict from theory that the aqueous nitrate species would preferentially adsorb in the Stern layer on the alumina surface in the 1st SILD cycle. In addition, the aqueous barium complex might once again begin to displace the oxidized alumina nanolayer. To functionalize the alumina surface so that it would attract the cationic barium complexes, the oxidized alumina surface first needed to be exposed to a solution of pH greater than its IEP. Thus, as was described in section 3.2, the NH_4OH SILD solution was first applied to the alumina surface in order to form a net negative surface charge above the alumina surface. Following two rinses, the $Ba(NO_3)_2$ solution was then applied to initiate the SILD of the barium oxide on the supported alumina thin film.

Table 3 summarizes the SILD experiments performed to produce Al_2O_3 and BaO thin films supported on silicon wafer fragments. After 45 SILD cycles and oxidation in air to 450^oC, XPS experiments confirmed the presence of alumina on the entire surface of the silicon wafer (Figure 19a) and AFM images indicated the presence of some textured alumina surface structures with island diameters of about 130-200 nm (Figure 20b). Appendix B contains additional AFM images and XPS spectra of several samples from Table 3.

Sample	SILD Soln. 1 [M]	SILD Soln. 1 Species	SILD Soln. 2 vol% / [M]	SILD Soln. 2 Species	SILD cycles	Residence Time (sec)
S31 A	0.02	$Al(NO_3)_3$	4.2	NH_4OH	30	90
S31 A+B	0.01	$Ba(NO_3)_2$	0.04	KOH	16	30
S35 A	0.01	$Al(NO_3)_3$	4.0	NH_4OH	45	90
S35 A+B	0.01	$Ba(NO_3)_2$	4.5	NH_4OH	5	30
S36 A	0.01	$Al(NO_3)_3$	4.0	NH_4OH	75	90
S36 A+B	0.01	$Ba(NO_3)_2$	4.5	NH_4OH	5	30
S32	0.01	$Ba(NO_3)_2$	0.04	KOH	50	30
S33	0.01	$Ba(NO_3)_2$	0.04	KOH	15	30
S34	0.01	$Ba(NO_3)_2$	0.04	KOH	5	30
S37	0.01	$Ba(NO_3)_2$	4.5	NH_4OH	5	30

Table 3. Summary of the SILD conditions for Al_2O_3 and BaO thin films synthesized on silicon wafer fragments as a part this study. In each case the SILD solutions contained 25% ethanol by volume and the balance DI water.

After SILD of barium oxide on the alumina thin film, XPS confirmed the presence of both barium and aluminum on the wafer surface, with the Al 2p signal from the alumina layer noticeably suppressed by the subsequent barium oxide coverage (Figure 19). AFM was used to characterize a sample in which 5 SILD cycles of barium oxide were deposited on 45 SILD cycles of alumina (Figure 20c). After heating the wafer to 450°C in air, the surface topography of this dispersed phase of barium oxide nanoislands on alumina remained unchanged, as characterized by AFM.

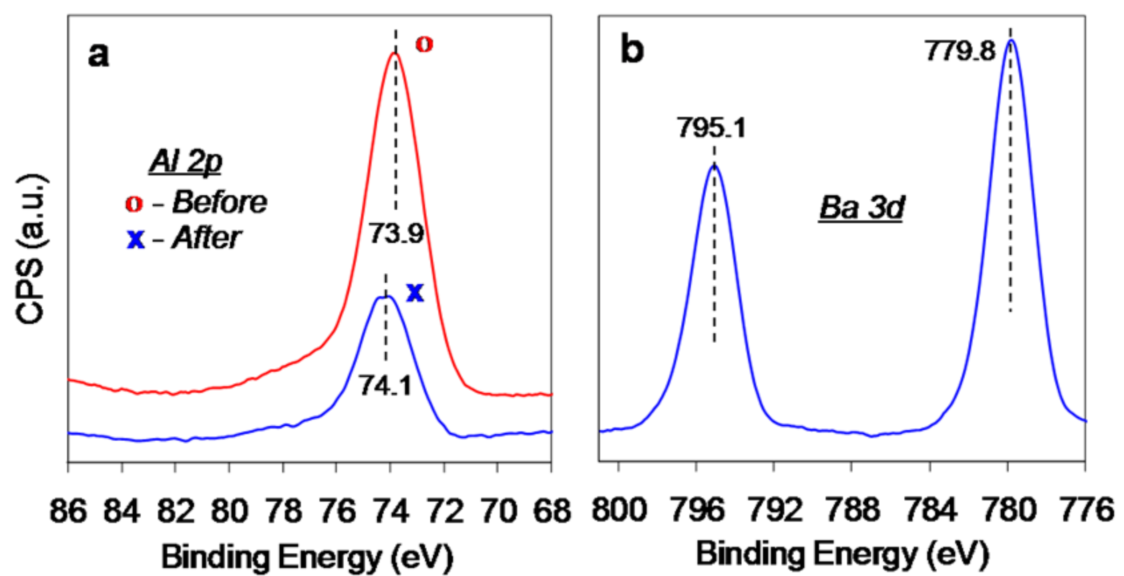

Figure 19. XPS peaks of (a) the SILD-deposited alumina layer before and after SILD of barium oxide and (b) the BaO nanoislands deposited on the alumina supported on a silicon wafer

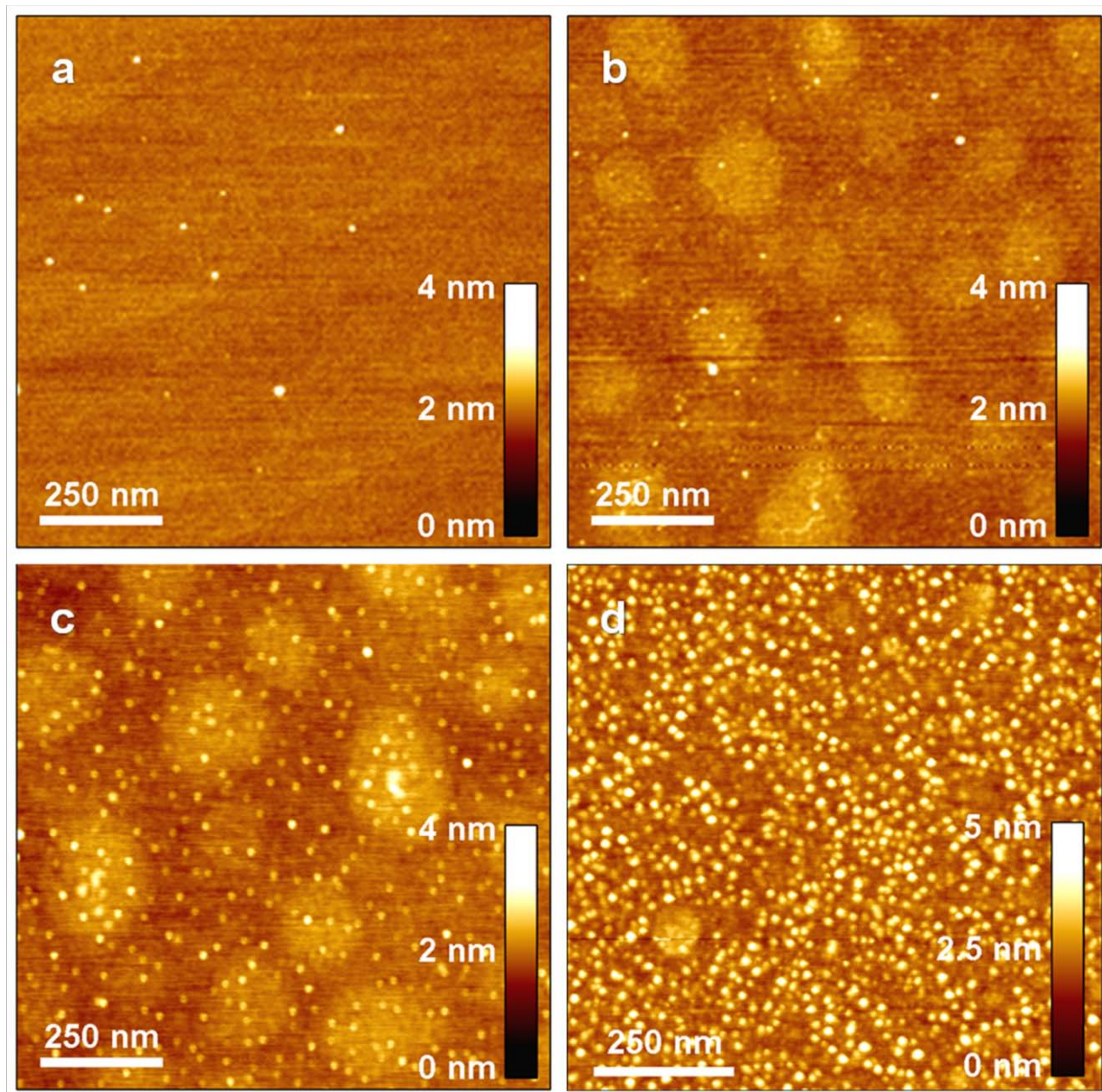

Figure 20. AFM images of (a) blank silicon wafer, (b) alumina deposited on the blank silicon wafer, (c) 5 cycles of barium oxide deposited on the alumina, and (d) an additional 11 cycles of barium oxide, all deposited using the SILD technique

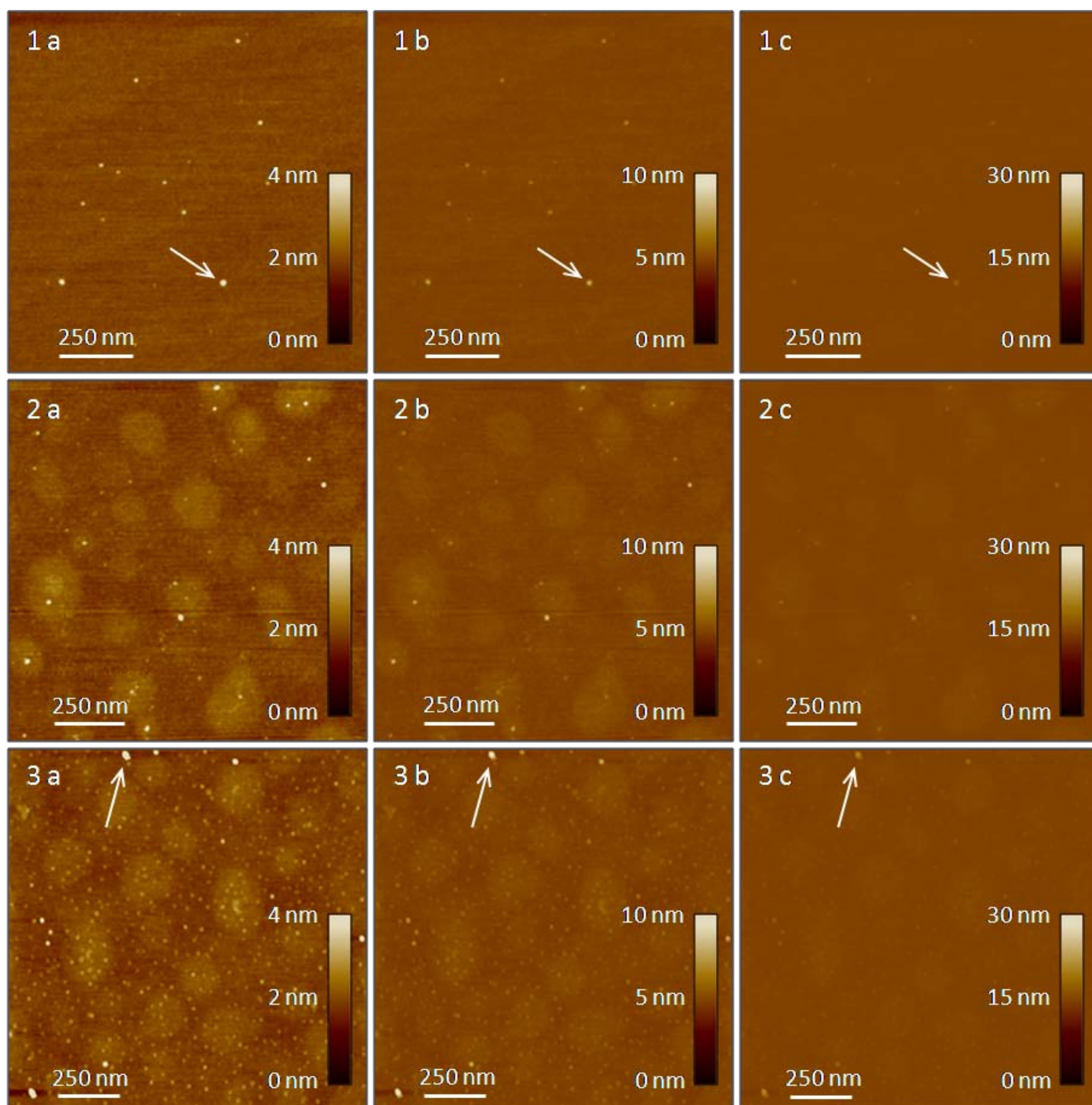

Figure 21. AFM images of three samples (same as Figure 20 a-c): (1) a blank silicon wafer, (2) alumina deposited via SILD on the blank silicon wafer, (3) barium oxide deposited on the alumina via SILD. AFM images (a) through (c) are identical for each of the three samples with only the z-height changing from 4 nm to 30 nm. These images highlight the difference between particles of contamination (indicated by arrows) and the alumina and barium oxide thin films.

The AFM image (Figure 20c) clearly shows the presence of uniform and dispersed nanoislands of BaO on top of Al_2O_3. Figure 21 confirms that the nanoislands represent BaO by distinguishing them from particles of contamination. The average diameter of the BaO nanoislands is 15 ± 2.0 nm, with an average height of 1.3 ± 0.6 nm. Increasing the number of SILD cycles of the $Ba(NO_3)_2$ solution to sixteen had the effect of completely covering the Al_2O_3 with BaO while only increasing the diameter of the BaO islands to 18 ± 2.0 nm (Figure 20d).

Post SILD treatment of the samples was completed to test the stability of the barium oxide and alumina SILD nanolayers. After heating the samples to 450°C in air, smaller sections of each wafer fragment were again washed several times with ethanol or acetone and then rinsed with DI water and reheated to 450°C in air to dry. Appendix B contains AFM images from some of these post-SILD rinses. The ethanol rinse had the effect of removing or redistributing the barium oxide and/or alumina on the surface of the silicon wafer. The effect of the acetone rinse was to perform a surface cleaning, such as the removal of organic contaminants from the surface, as evidenced by less dust on the surface under AFM. For the two samples analyzed, the acetone rinse post-SILD did not appear to damage the barium oxide or alumina surface in any manner.

3.5 Conclusions

In this chapter, SILD was used to synthesize disperse nanoislands or rafts of barium oxide on larger rafts of alumina supported on a silicon wafer. Several modifications to the conventional SILD procedure were necessary to facilitate the successful synthesis of BaO and alumina thin films. Most notably, for the 2nd SILD

solution to hydrolyze the adsorbed aluminum complex and form a surface metal hydroxide, a weaker base than potassium hydroxide was necessary in the 2nd SILD solution. Ammonium hydroxide as the 2nd SILD solution was able to provide the oxygen source for the surface-bound aluminum hydroxide without removing each SILD layer of aluminum hydroxide.

Theory-guided decisions relating to (1) the isoelectric points of silica, alumina, and barium oxide and (2) Stern's model of the electrical double layer formed on a solid surface in an aqueous environment (refer to section 1.2 of Chapter 1) enabled the successful SILD of barium oxide on alumina on silica. This chapter demonstrates that predicting the outcome of a SILD synthesis experiment with sufficient accuracy is possible by knowing the isoelectric points of the support and the desired oxide thin film, as well as the pH of the SILD solutions.

The highly-dispersed BaO phase, characterized by AFM as thin rafts supported on a layer of alumina, was determined to be thermally stable up to at least 450ºC. This temperature was arbitrarily chosen to make certain the thin film of BaO was completely oxidized. Organic contamination was then cleaned from the surface of the oxidized thin film of BaO by rinsing the surface with acetone. The robustness, thermal and chemical stability of the SILD-deposited BaO thin film was remarkable. Future work may prove that SILD is a powerful technique for preparing uniform, nanodispersed thin oxide films that are stable under even harsher conditions and temperatures beyond 450ºC. In the next chapter, the SILD method will be extended to deposit barium oxide on higher surface area alumina supports.

Chapter 4

SILD of Barium Oxide on Fused Alumina Powder

4.1 Introduction

As already introduced in Chapter 3, several studies suggest that γ-alumina supported noble metal catalysts, containing a highly dispersed phase of barium oxide for NO_x storage, are more effective catalysts than those containing a bulk-like phase of barium oxide [48-51]. The Pt/BaO/alumina system is one example of many systems that exhibit interesting catalyst-support interactions [53], where the extent of dispersion of the active species on the support influences the overall catalytic performance.

The purpose of this chapter was to develop a synthesis procedure that would allow the controlled synthesis of a highly dispersed phase of BaO on alumina. There is evidence that the physical distance of noble metal particles from BaO particles plays an important role in overall NO_x storage behavior via oxygen spillover during storage or hydrogen spillover or reverse spillover of NO_x species from BaO to the noble metal catalyst particles during regeneration [54,55]. Coating alumina with closely-spaced, highly dispersed rafts of BaO to the extent of near complete coverage would, in principle, decrease the spacing between noble metal particles and the NO_x storage material, thus enhancing the effectiveness of the lean NO_x trap system.

Adsorption of NO_2 on highly dispersed BaO particles located at pentacoordinate sites of the γ-alumina support has been demonstrated by experiment and theory to have a

lower energetic barrier for NO_2 uptake [50,51]. Temperature programmed desorption (TPD) studies have indicated that this highly dispersed phase of BaO also releases adsorbed NO_2 at lower temperatures around 430ºC, whereas the bulk-like phase of larger BaO particles releases NO_2 at temperatures above 520ºC (Figure 22, used with permission) [48,49].

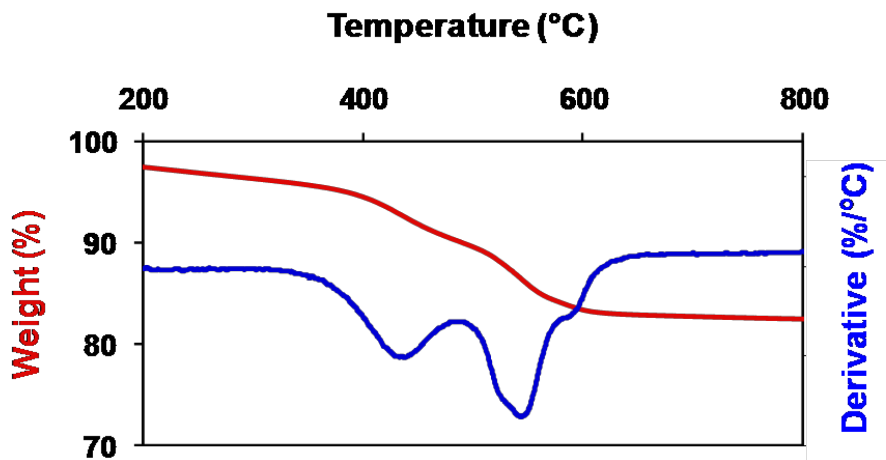

Figure 22. Thermogravimetric analysis (TGA) of NO_2 released from 21.4 wt% BaO supported on γ-alumina (252 m^2/g) as the sample is heated to 800ºC at 2ºC/min. The percentage of BaO in the dispersed and bulk-like phases was reported to be 44% and 56%, respectively [49].

Increasing the ratio of BaO synthesized in the dispersed phase compared to the bulk-like phase is challenging using conventional loading techniques such as wet impregnation. The previously mentioned TPD study reported that the less stable, dispersed phase saturates at 0.14 grams of BaO per gram of Al_2O_3 support, beyond which point increased loading of BaO using the wet impregnation technique results in the formation of bulk-like BaO, with respect to NO_2 adsorption behavior. Even at a 14 wt%

BaO loading, approximately 40% of the BaO exists in the bulk-like phase (Figure 23, used with permission) [49].

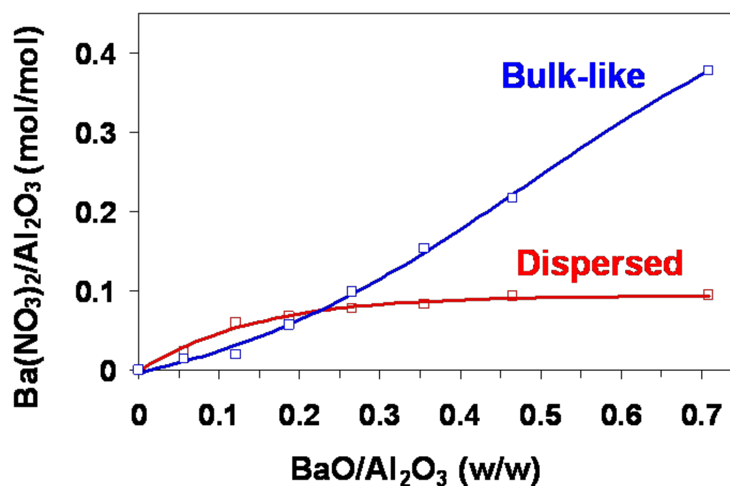

Figure 23. Molar ratio of $Ba(NO_3)_2$ to alumina support (252 m^2/g) after NO_2 adsorption vs. the total weight loading of BaO via wet impregnation. Molar quantities of $Ba(NO_3)_2$ assigned to the bulk-like and dispersed phases were derived from integration of TGA derivative peaks from NO_2 TPD experiments [49].

Enhancing the dispersion of highly loaded catalysts synthesized by wet impregnation, or other bulk scale loading techniques, is often difficult because catalyst dispersion tends to decrease as weight loading increases. Bulk scale catalyst synthesis techniques synthesize supported catalyst nanoparticles of which only a fraction of the catalyst mass can directly be influenced by the support. Furthermore, on many supports post-deposition drying and calcination lead to the agglomeration of the dispersed catalyst phases into less active and more bulk-like catalyst particles [56,57]. The ability to selectively synthesize a purely dispersed phase on a support would enable a more detailed characterization of the effects of catalyst-support interactions on overall catalytic activity.

Because of its ability to control uniform deposition at the nanometer scale, SILD was chosen as the synthesis technique for producing a highly dispersed BaO oxide phase on alumina. Although not yet incorporating noble metal catalyst particles, this chapter focuses on SILD as an enabling synthesis method for depositing highly dispersed BaO on alumina, a prerequisite for enhanced utilization of the noble metal catalysts.

Chapter 3 of this dissertation provided a fundamental understanding of the appropriate SILD conditions that were required to synthesize a dispersed phase of barium oxide on a two-dimensional model support. This chapter uses the knowledge gained to extend the SILD method to three-dimensional support structures by synthesizing a purely dispersed phase of barium oxide on fused alumina powder.

4.2 Equipment, Procedures, and Materials

The SILD apparatus used for deposition of barium oxide on fused alumina powder consisted of an 87 ml Coors Büchner funnel, 0.45µm Millipore filter paper, a side arm flask, and a Welch 2522B vacuum pump.

Fused alumina powder (>99.99%, Atlantic Equipment Engineers) of particle size 1-2 µm (determined by SEM) was used as the support for the SILD of barium oxide in the Büchner funnel apparatus. At closer inspection by TEM, these fused alumina particles contained dense crystallites of approximately 150 nm diameter and 50 to 100 nm wide pores (Figure 24).

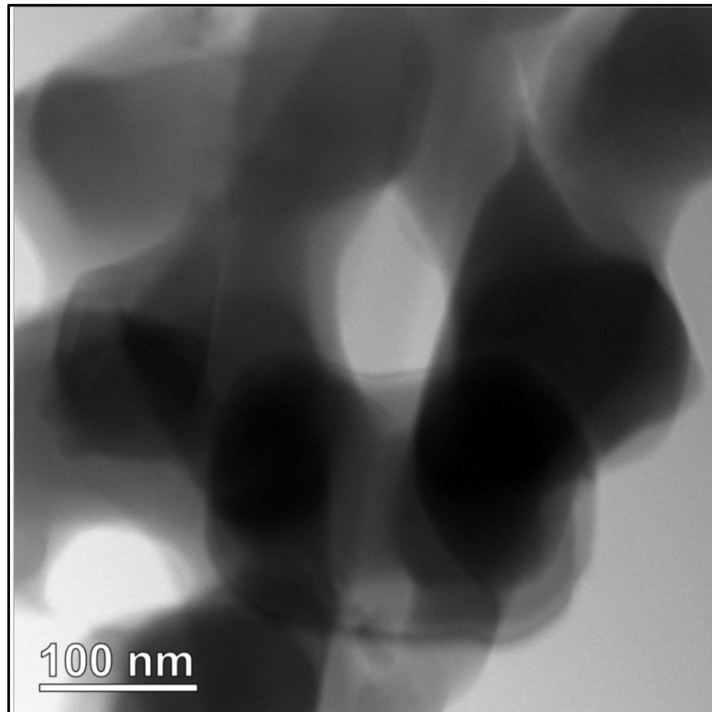

Figure 24. TEM image of fused alumina

This fused alumina support with large pores was chosen as a suitable support material to avoid capillary transport of SILD solutions and precipitation of bulk-like BaO particles during SILD that one would expect to occur in higher surface area alumina with smaller pores. This method confines loading of the dispersed BaO rafts to the fused alumina surface during SILD and facilitates a direct comparison to conventional wet impregnation techniques. The latter technique has been shown to yield a significant percentage of bulk-like BaO particles even at low weight loadings or modest surface coverage [48,49].

The BET surface area of the fused alumina support was measured at 6.57 m^2/g, porous enough for characterization using bulk gas adsorption techniques. The choice of

fused alumina as the support for these experiments does not imply that SILD could not be used to deposit BaO onto higher surface area alumina supports, or even onto washcoated monoliths. However, in this study we chose to use a relatively non-porous alumina as a model support for a clearer confirmation that SILD leads to nanostructures distinguishable from those achievable with conventional wet impregnation. The rationale was that on less highly porous supports SILD of BaO would lead exclusively to surface deposition, without confounding the characterization by additional nanoparticle deposition which would likely occur via capillary transport and precipitation of BaO in small pores of the support.

The SILD of barium oxide on fused alumina powder over filter paper in a Büchner funnel was performed using the same 0.01 M $Ba(NO_3)_2$ and 4.5% NH_4OH solutions in 25% ethanol and DI water as described in chapter 3, section 3.2. The procedure for the SILD of BaO on the fused alumina was initiated just as was done to deposit BaO on a thin film alumina sample with the NH_4OH solution applied first, followed by two to four rinses, and then the barium nitrate SILD solution followed by another two to four rinses. This pattern of solutions was repeated for up to 5 SILD cycles. The residence time or contact time between the SILD solutions and the fused alumina powder was dependent on the vacuum pressure on the side arm flask and the filtration rate through the filter paper in the Büchner funnel. Typical residence times ranged from 90 seconds to 3 minutes for each SILD solution and rinse. Between 2 and 3 grams of fused alumina support were used in each BaO deposition experiment. After the SILD procedure, the alumina samples were dried in air to 110°C for 24 hours and heated to 450°C for 6 hours to form BaO.

4.3 Characterization

A Kratos Axis Ultra XPS instrument with an Al Kα x-ray source and a charge neutralizing flood gun was used to characterize the elemental surface composition. In XPS, line positions were corrected relative to a carbon 1s position of 284.5 eV. Electron microscopy was performed on a FEI Nova Nanolab SEM instrument with a Schottky FEG and a JEOL 2010F TEM. BET surface areas were determined by nitrogen physisorption experiments on a Micromeritics ASAP 2020 instrument.

The deposition of BaO on fused alumina by the SILD technique was characterized by XPS (Figure 25) and BET surface area measurements. The BET surface area of the alumina support was measured at 6.57 m^2/g. After SILD of BaO the BET surface area was approximately the same, increasing only to 7.06 m^2/g.

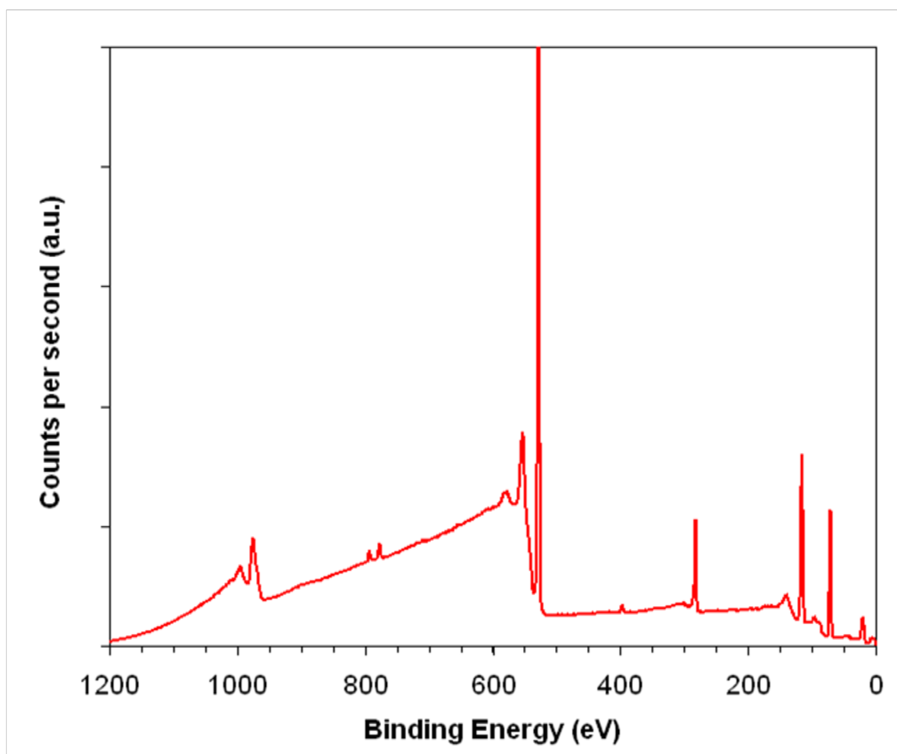

Figure 25. XPS spectra of barium oxide synthesized by SILD on fused alumina powder

4.4 Control Experiment

The objective of the wet impregnation control experiments was to compare the BaO dispersion on samples using the SILD technique to the dispersion of conventionally loaded BaO using the wet impregnation technique. Six BaO-loaded samples on fused alumina and three blank fused alumina samples were prepared in the following manner. The first two BaO-loaded samples were prepared through five cycles of the previously described SILD technique. The next two samples were prepared as a single step loading of $Ba(NO_3)_2$ precursor using the wet impregnation technique [48]. The last two samples were prepared through five sequential wet impregnation steps where each step deposited one fifth of the total BaO weight loading (Figure 26). The purpose of dividing the wet impregnation procedure into five sequential steps was to directly compare the surface deposition of BaO on a per-step basis to the SILD-synthesized samples of five SILD cycles. The wet impregnation samples were likewise dried in air to 110°C for 24 hours and heated to 450°C for 6 hours. The three blank samples of fused alumina were prepared in a similar manner as the BaO-loaded samples, only DI water was used rather than $Ba(NO_3)_2$.

The target weight loadings were 0.10 and 0.20 wt% BaO on the fused alumina. Assuming a linear relationship between barium oxide surface coverage and alumina surface area, these BaO weight loadings on fused alumina correspond to 3.8 and 7.6 wt% BaO loadings on a typical 250 m^2/gram, high surface area alumina support.

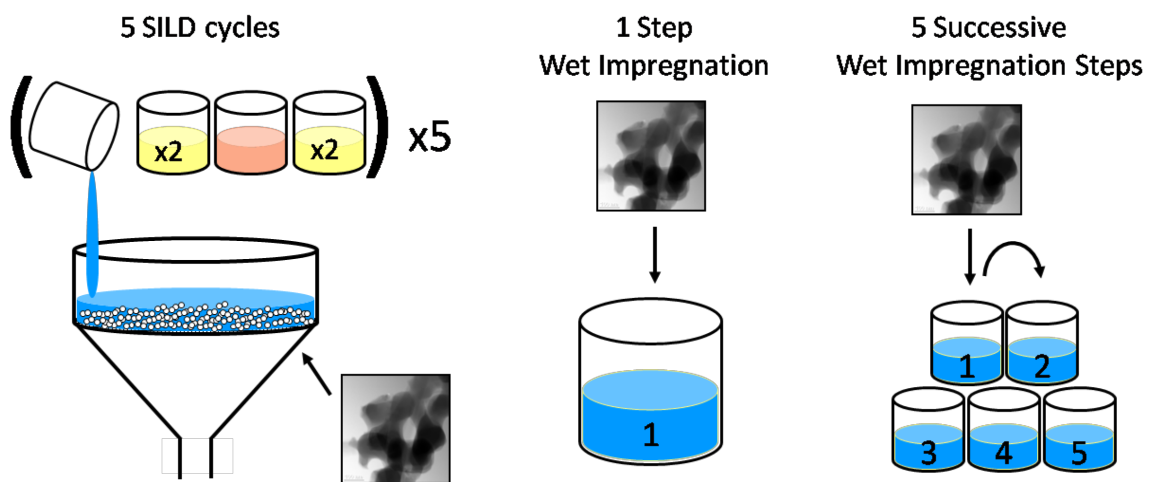

Figure 26. Illustration of the three different synthesis techniques used to compare SILD to the conventional wet impregnation technique

4.5 Temperature Programmed Desorption Experiments

To confirm the uniqueness of this highly dispersed phase of BaO, NO_2 temperature programmed desorption (TPD) experiments were performed on SILD-synthesized samples and equally weight loaded samples prepared by the conventional wet impregnation technique. The highly dispersed BaO rafts on fused alumina synthesized by SILD were expected to release NO_2 at a lower temperature during TPD than the predominantly bulk-like BaO nanoparticles synthesized by wet impregnation (refer to Figure 22).

The nine fused alumina samples, six containing BaO and three blanks, were each placed in a 4.7 ml glass U-tube inside a vertical tube furnace, heated in flowing 5000 ppm NO_2 (balance helium) to 650°C followed by ballistically cooling in the same gas to 25°C. The temperature of 650ºC is significant because it ensures on all samples that the barium is completely oxidized and contains no leftover nitrates (dispersed or bulk-like) that may have been present from the synthesis procedure.

The samples were then transferred to platinum weigh pans for thermogravimetric analysis (TGA) in a TA Q500 with effluent gases connected to a Thermo Scientific TGA/FT-IR Interface and Nicolet 380 FT-IR. Weight loss of NO_2 was measured with respect to temperature by the TA Q500 as the samples were ramped from 25°C to 800°C at 10°C per minute in pure N_2 flowing at a rate of 100 ml (STP)/min. For each sample, multiple TGA experiments were conducted to assure reproducibility. The weight loss of each of the six BaO-loaded alumina samples was corrected for NO_2 weight loss from the corresponding blank alumina samples. The corresponding IR traces for NO_2 desorbing from the samples during TPD were integrated as a function of TGA temperature,

adjusting for flow rate and lag time for gas transfer from the TGA to the IR instrument. These experiments were designed as a method to highlight SILD as a novel technique for preparation of highly dispersed catalysts through direct comparison of the derivative weight loss peaks with respect to temperature.

4.6 Results and Discussion

After determining the SILD parameters suitable for depositing barium oxide on an alumina model surface (refer to Chapter 3), a highly dispersed phase of BaO was loaded on a three dimensional alumina support via the SILD technique. Fused alumina particles 1-2 μm in diameter were suspended by filter paper in a Büchner funnel as the SILD solutions were applied. During SILD, the alumina slurry (support plus aqueous solution) was manually mixed using a stainless steel spatula. The alumina slurry was observed to be more viscous initially, and became easier to stir after a few SILD cycles. Physically mixing the slurry over the filter paper occasionally caused the filter paper to tear. When tearing of the filter paper occurred the sample was lost through the Büchner funnel with the filtrate. Additional efforts to automate the SILD procedure for deposition on three dimensional powder supports are recommended to improve efficiency and reproducibility.

The ratio of BaO present on the fused alumina in the dispersed phase as compared to the bulk-like phase was calculated from the NO_2 weight loss curves. The NO_2 weight loss of the three blank alumina support samples were subtracted from the actual experimental weight loss of the corresponding BaO-containing samples synthesized via SILD, one-step wet impregnation, or five-step wet impregnation. Net weight loss (after

subtracting the weight loss of the blanks) between 300ºC and 500ºC was considered to be NO_2 released from dispersed BaO; whereas, weight loss above 500ºC corresponded to bulk-like BaO. Figure 27 and Figure 28 show representative NO_2 weight loss curves for a BaO on alumina sample loaded by wet impregnation and a blank alumina sample, respectively. Figure 29 shows the net weight loss curve (Figure 27 less Figure 28) representing only the NO_2 that was adsorbed on the BaO. To calculate the mass of BaO in the dispersed and bulk-like phases, the mass loss from $Ba(NO_3)_2$ decomposition (represented as NO_2-NO_3) to form BaO was converted to moles of NO_2-NO_3 and then converted to mass of BaO. The 1.416 conversion factor represents 1.416 grams of BaO loaded on the alumina per 1.000 grams of NO_2-NO_3 released during TPD.

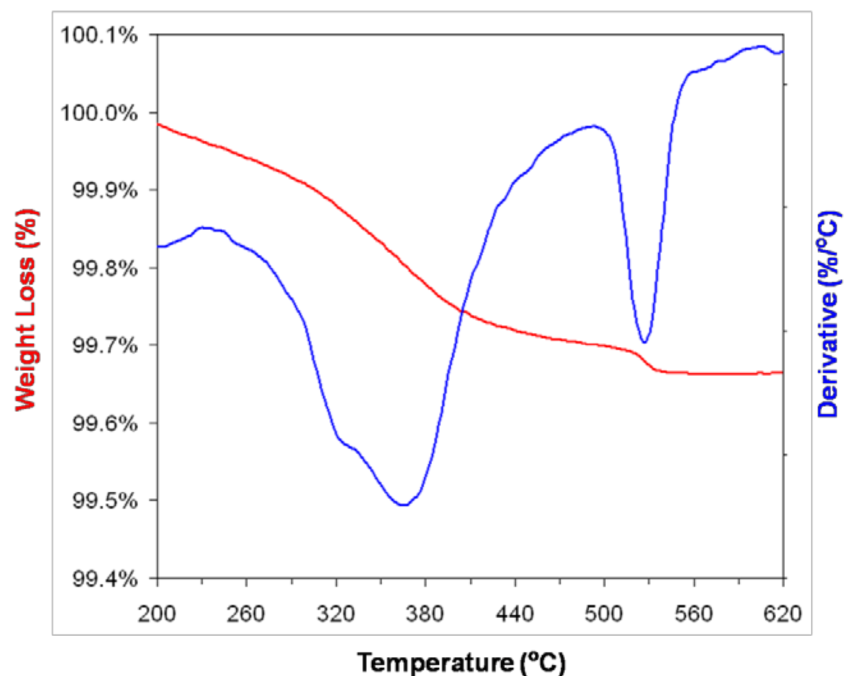

Figure 27. Weight loss of NO_2 during TPD from a BaO / fused alumina sample in which the BaO was loaded using the single step wet impregnation technique

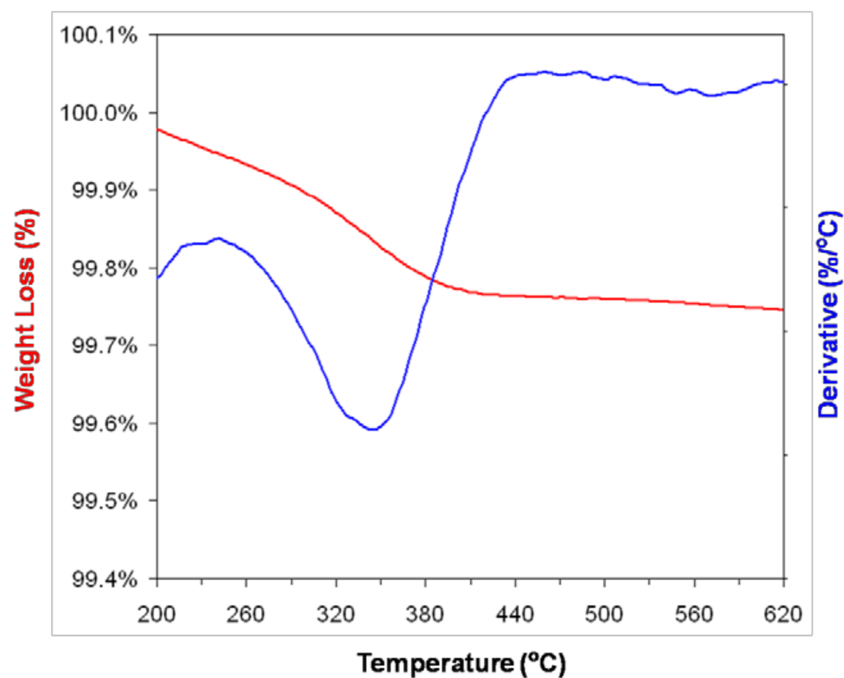

Figure 28. Weight loss of NO_2 during TPD from a blank fused alumina sample

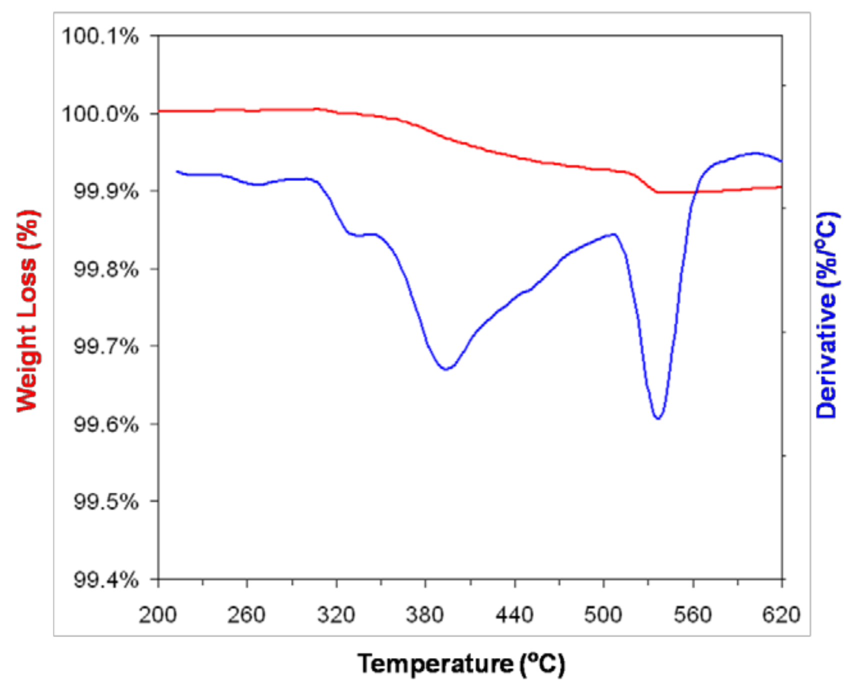

Figure 29. Net weight loss of NO_2 during TPD corresponding to only the BaO

A comparison of the percentage of BaO in the dispersed phase vs. the bulk phase was made between the samples synthesized by the SILD technique and the control samples prepared via the wet impregnation technique. The relative percentage of BaO in one phase or the other is calculated from the NO_2 weight loss observed over the temperature intervals corresponding to each phase. Table 4 summarizes the results of the TPD experiments on each of the six BaO-loaded samples.

Sample	BaO loading technique	BaO loading steps or SILD cycles (#)	Target BaO loading on fused Al_2O_3 (wt%)	TGA samples[a]		Final BaO loading on fused Al_2O_3 (wt%)[b]	BaO phase distribution (%)[c]	
				Run	Weight (mg)		Dispersed	Bulk-like
1	SILD	5	0.10	1	31.225	0.09	100	0
				2	52.216	0.12	100	0
2	SILD	5	0.20	1	64.460	0.18	96	4
				2	60.624	0.18	97	3
3	Wet Impregnation	5	0.10	1	65.437	0.07	86	14
				2	70.910	0.10	90	10
4	Wet Impregnation	5	0.20	1	61.727	0.11	79	21
				2	63.443	0.13	80	20
5	Wet Impregnation	1	0.10	1	50.180	0.05	70	30
6	Wet Impregnation	1	0.20	1	51.538	0.15	72	28

[a] Only one or two representative samples shown. Additional TPD experiments were reproducible +/- 0.03 wt%

[b] Adjusted for NO_2 weight loss of blank Al_2O_3 samples (prepared identically except barium precursor was absent)

[c] Estimates calculated from weight loss in NO_2 TPD experiments

Table 4. Distribution of dispersed and bulk-like barium oxide in samples prepared via the SILD and wet impregnation techniques.

For the fused alumina samples loaded with BaO by the two wet impregnation routes, the evident high-temperature derivative weight loss peaks above 500ºC (Figure 29 and Figure 30) demonstrate that wet impregnation leads to the formation of the bulk-like phase of BaO. In contrast, the predominant weight loss feature in the SILD-synthesized samples falls in the low temperature range characteristic of the dispersed BaO phase. Although a trace amount of weight loss above 500ºC was measured in the 0.18 wt% SILD-synthesized sample, there is no well-defined NO_2 derivative weight loss feature above 500ºC that would suggest the formation of bulk-like BaO via SILD. Analysis of the effluent gases in the FT-IR instrument indicates that only NO_2 is desorbing from the samples during the TPD experiments (Figure 31).

The thermal stability to 650ºC of the dispersed BaO phase on the fused alumina is also a significant achievement. This remarkable stability of the thin BaO rafts on the alumina was not necessarily expected. As was mentioned in the introduction, drying and calcination post-synthesis often result in the agglomeration of dispersed phases into bulk-like particles. After the wet impregnation of $Ba(NO_3)_2$ and subsequent drying and calcination to load an equivalent surface coverage (as compared to the 0.10 wt% BaO on fused alumina) of BaO on high surface area alumina would normally result in at most 65% of the deposited BaO remaining in the dispersed phase. Whereas, via the SILD technique, almost 100% of the BaO was determined to be in the dispersed phase on the fused alumina, even after post-synthesis drying and calcination to 650ºC.

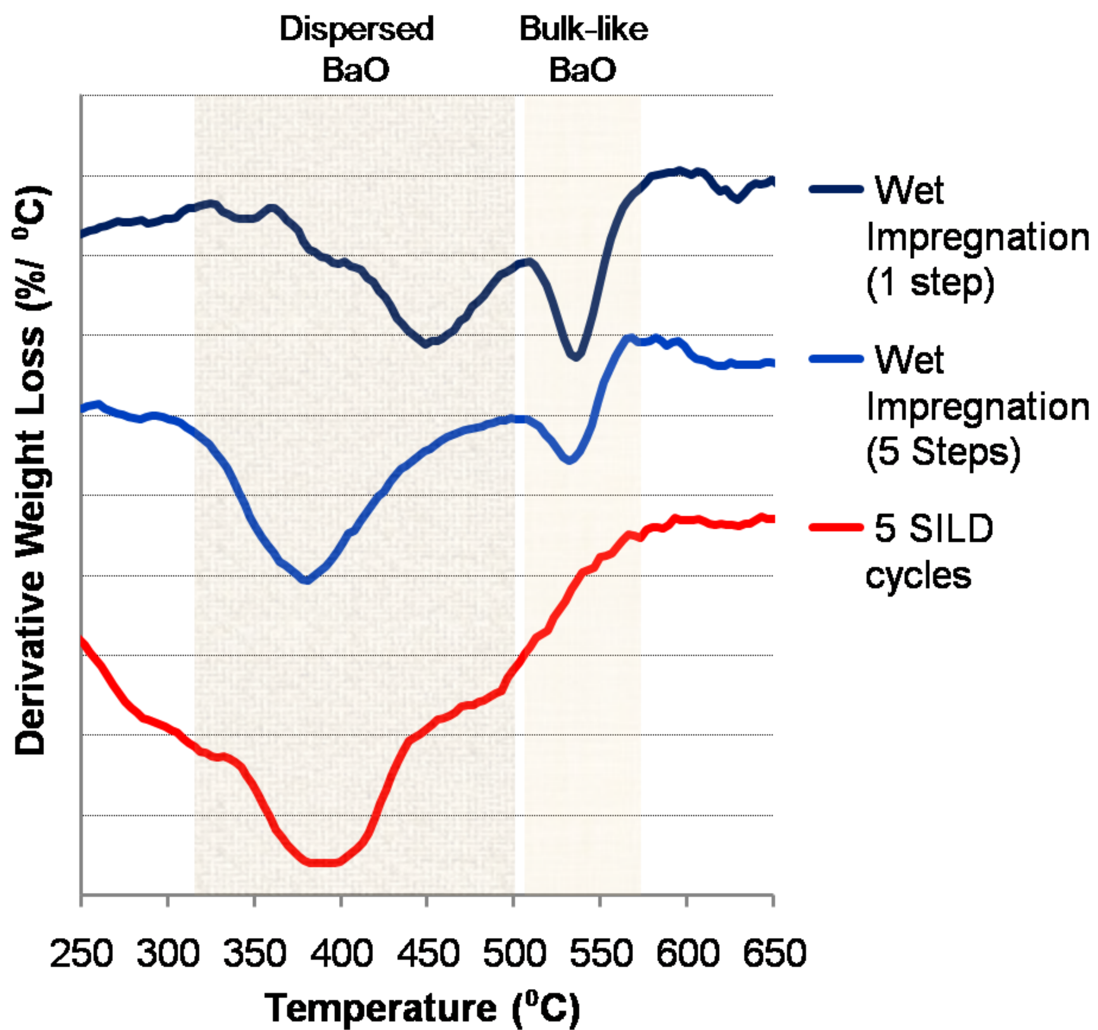

Figure 30. Derivative NO_2 weight loss peaks comparing the BaO dispersion of samples synthesized using the SILD technique to wet impregnation samples

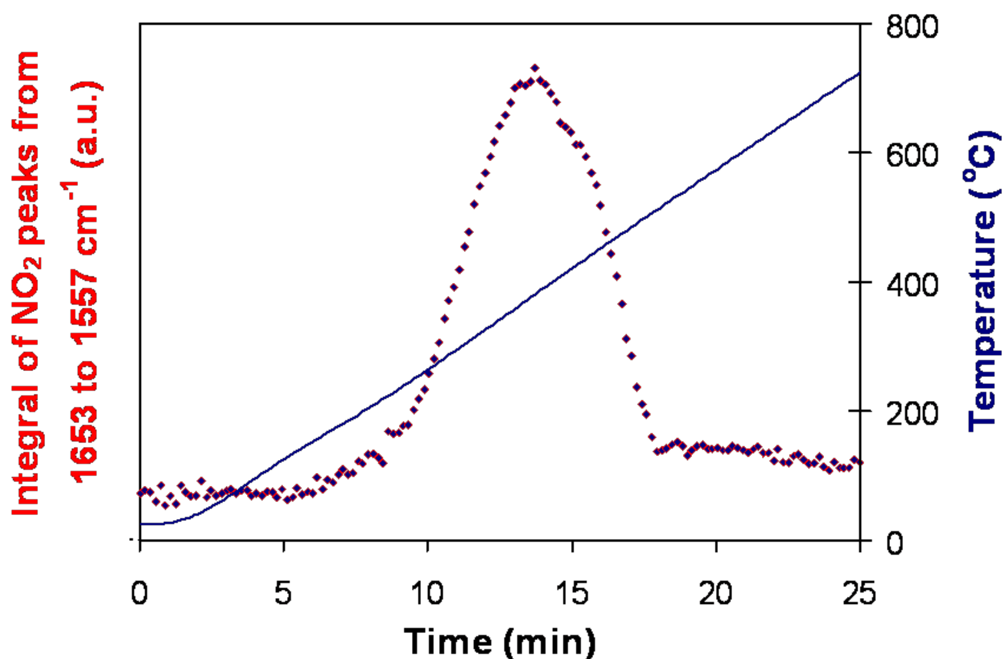

Figure 31. Bell-shaped curve represents the integral of the signature IR peaks for the characteristic wave numbers corresponding to NO_2 with respect to time. The solid line represents the TGA temperature profile during TPD at a constant ramp rate of 30ºC/min

In almost every case, the BaO loading calculated from the observed NO_2 weight loss during thermogravimetric analysis is less than the BaO loading targeted by the synthesis technique. In SILD, the target weight loading is somewhat nebulous as the average deposition rate per SILD cycle was estimated from AFM measurements on two-dimensional surfaces. Whereas, the lower than anticipated weight loadings of the samples prepared by wet impregnation was not expected. There are at least two possible explanations for this discrepancy between the experimentally measured loading by $Ba(NO_3)_2$ impregnation and the calculated BaO weight loading from NO_2 TPD experiments. First, during the wet impregnation, the aqueous barium species may have been preferentially attracted to the walls of the glass beaker that was used to contain the

fused alumina support rather than depositing on the fused alumina surface. Likewise, during the drying step the barium may also have preferentially precipitated on the glass beaker. Second, the innermost core of the bulk-like BaO particles synthesized via wet impregnation may not have adsorbed NO_2 and been converted to $Ba(NO_3)_2$ prior to the TPD experiments. Thus, the net BaO weight loading calculated from NO_2 weight loss during TPD would not necessarily reflect the total BaO present on the alumina samples.

4.7 Conclusions

The results of this study demonstrate that the SILD technique is capable of selectively synthesizing a highly-dispersed BaO phase as a conformal coating on three-dimensional alumina supports. Such a selective and uniform deposition of nanoscale BaO rafts would be difficult, if not impossible, to achieve with traditional impregnation-based synthesis techniques. Though not part of this study, one could envision using SILD to also deposit the platinum particles on the surface of the BaO rafts to create a lean NO_x trap catalyst. However, given the relatively low noble metal loadings of typical NO_x trap catalysts, the conventional impregnation techniques may be sufficient to deposit the highly dispersed platinum nanoparticles.

This study is one of the first attempts to extend SILD from its role as a 2-dimensional thin film deposition technique toward becoming a 3-dimensional conformal coating technique of interest for catalyst synthesis. The SILD of BaO on the fused alumina was confirmed initially by XPS spectra identifying barium on the alumina surface and then physisorption experiments indicating no significant change in BET surface area as compared to the blank alumina. The SILD of BaO was later confirmed by

careful NO_2 TPD experiments. The SILD-synthesized BaO was determined to be thermally stable in a highly dispersed phase after post-SILD drying and calcination to 650ºC by subsequent NO_2 TPD experiments. To what extent the remarkable thermal stability of highly dispersed BaO will be sustainable on a fully formulated noble metal containing monolith under realistic automotive exhaust conditions remains to be seen. SILD may prove to become a powerful method for preparing uniform nanodispersed materials that are stable under harsh operating temperatures even beyond 650ºC.

Chapter 5

Conclusions and Future Recommendations

5.1 Conclusions

The objectives of this dissertation were to study empirical aspects of the SILD technique by characterizing the thin oxide films synthesized on model two dimensional supports and then extend the SILD technique to the practical synthesis of supported oxide nanostructures on three dimensional supports of interest to catalysis.

AFM surface profiles, XPS spectra, and SEM images provided significant insight into the SILD of zirconia, alumina, and barium oxide thin films on silicon wafers. The most significant SILD conditions that affected the final surface morphology of the thin films were the selection of aqueous metal salt precursors comprising the SILD solutions and the total number of SILD cycles. The additional SILD variables analyzed in the zirconia thin film study (chapter 2) all had statistically insignificant effects on the resultant morphology of the thin ZrO_2 films. Fundamental aspects pertaining to the SILD mechanism were confirmed as surface potential theory guided some necessary modifications to the conventional SILD procedure to enable the synthesis of BaO and alumina thin films on silicon wafers (chapter 3). In the effort to synthesize an alumina thin film on a silicon wafer, a potassium-containing thin film was deposited for the first time by means of the SILD technique.

The NO_2 storage behavior of SILD-synthesized thin films of barium oxide on fused alumina powder confirmed that a highly dispersed phase of BaO was able to be deposited for the first time on three dimensional powder supports through the SILD technique. Chapter 4 describes how a lower decomposition temperature of $Ba(NO_3)_2$ (formed by flowing NO_2 over supported BaO) during TPD experiments suggest that the SILD-synthesized thin films of BaO are more highly dispersed on alumina than the BaO deposited on alumina by the conventional catalyst loading technique of wet impregnation.

Additional insights related to the SILD procedure were also observed in this study. For example, unless there is a clear, physical path whereby the SILD solutions may be rinsed from the support, deposition by co-precipitation of the SILD solutions in the diffusion layer near the support surface is also likely to occur (such as in Figure 6). The co-precipitation of the SILD solutions in the aqueous medium becomes particularly important when one uses SILD to deposit thin films on high surface area powders. Creative engineering with regards to the construction of the SILD apparatus as well as thorough support rinsing to remove undesired ions or precipitate from the diffusion layer after each step in the SILD cycle will become increasingly important in effectively using SILD to deposit conformal thin films on higher surface area supports including γ-alumina, carbon nanotubes, and cordierite monoliths.

5.2 Future Recommendations

The ability of SILD to synthesize a highly disperse and uniform conformal coating of oxides on three dimensional supports has the potential to provide many fundamental insights into the way catalysts interact with supports. The ability to

maintain high catalyst dispersion on a support before, during, and after the reaction would be enormously beneficial for understanding many catalyst systems. By utilizing the ionic interactions between the support and the aqueous precursors during the deposition cycles, SILD has been shown able to adhere nanodispersed oxides as thin films or rafts on the support surface such that they remain stable and highly dispersed even at elevated temperatures. The potential for this thermal stability to persist between multilayers deposited using the SILD technique also exists (Figure 32).

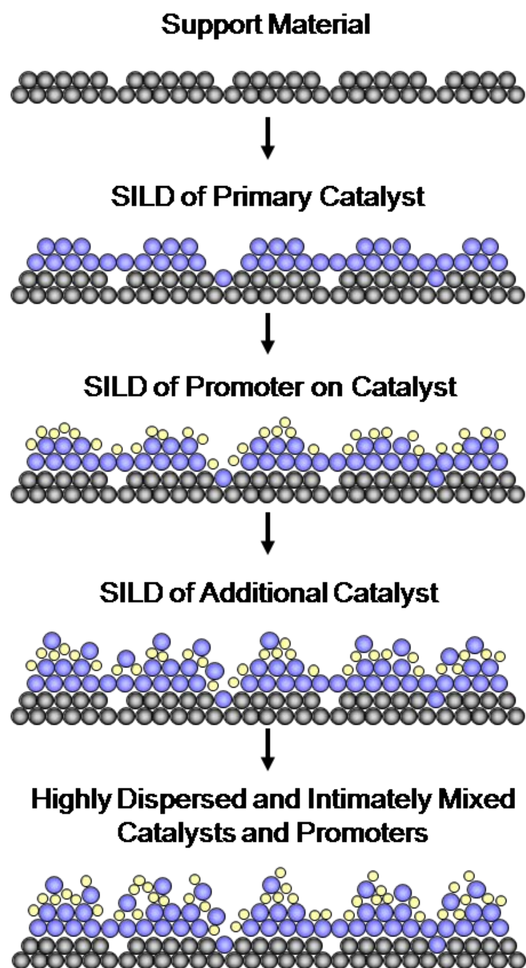

Figure 32. Illustration of the ability of SILD to synthesize highly dispersed and intimately mixed multicomponent thin films on a support

A recommended next step for future work is to continue synthesizing thin films of BaO on fused alumina via the SILD technique. A valuable set of experiments would involve increasing the number of SILD cycles, or increasing the total weight loading, of BaO on the fused alumina. The thickness of the BaO thin film on the alumina surface would continue to increase with more and more SILD cycles. It would be interesting to observe at what weight loading (or total alumina surface coverage) the bulk-like phase of BaO begins to form. Additional NO_2 TPD experiments and wet impregnation control samples should be coupled with the SILD synthesis experiments to evaluate the higher weight loaded samples.

Additionally, the manual, step-wise procedure used in performing the SILD of BaO on the fused alumina could be improved. The procedure was labor intensive making it difficult to control and identically reproduce the SILD conditions from one sample to the next. The filter paper in the Buckner funnel was subject to tearing and was often clogged with the nanopowder support, reducing solution flow and increasing the SILD solution residence times from one cycle to the next. The construction and use of an automated apparatus for the SILD of thin films on powder supports would be expected to improve experimental consistency in the amount of BaO deposited during the SILD synthesis experiments on the fused alumina supports.

Experiments designed to measure the actual lean NO_x trap performance would also be a worthwhile future study. Incorporating platinum or other precious metals with the highly dispersed phase of barium oxide on fused alumina would be able to test the NO_x storage (and reduction) behavior of a fully formulated catalyst. This study would

likely provide mechanistic insight into the proximity effects between the BaO and the precious metal catalysts.

Finally, SILD may prove to be useful in synthesizing and exploring many other catalyst systems that have been theorized to be more active or selective but are difficult to synthesize. Some of these catalyst systems may be those in which the catalyst-support interface has been shown to have a significant effect on the activity and/or selectivity of the catalyst.

APPENDIX A. Successive Ionic Layer Deposition of Zirconia

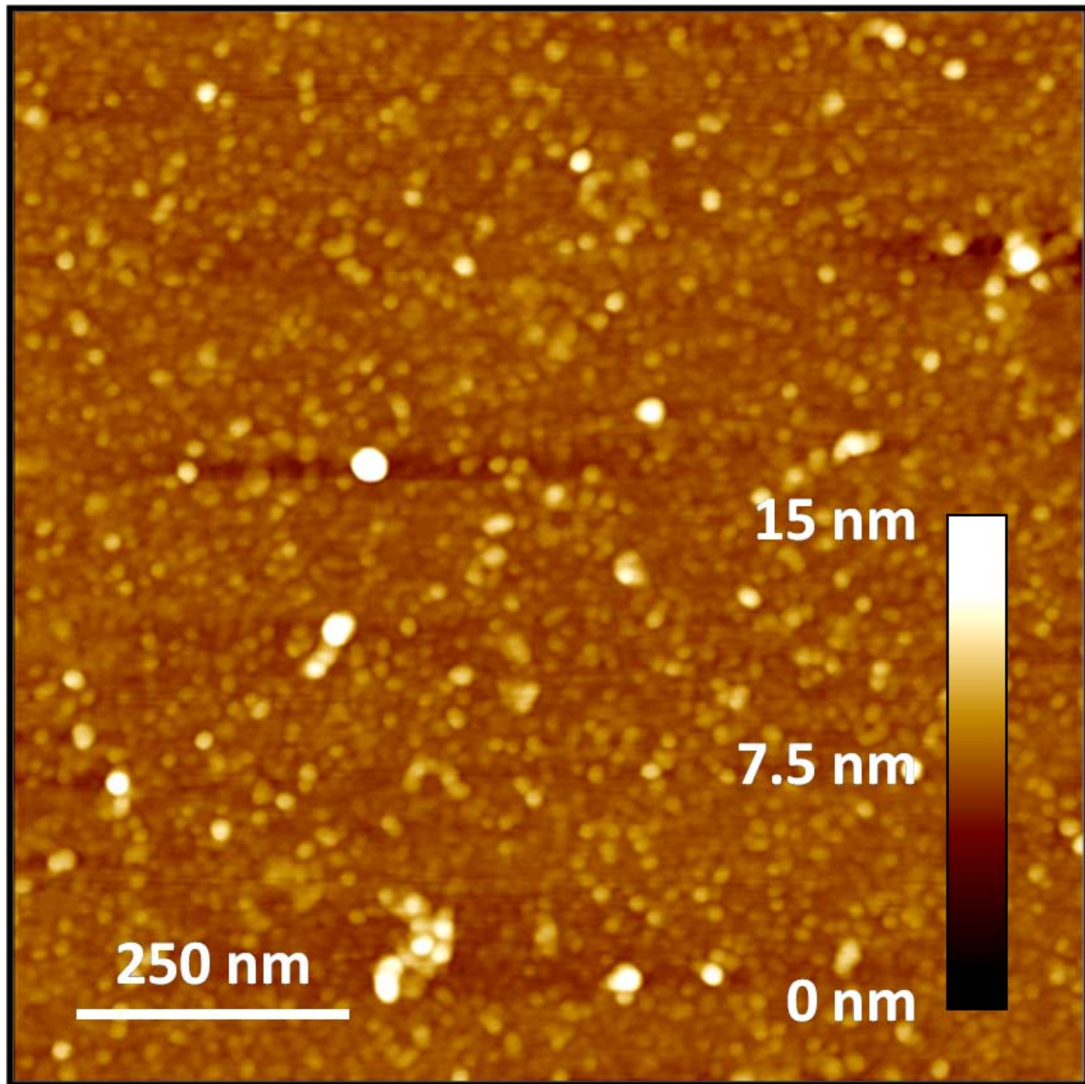

Figure A.1. AFM image of a zirconia thin film that was synthesized on a silicon wafer through 10 SILD cycles of alternating 0.005 M $ZrO(NO_3)_2$ and 0.04 M KOH solutions in 25% ethanol & 75% DI water (by volume) according to the SILD procedure described in Section 2.2. The residence time in which each SILD solution was in contact with the surface was approximately 60 seconds.

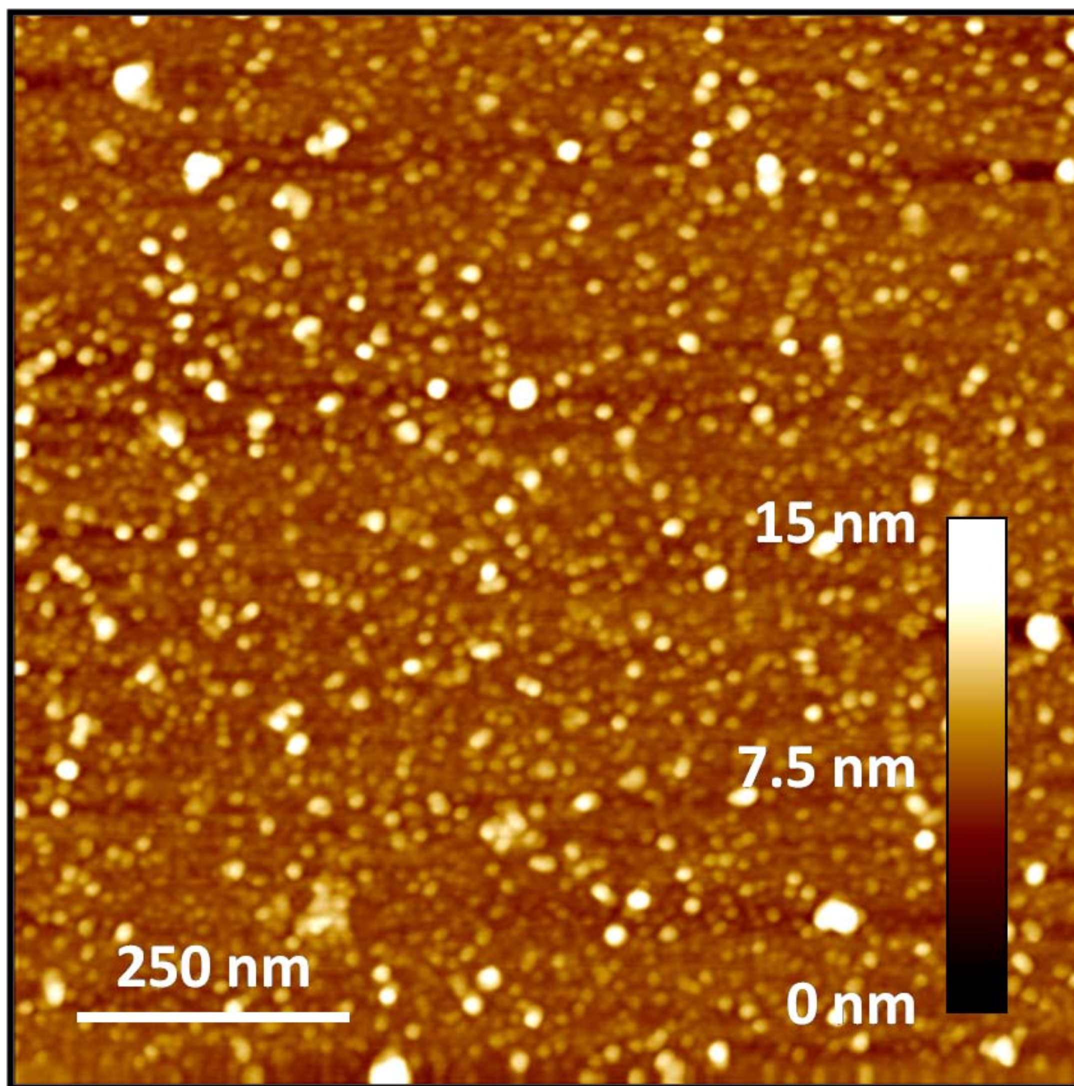

Figure A.2. AFM image of a zirconia thin film that was synthesized on a silicon wafer through 50 SILD cycles of alternating 0.005 M $ZrO(NO_3)_2$ and 0.04 M KOH solutions in 25% ethanol & 75% DI water (by volume) according to the SILD procedure described in Section 2.2. The residence time in which each SILD solution was in contact with the surface was approximately 60 seconds.

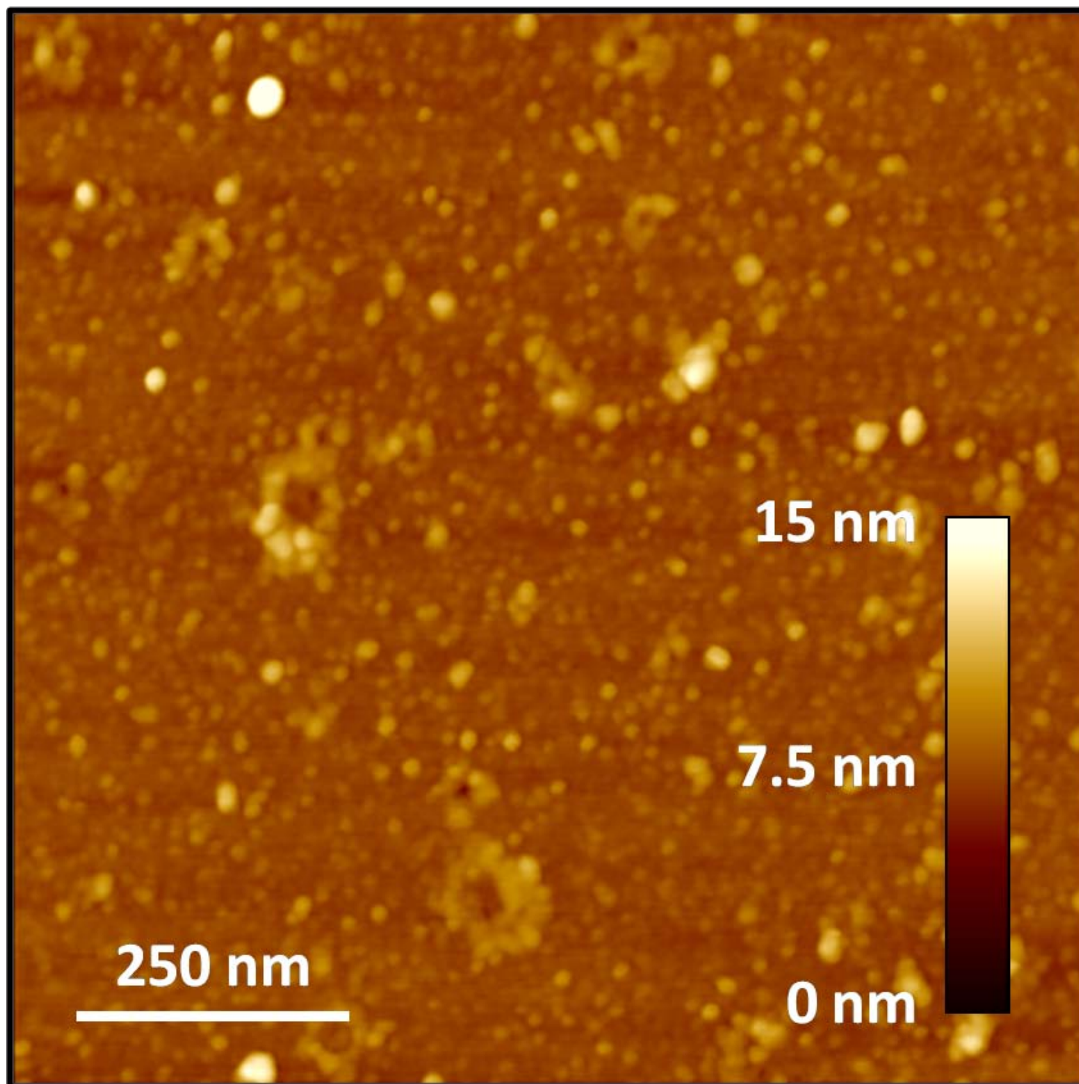

Figure A.3. AFM image of a zirconia thin film that was synthesized on a silicon wafer through 10 SILD cycles of alternating 0.01 M $ZrO(NO_3)_2$ and 0.01 M KOH solutions in 25% ethanol & 75% DI water (by volume) according to the SILD procedure described in Section 2.2. The residence time in which each SILD solution was in contact with the surface was approximately 60 seconds.

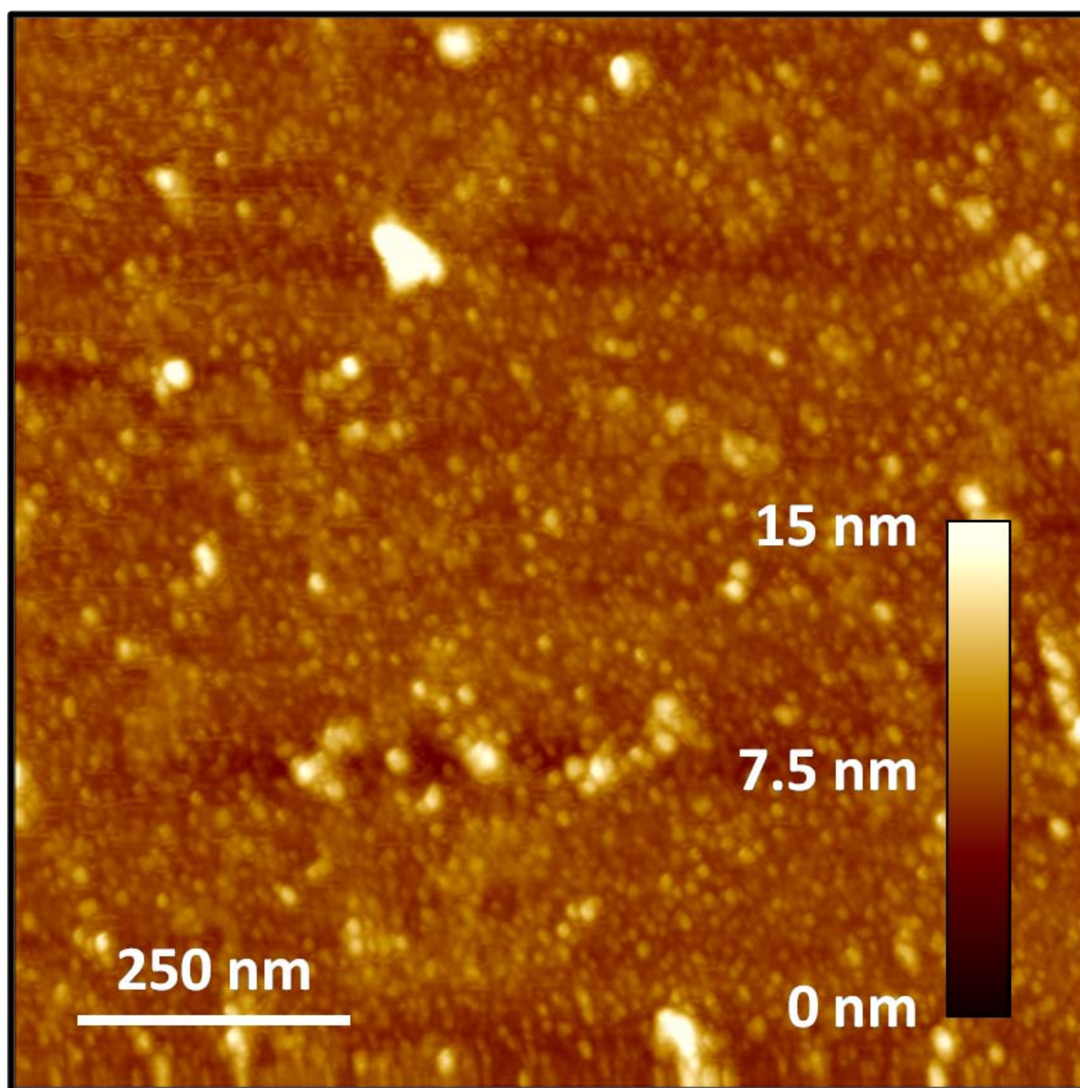

Figure A.4. AFM image of a zirconia thin film that was synthesized on a silicon wafer through 50 SILD cycles of alternating 0.01 M $ZrO(NO_3)_2$ and 0.01 M KOH solutions in 25% ethanol & 75% DI water (by volume) according to the SILD procedure described in Section 2.2. The residence time in which each SILD solution was in contact with the surface was approximately 60 seconds.

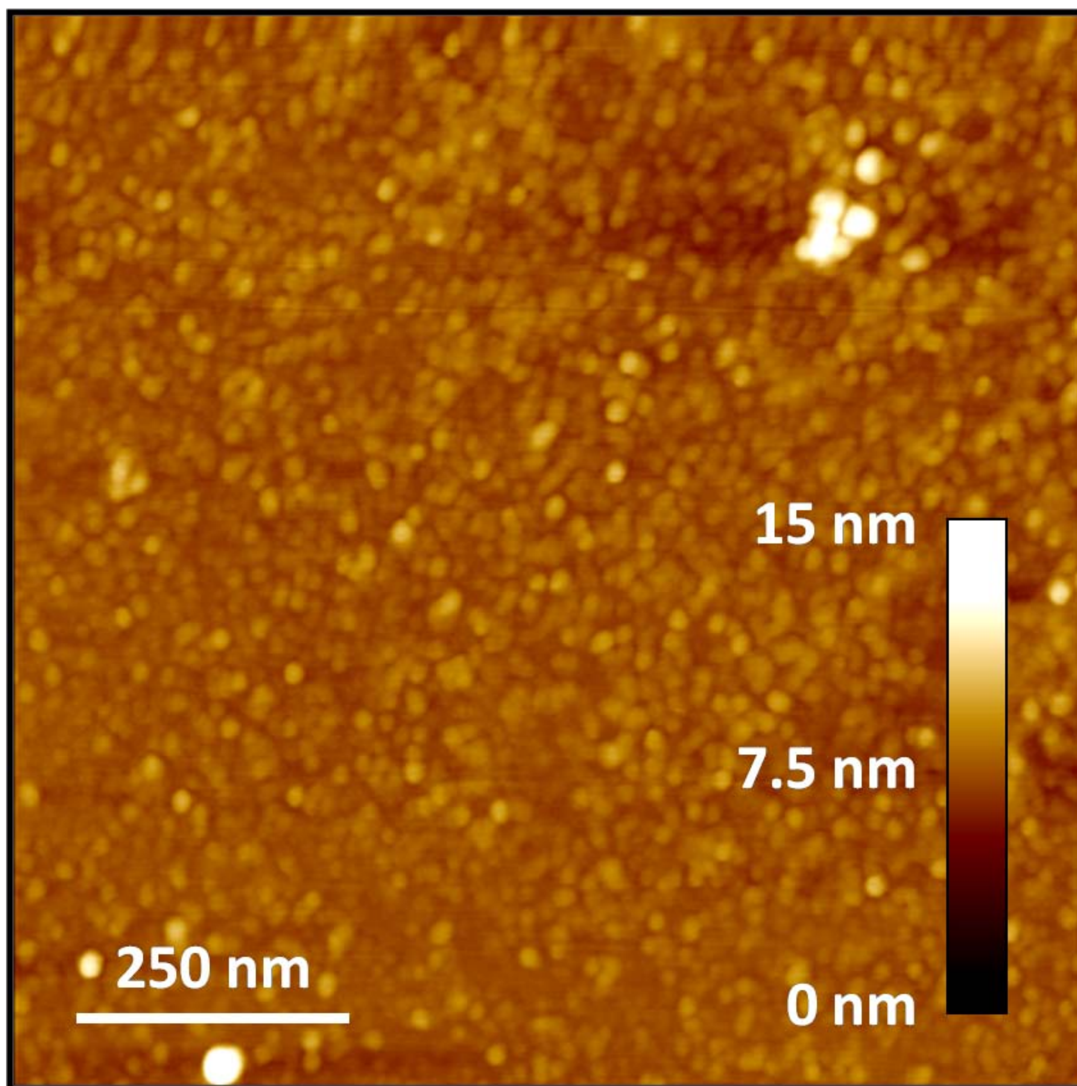

Figure A.5. AFM image of a zirconia thin film that was synthesized on a silicon wafer through 10 SILD cycles of alternating 0.01 M $ZrO(NO_3)_2$ and 0.04 M KOH solutions in 100% DI water according to the SILD procedure described in Section 2.2. The residence time in which each SILD solution was in contact with the surface was approximately 60 seconds.

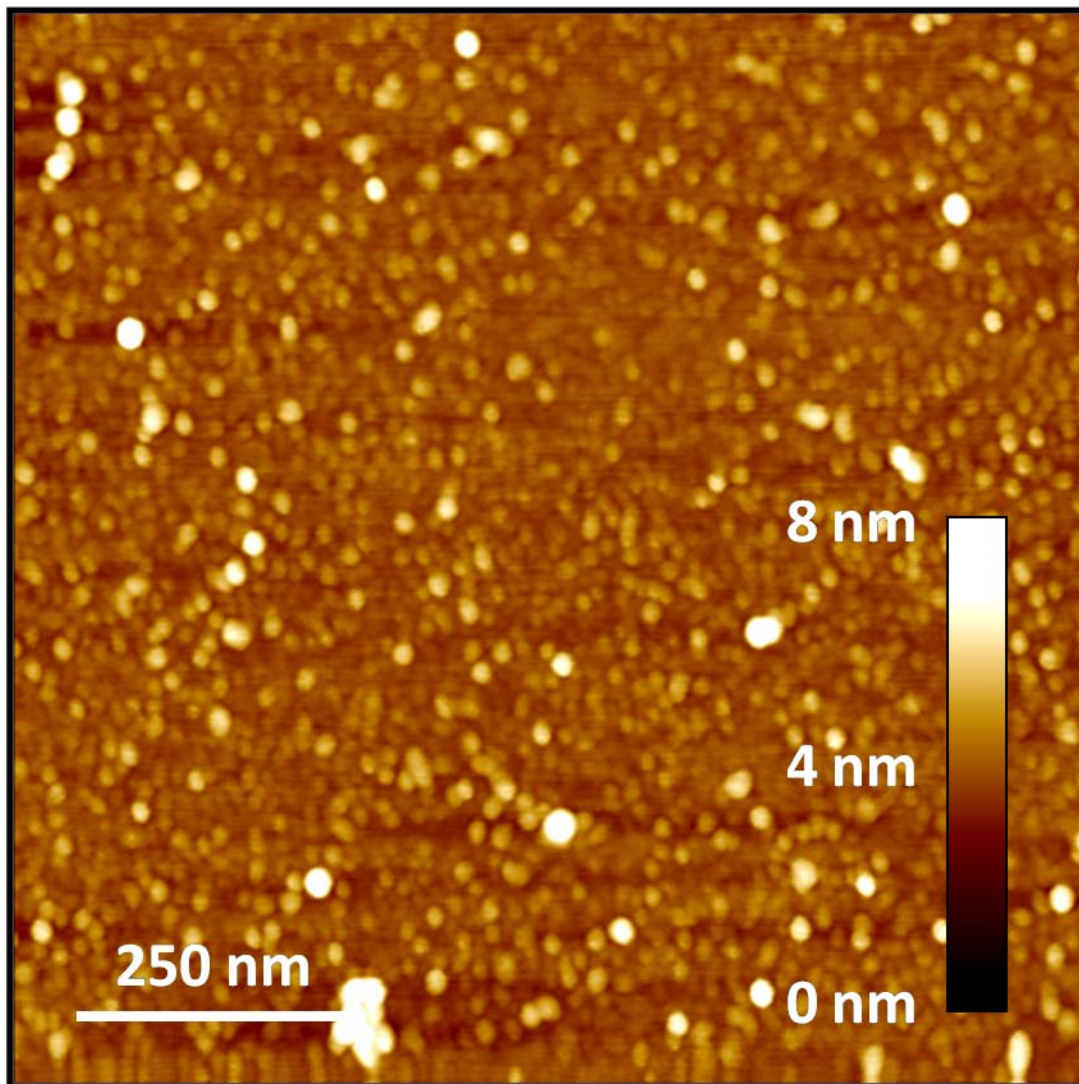

Figure A.6. AFM image of a zirconia thin film that was synthesized on a silicon wafer through 50 SILD cycles of alternating 0.01 M $ZrO(NO_3)_2$ and 0.04 M KOH solutions in 100% DI water according to the SILD procedure described in Section 2.2. The residence time in which each SILD solution was in contact with the surface was approximately 60 seconds.

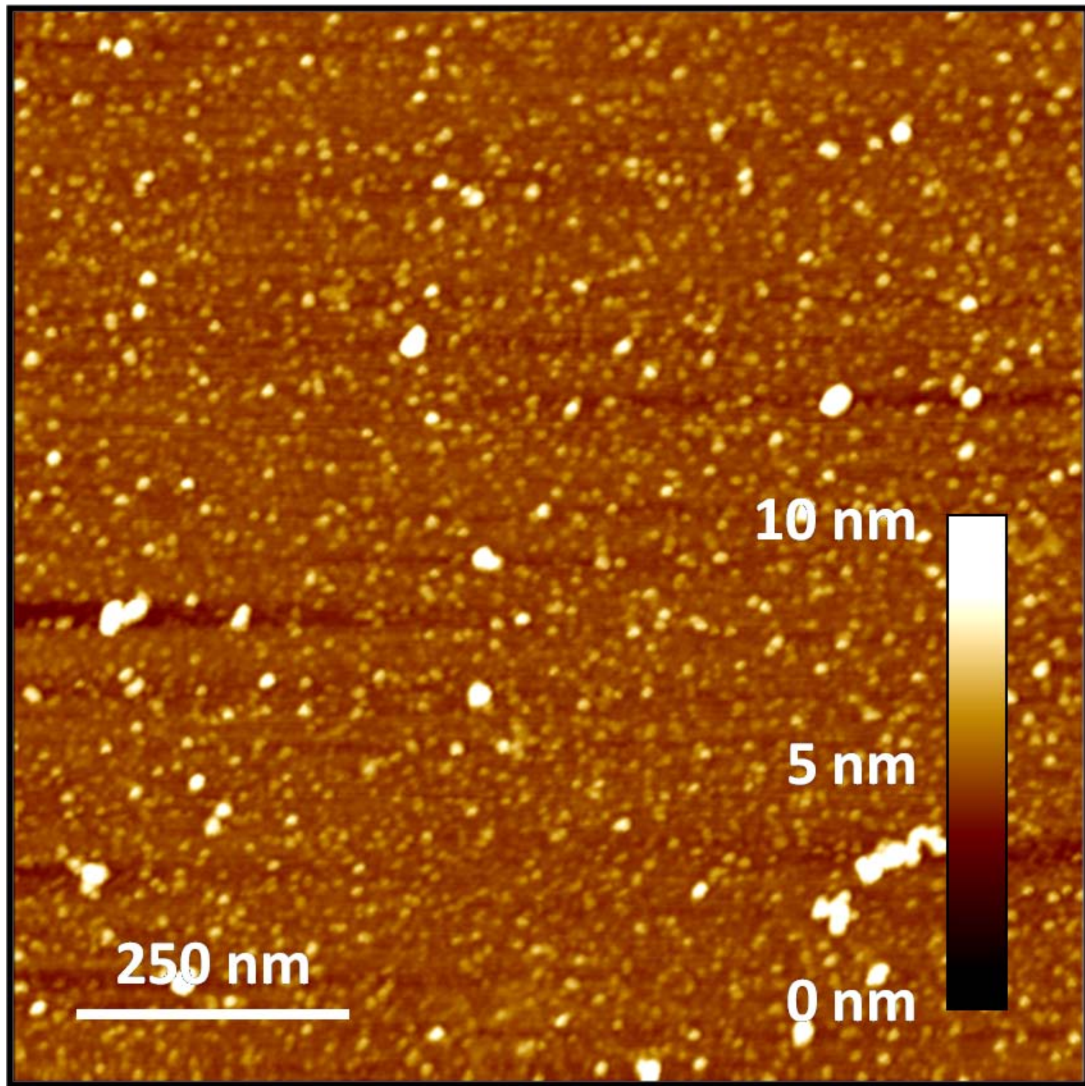

Figure A.7. AFM image of a zirconia thin film that was synthesized on a silicon wafer through 5 SILD cycles of alternating 0.01 M $ZrO(NO_3)_2$ and 0.04 M KOH solutions in 25% ethanol & 75% DI water according to the SILD procedure described in Section 2.2. The residence time in which each SILD solution was in contact with the surface was approximately 30 seconds.

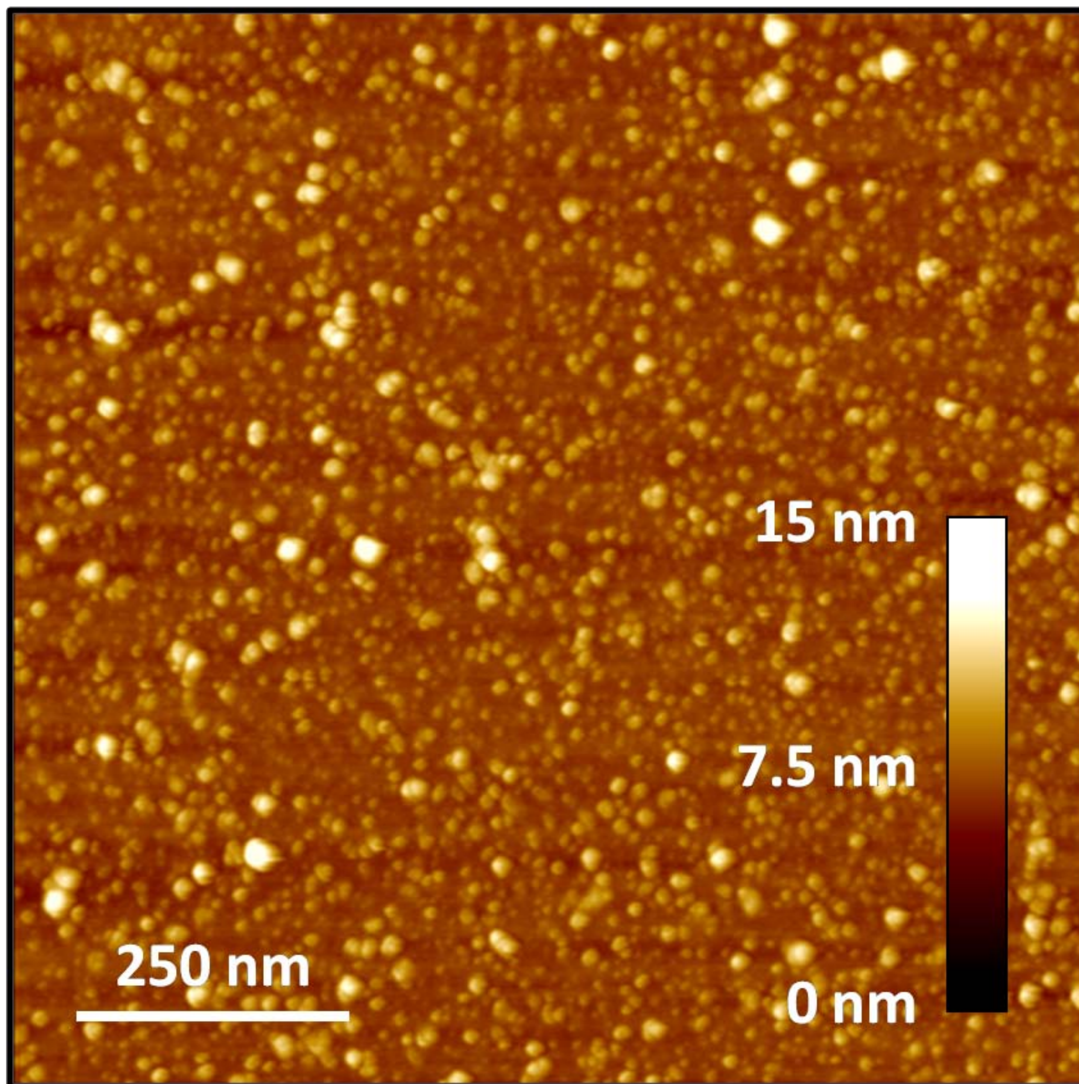

Figure A.8. AFM image of a zirconia thin film that was synthesized on a silicon wafer through 5 SILD cycles of alternating 0.01 M $ZrO(NO_3)_2$ and 0.04 M KOH solutions in 25% ethanol & 75% DI water according to the SILD procedure described in Section 2.2. The residence time in which each SILD solution was in contact with the surface was approximately 60 seconds.

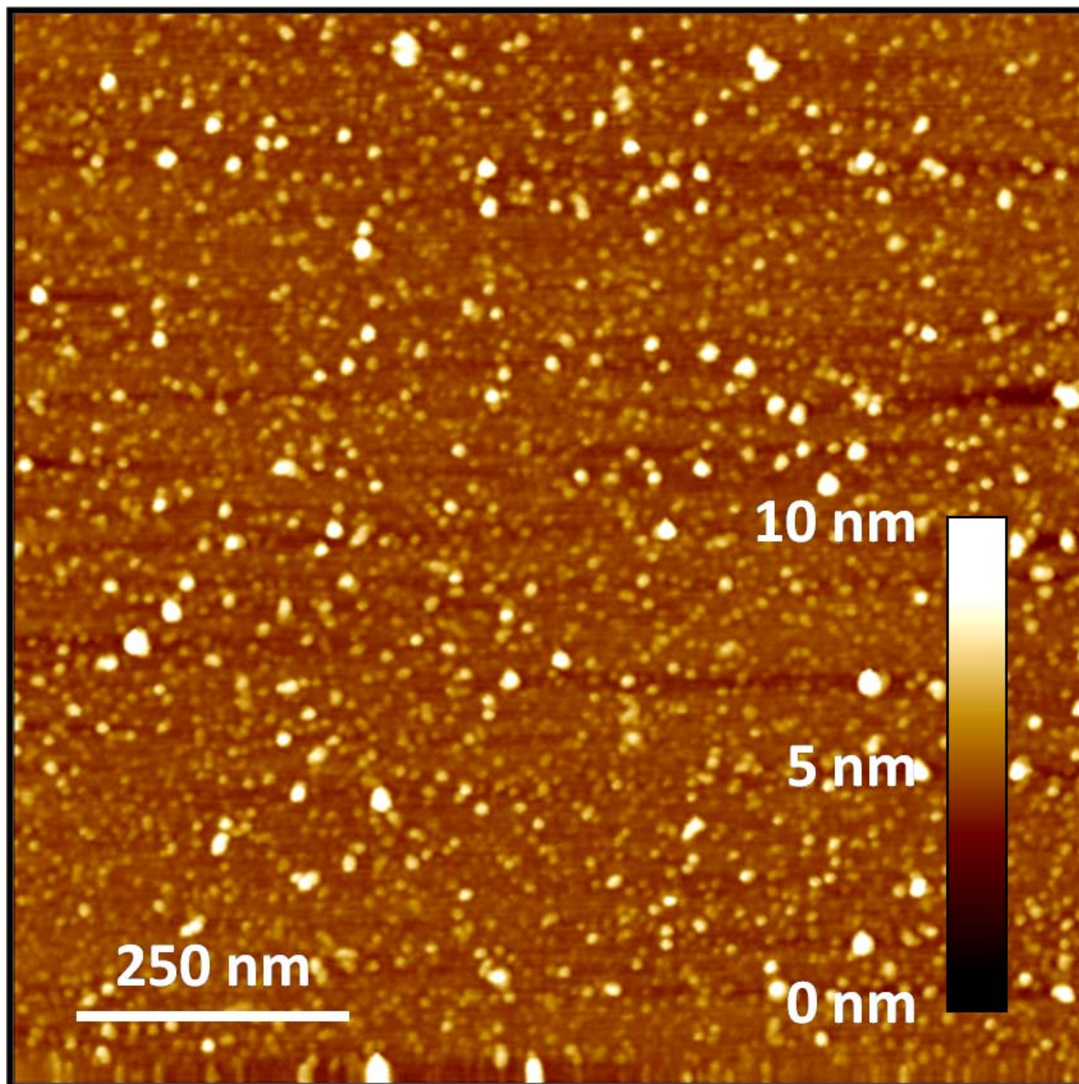

Figure A.9. AFM image of a zirconia thin film that was synthesized on a silicon wafer through 5 SILD cycles of alternating 0.01 M $ZrO(NO_3)_2$ and 0.04 M KOH solutions in 25% ethanol & 75% DI water according to the SILD procedure described in Section 2.2. The residence time in which each SILD solution was in contact with the surface was approximately 90 seconds.

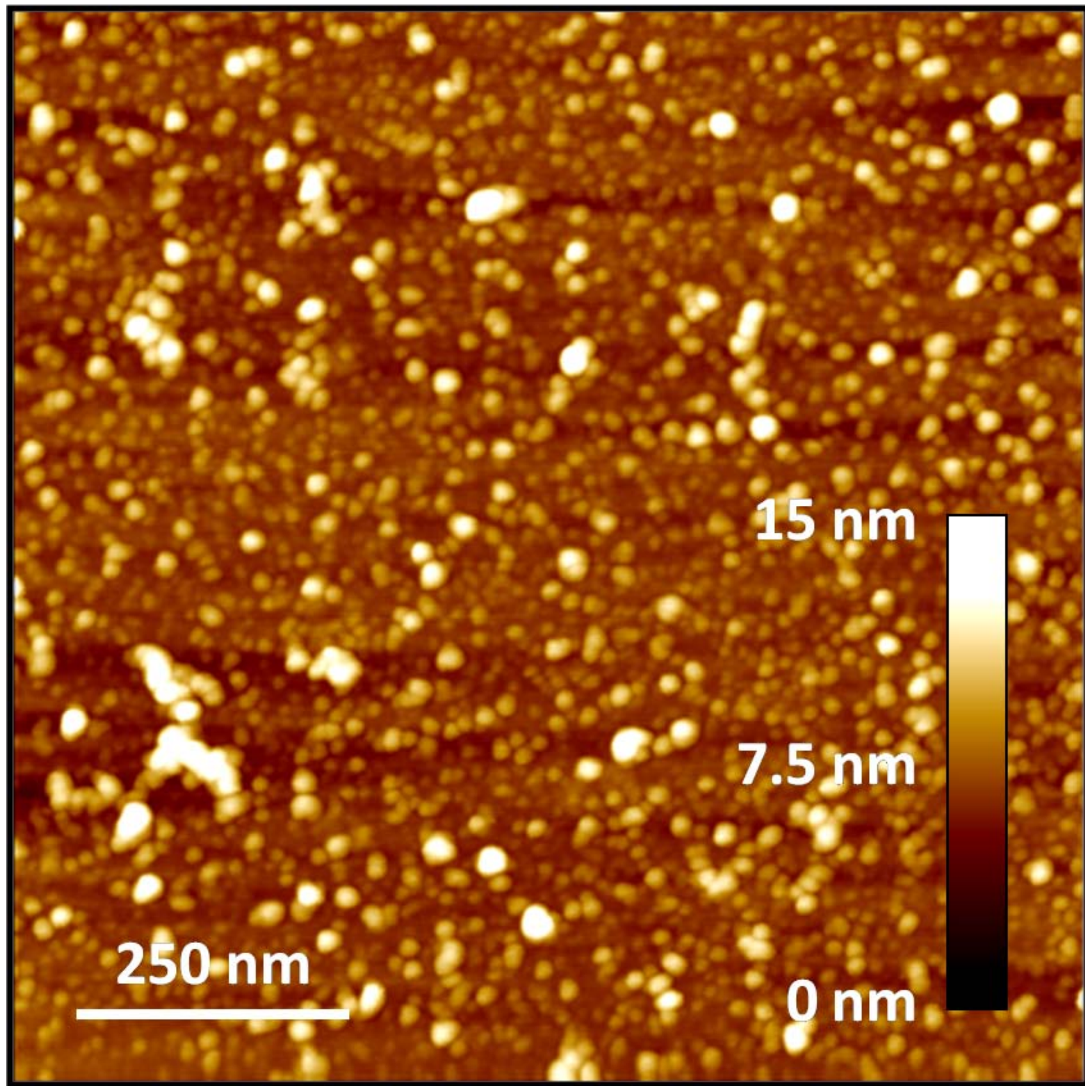

Figure A.10. AFM image of a zirconia thin film that was synthesized on a silicon wafer through 10 SILD cycles of alternating 0.01 M $ZrO(NO_3)_2$ and 0.04 M KOH solutions in 25% ethanol & 75% DI water according to the SILD procedure described in Section 2.2. The residence time in which each SILD solution was in contact with the surface was approximately 30 seconds.

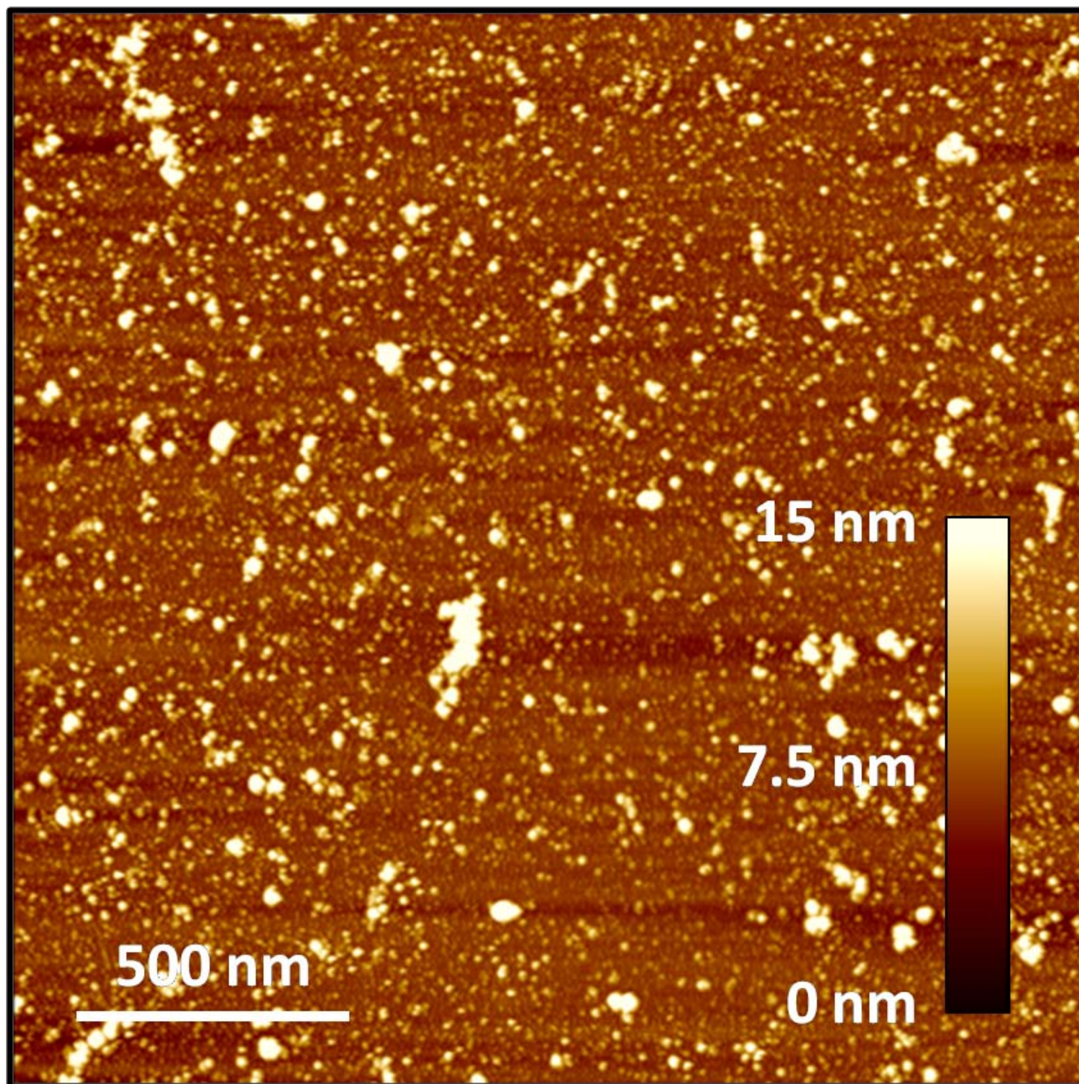

Figure A.11. AFM image of a zirconia thin film that was synthesized on a silicon wafer through 10 SILD cycles of alternating 0.01 M $ZrO(NO_3)_2$ and 0.04 M KOH solutions in 25% ethanol & 75% DI water according to the SILD procedure described in Section 2.2. The residence time in which each SILD solution was in contact with the surface was approximately 60 seconds.

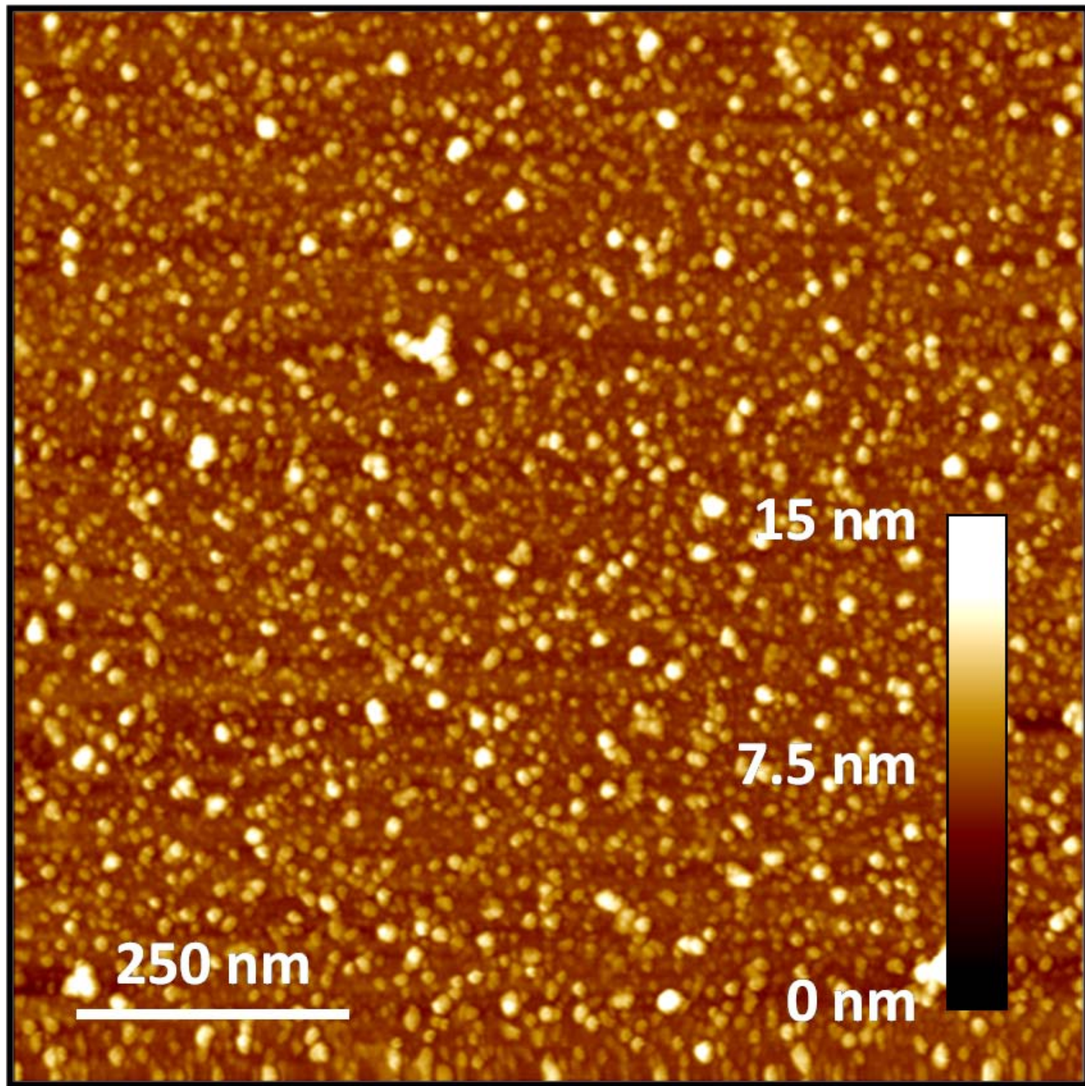

Figure A.12. AFM image of a zirconia thin film that was synthesized on a silicon wafer through 10 SILD cycles of alternating 0.01 M $ZrO(NO_3)_2$ and 0.04 M KOH solutions in 25% ethanol & 75% DI water according to the SILD procedure described in Section 2.2. The residence time in which each SILD solution was in contact with the surface was approximately 90 seconds.

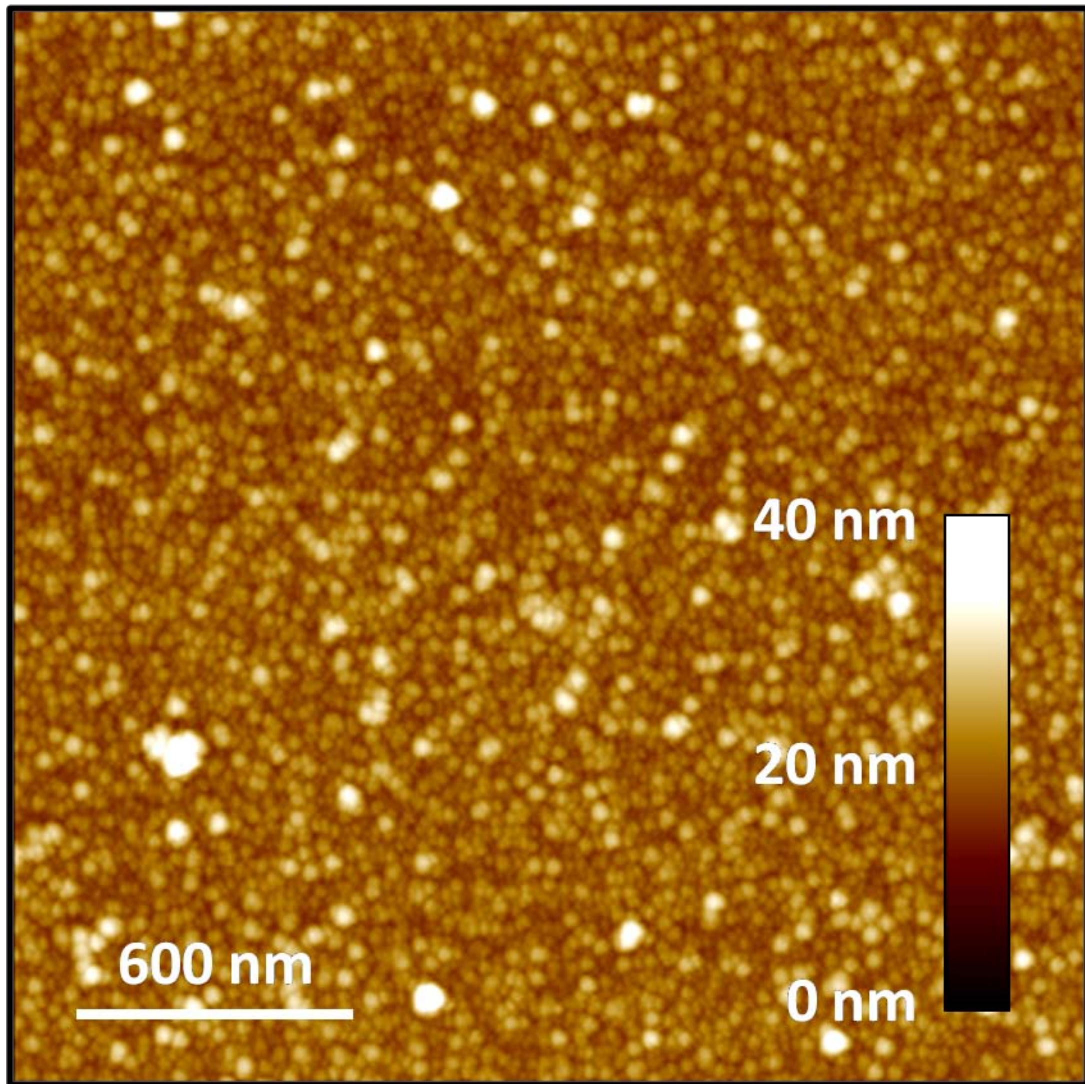

Figure A.13. AFM image of a zirconia thin film that was synthesized on a silicon wafer through 45 SILD cycles of alternating 0.01 M $ZrO(NO_3)_2$ and 0.04 M KOH solutions in 25% ethanol & 75% DI water according to the SILD procedure described in Section 2.2. The residence time in which each SILD solution was in contact with the surface was approximately 30 seconds.

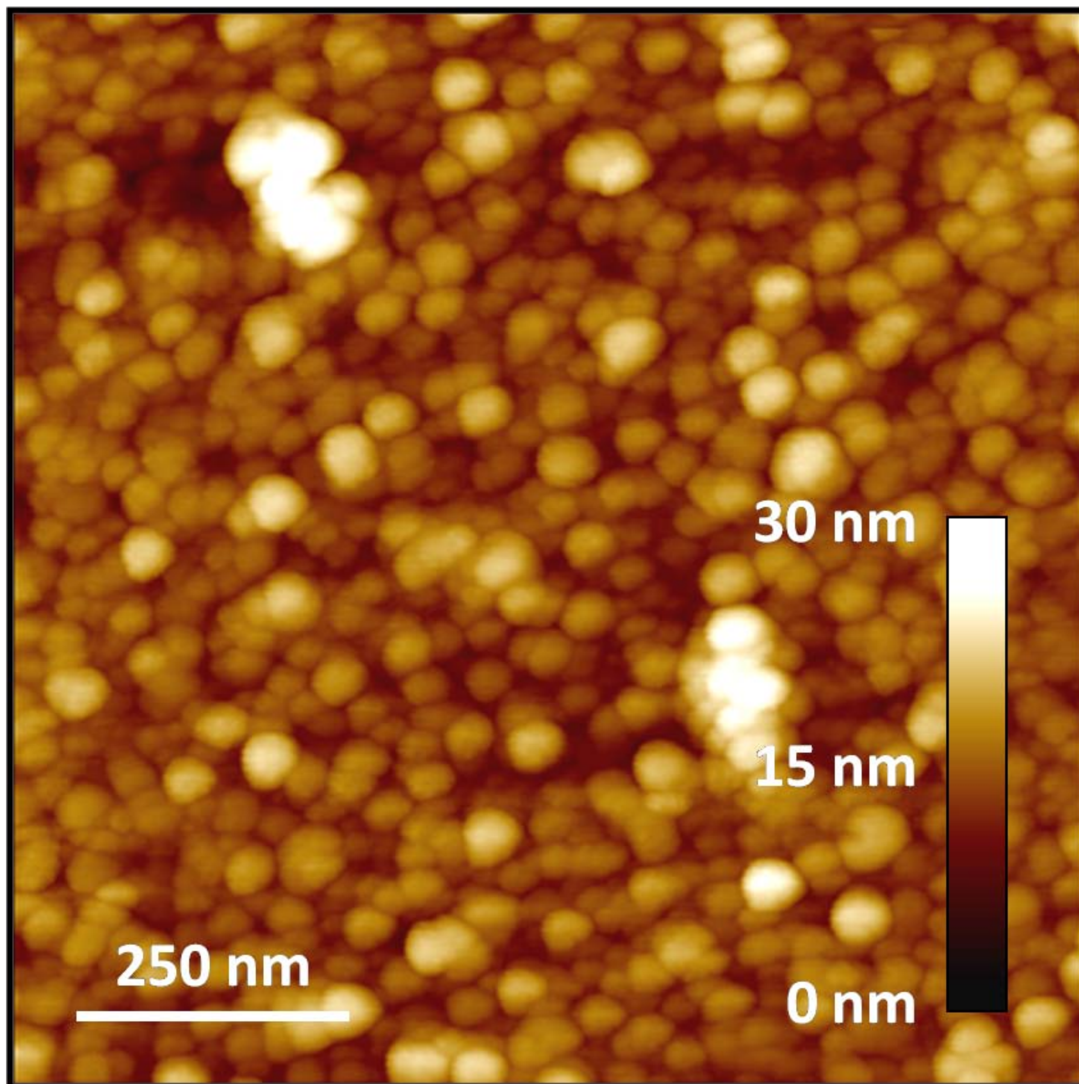

Figure A.14. AFM image of a zirconia thin film that was synthesized on a silicon wafer through 50 SILD cycles of alternating 0.01 M $ZrO(NO_3)_2$ and 0.04 M KOH solutions in 25% ethanol & 75% DI water according to the SILD procedure described in Section 2.2. The residence time in which each SILD solution was in contact with the surface was approximately 30 seconds.

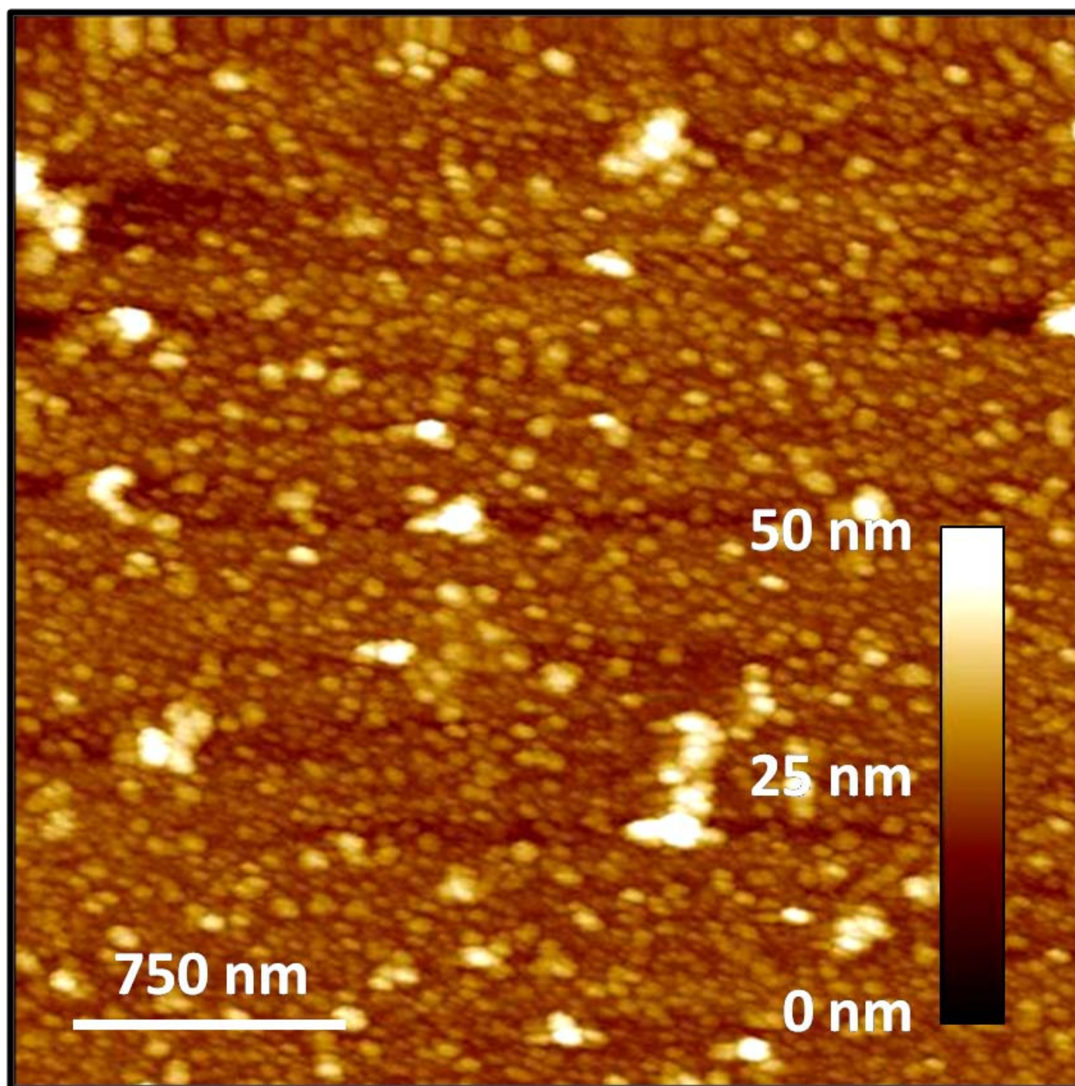

Figure A.15. AFM image of a zirconia thin film that was synthesized on a silicon wafer through 50 SILD cycles of alternating 0.01 M $ZrO(NO_3)_2$ and 0.04 M KOH solutions in 25% ethanol & 75% DI water according to the SILD procedure described in Section 2.2. The residence time in which each SILD solution was in contact with the surface was approximately 30 seconds. This is a repeat synthesis of the sample in Figure A.14.

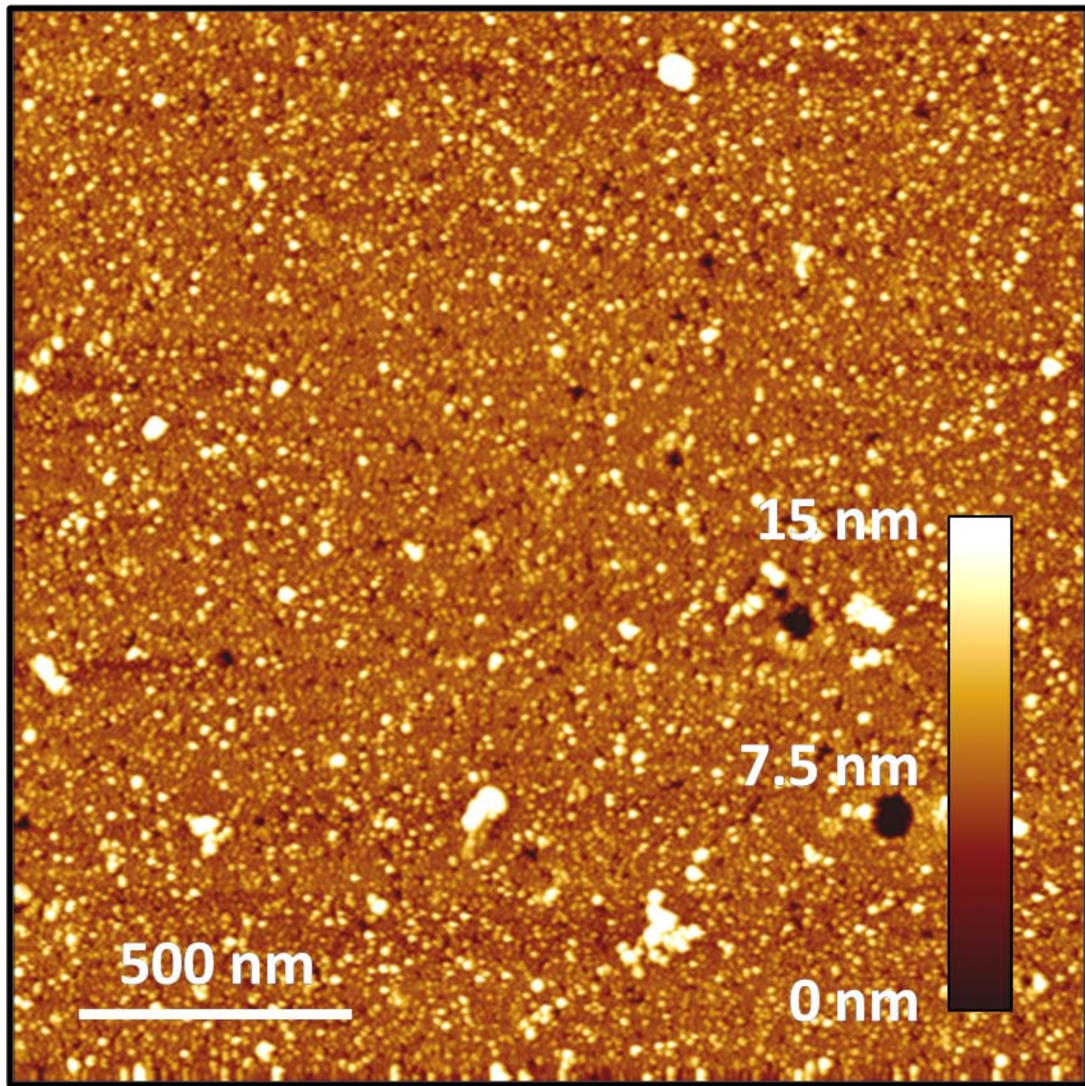

Figure A.16. AFM image of a zirconia thin film that was synthesized on a silicon wafer through 50 SILD cycles of alternating 0.01 M $ZrO(NO_3)_2$ and 0.04 M KOH solutions in 25% ethanol & 75% DI water according to the SILD procedure described in Section 2.2. The residence time in which each SILD solution was in contact with the surface was approximately 60 seconds.

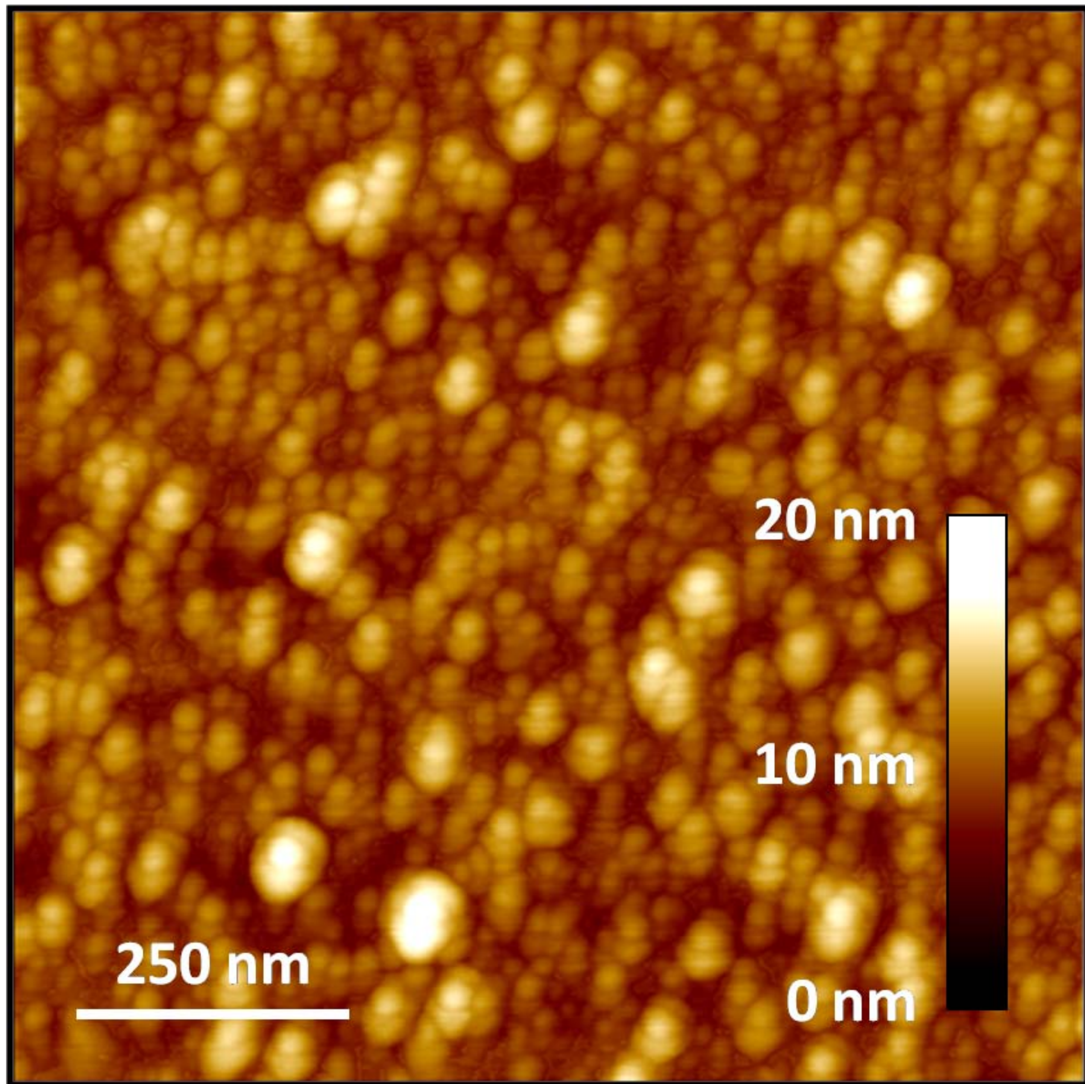

Figure A.17. AFM image of a zirconia thin film that was synthesized on a silicon wafer through 50 SILD cycles of alternating 0.01 M $ZrO(NO_3)_2$ and 0.04 M KOH solutions in 25% ethanol & 75% DI water according to the SILD procedure described in Section 2.2. The residence time in which each SILD solution was in contact with the surface was approximately 90 seconds.

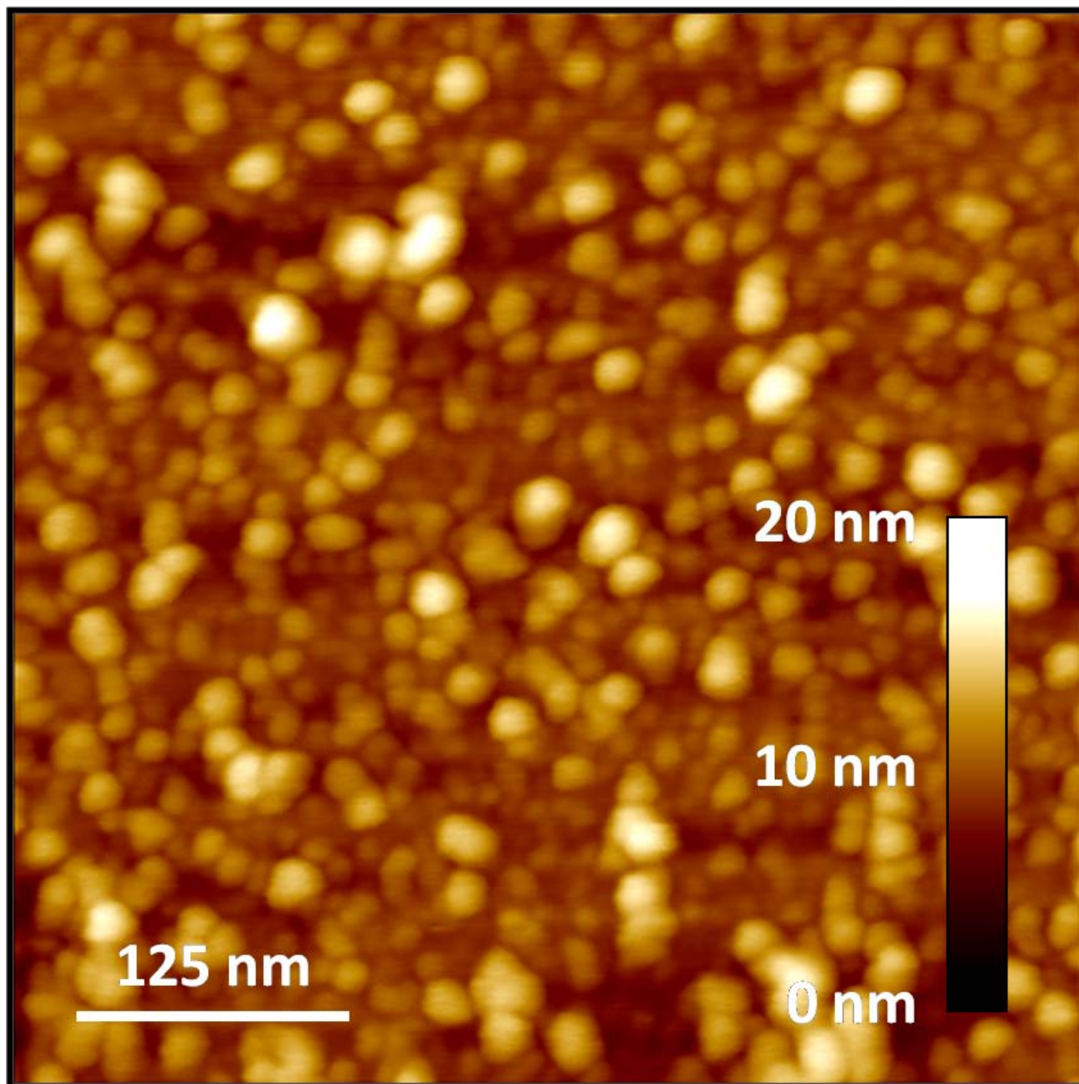

Figure A.18. AFM image of a zirconia thin film that was synthesized on a silicon wafer through 100 SILD cycles of alternating 0.01 M $ZrO(NO_3)_2$ and 0.04 M KOH solutions in 25% ethanol & 75% DI water according to the SILD procedure described in Section 2.2. The residence time in which each SILD solution was in contact with the surface was approximately 5 seconds.

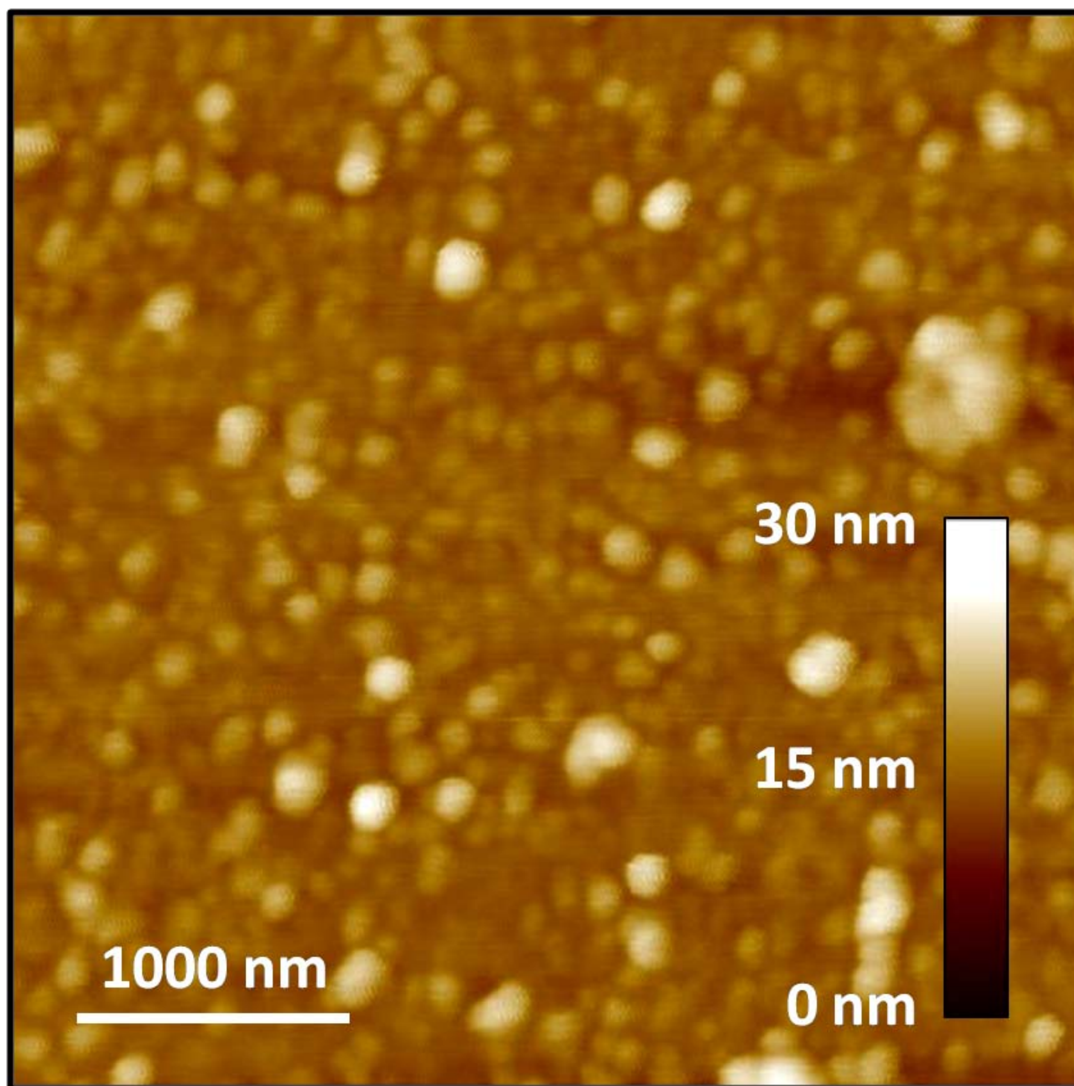

Figure A.19. AFM image of a zirconia thin film that was synthesized on a silicon wafer through 150 SILD cycles of alternating 0.01 M $ZrO(NO_3)_2$ and 0.04 M KOH solutions in 25% ethanol & 75% DI water according to the SILD procedure described in Section 2.2. The residence time in which each SILD solution was in contact with the surface was approximately 5 seconds.

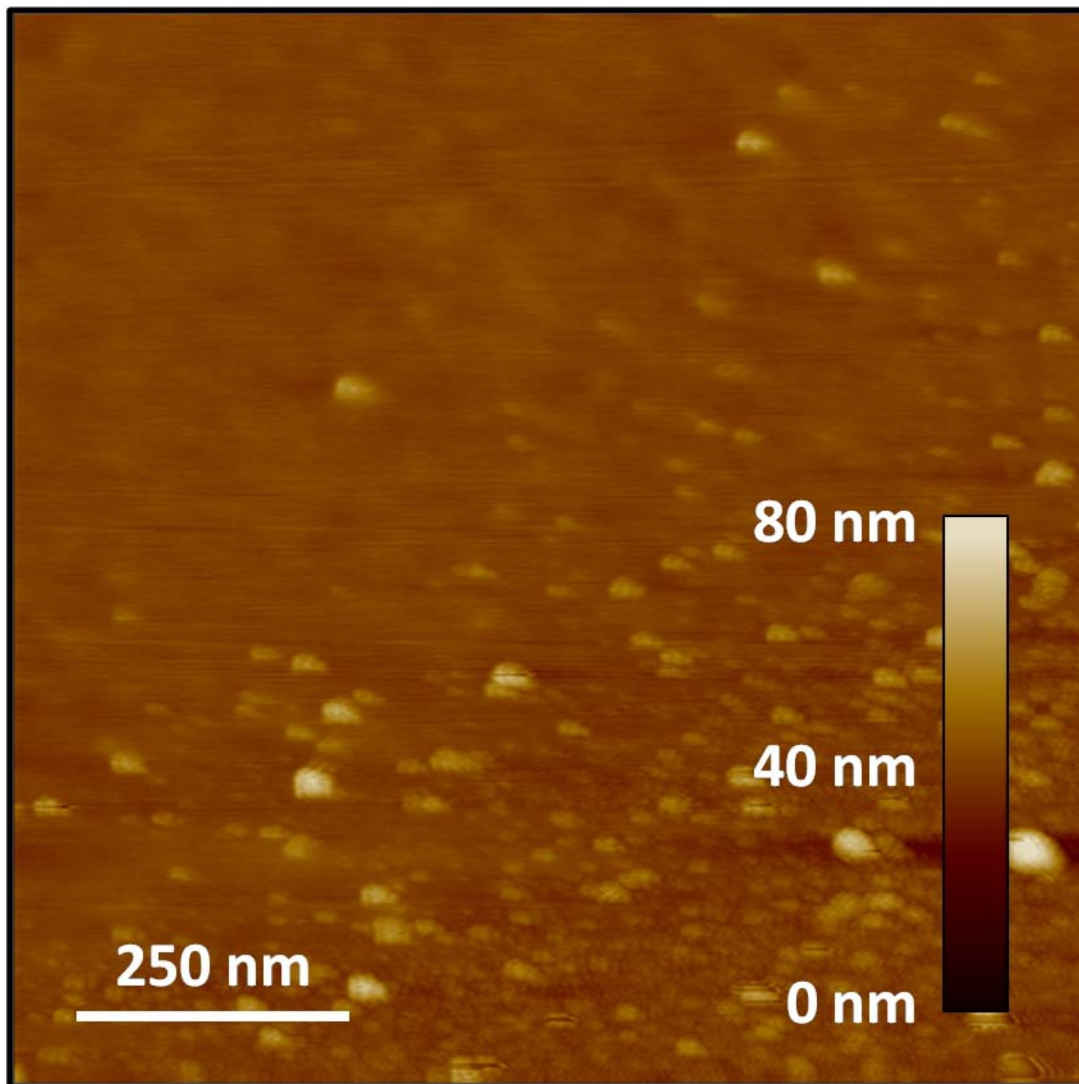

Figure A.20. AFM image of a zirconia thin film that was synthesized on a silicon wafer through 10 SILD cycles of alternating 0.04 M $ZrO(NO_3)_2$ and 0.01 M KOH solutions in 100% DI water according to the SILD procedure described in Section 2.2. The residence time in which each SILD solution was in contact with the surface was approximately 60 seconds.

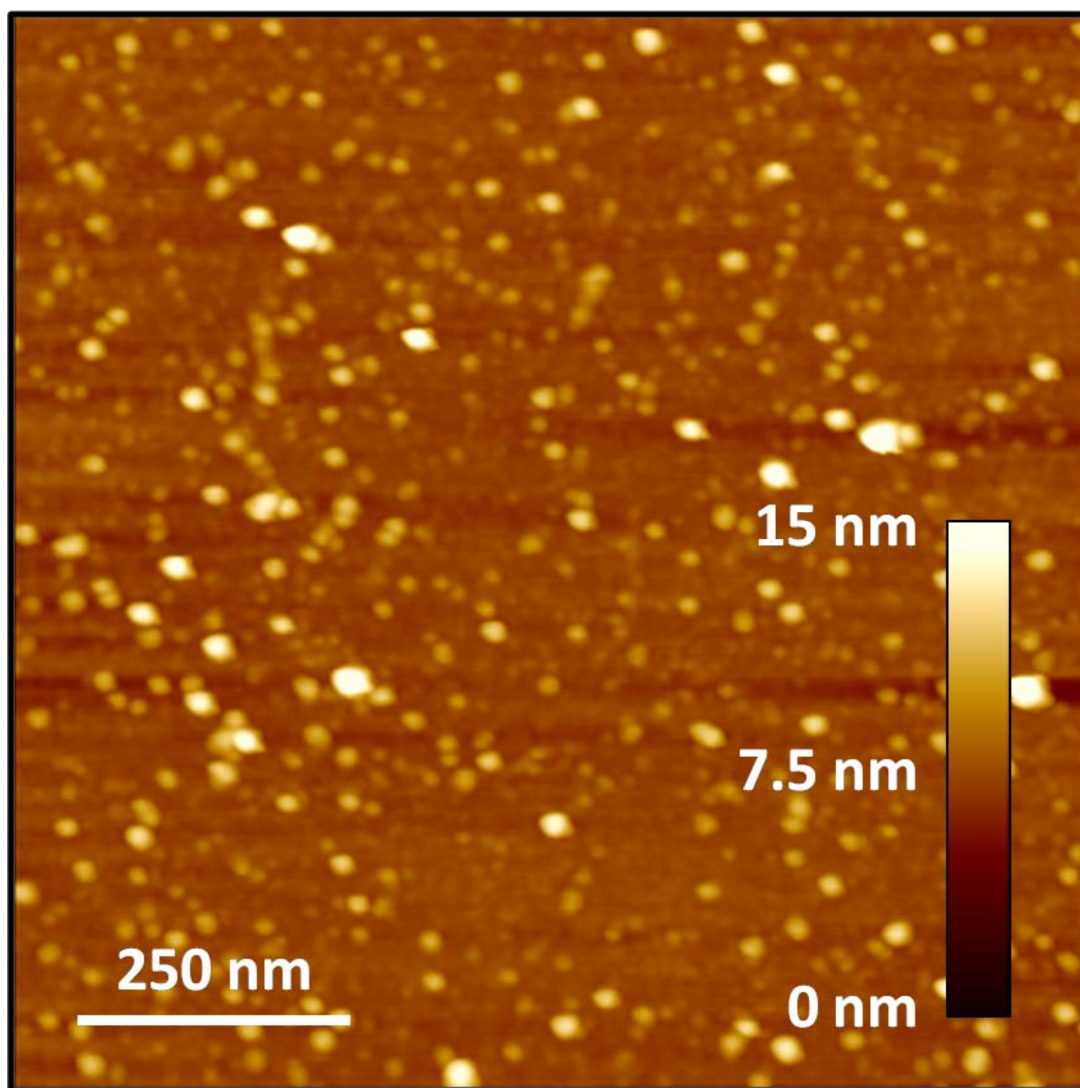

Figure A.21. AFM image of a zirconia thin film that was synthesized on a silicon wafer through 50 SILD cycles of alternating 0.04 M $ZrO(NO_3)_2$ and 0.01 M KOH solutions in 100% DI water according to the SILD procedure described in Section 2.2. The residence time in which each SILD solution was in contact with the surface was approximately 60 seconds.

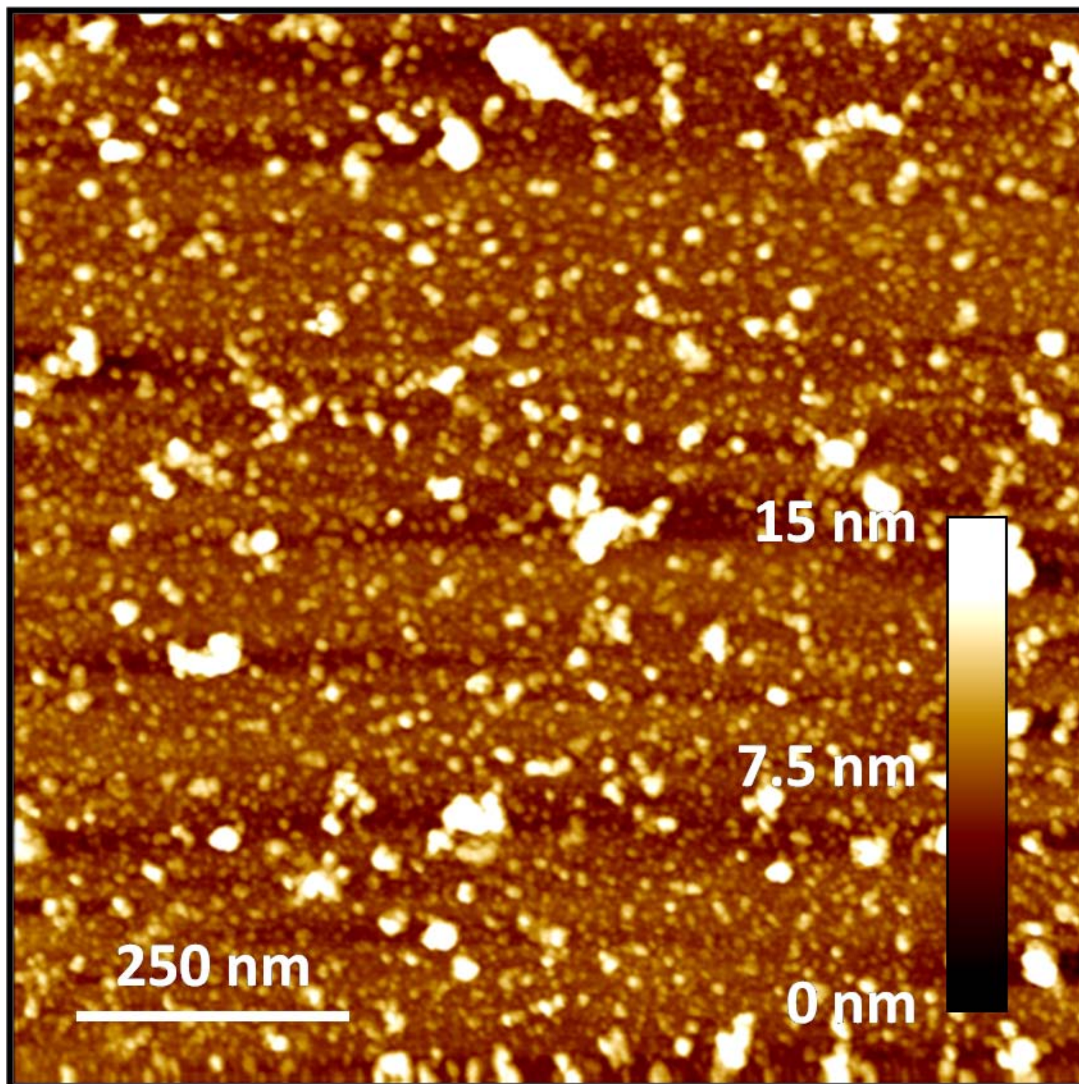

Figure A.22. AFM image of a zirconia thin film that was synthesized on a silicon wafer through 10 SILD cycles of alternating 0.04 M $ZrO(NO_3)_2$ and 0.01 M KOH solutions in 25% ethanol & 75% DI water according to the SILD procedure described in Section 2.2. The residence time in which each SILD solution was in contact with the surface was approximately 60 seconds.

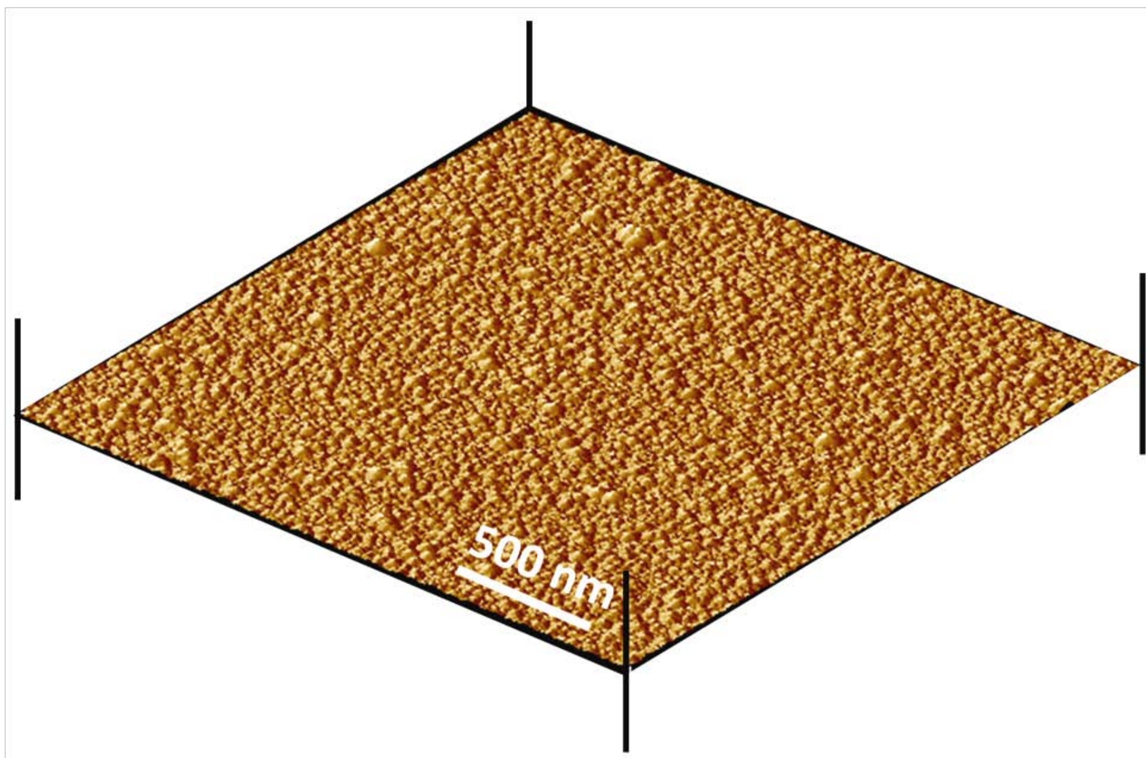

Figure A.23. Three-dimensional AFM representation of a zirconia thin film synthesized on a silicon wafer through 45 SILD cycles of alternating 0.01 M $ZrO(NO_3)_2$ and 0.04 M KOH solutions in 25% ethanol & 75% DI water according to the SILD procedure described in Section 2.2. This image is from the same sample as Figure A.13.

APPENDIX B. Successive Ionic Layer Deposition of Alumina

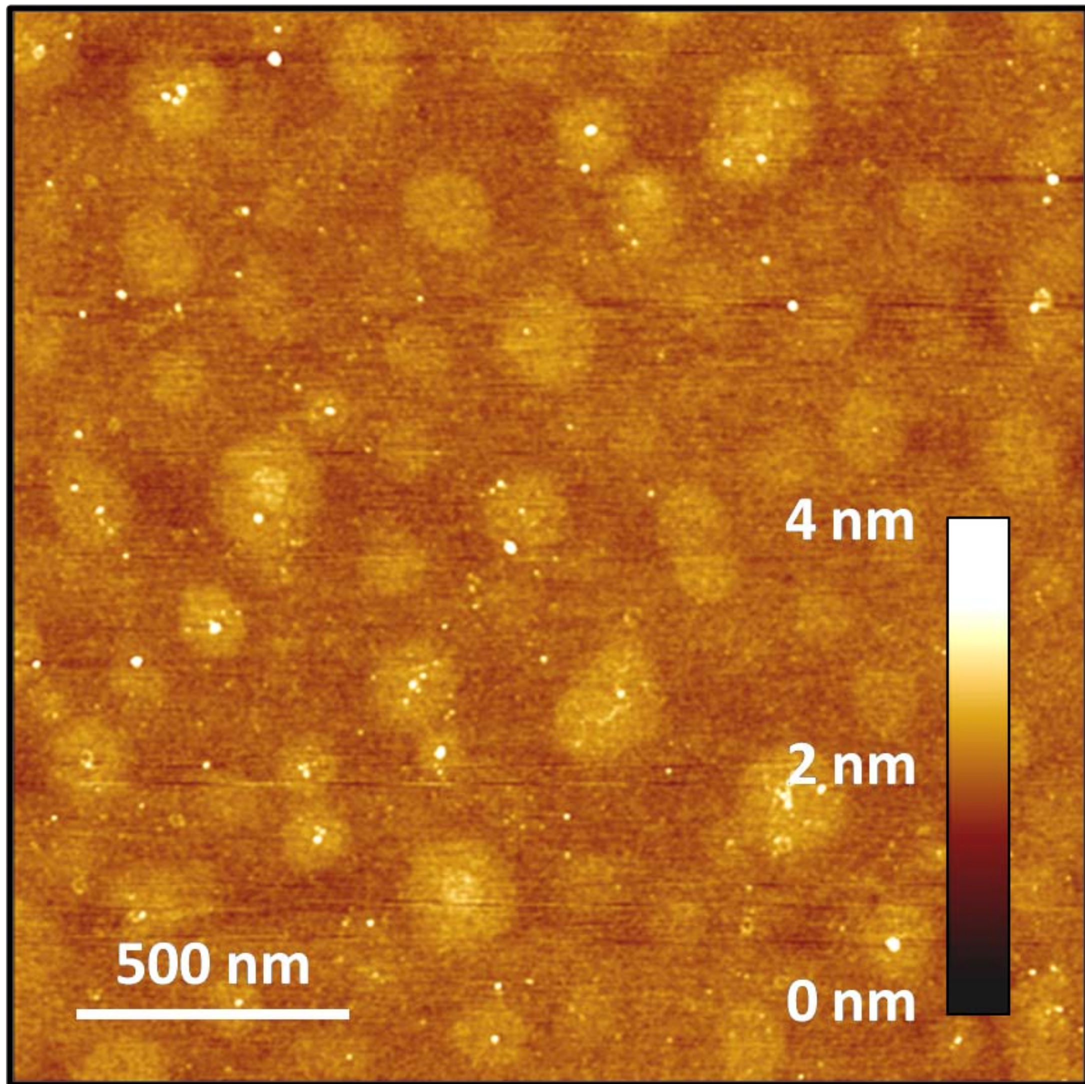

Figure B.1. AFM image of an alumina thin film that was synthesized on a silicon wafer through 45 SILD cycles of alternating 0.01 M $Al(NO_3)_3$ and 4.0 wt% NH_4OH solutions in 25% ethanol & 75% DI water according to the SILD procedure described in Sections 3.2 and 3.4. The residence time in which each SILD solution was in contact with the surface was approximately 90 seconds.

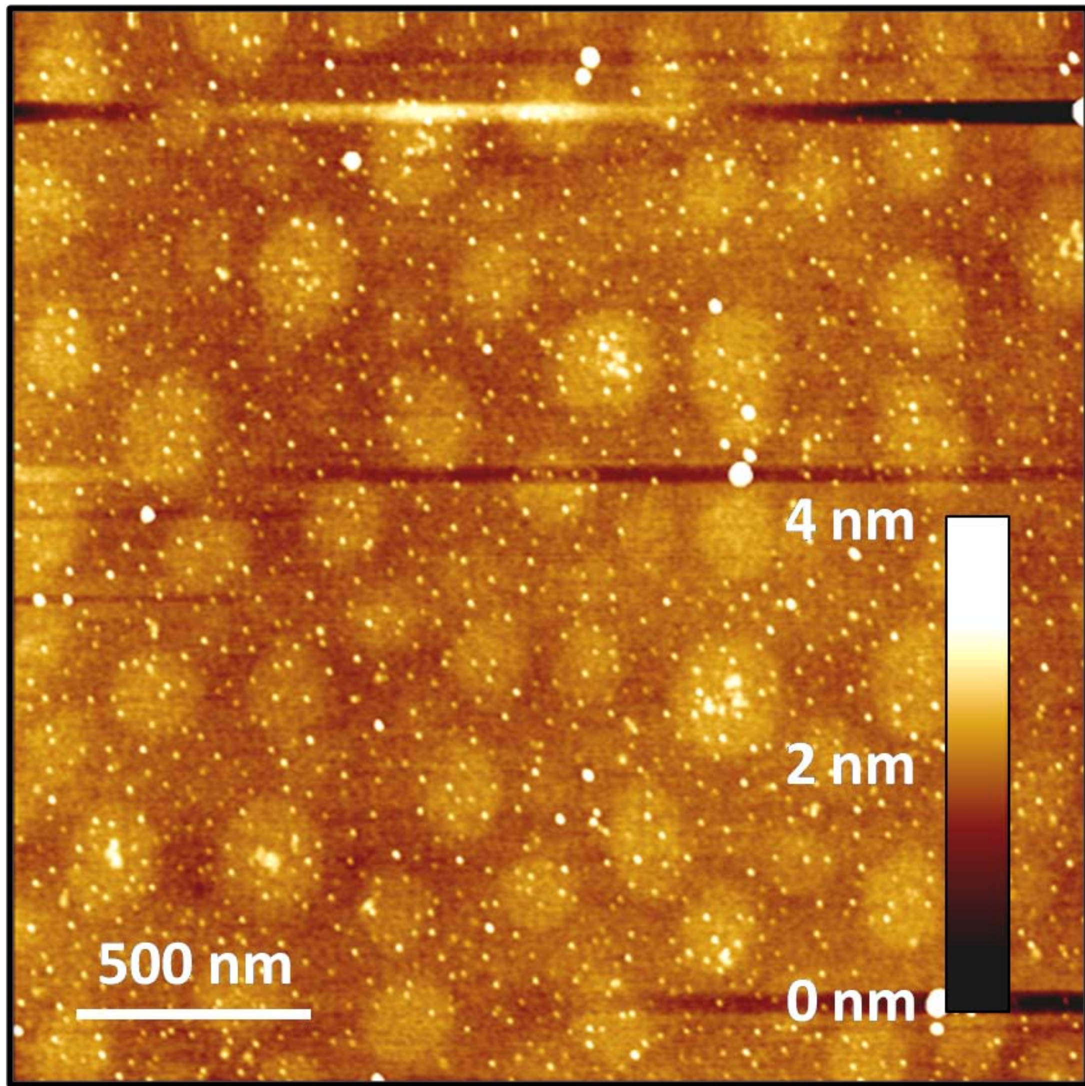

Figure B.2. AFM image of the underlying alumina thin film of Figure B.1 supported on a silicon wafer and dried at 450ºC for 2 hours that was followed by subsequent deposition of barium oxide through 5 SILD cycles of alternating 0.01 M $Ba(NO_3)_2$ and 4.5 wt% NH_4OH solutions in 25% ethanol & 75% DI water according to the SILD procedure described in Sections 3.2 and 3.4. The residence time in which each SILD solution was in contact with the surface was approximately 30 seconds.

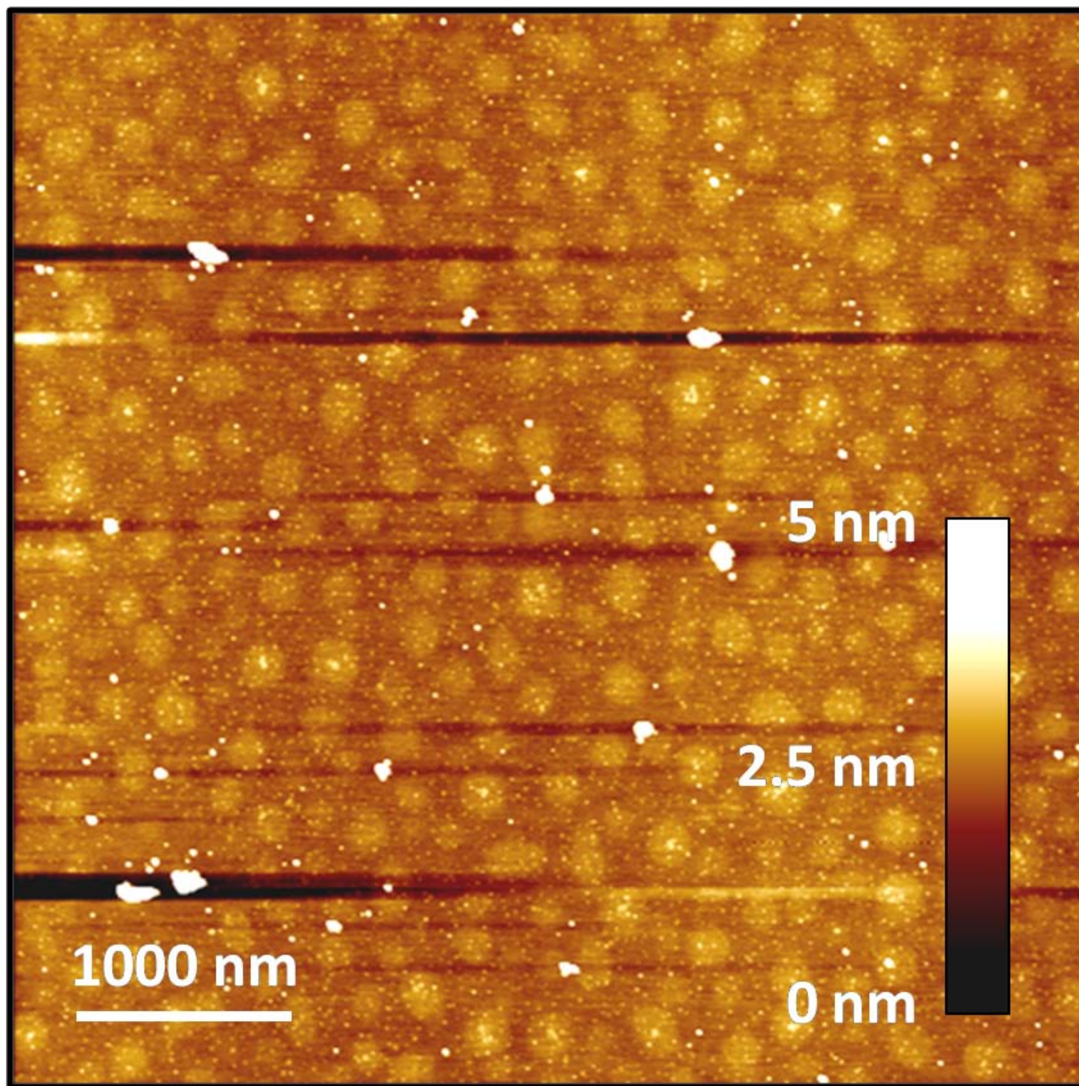

Figure B.3. Another AFM image of the sample prepared as described in the caption of Figure B.2 containing smaller barium oxide islands supported on larger alumina rafts all supported on a silicon wafer.

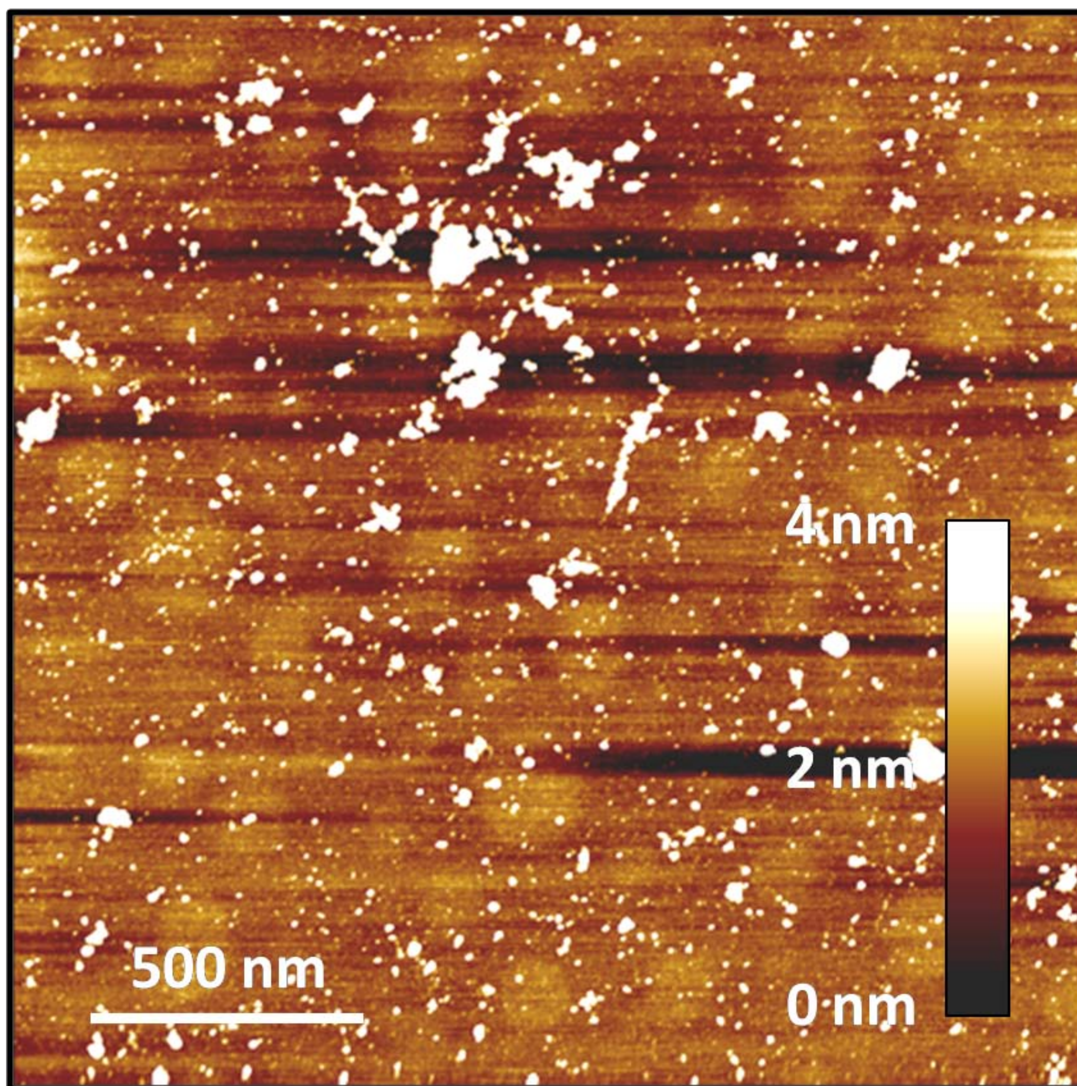

Figure B.4. AFM image of an alumina thin film that was synthesized on a silicon wafer through 75 SILD cycles of alternating 0.01 M $Al(NO_3)_3$ and 4.0 wt% NH_4OH solutions in 25% ethanol & 75% DI water according to the SILD procedure described in Sections 3.2 and 3.4. The residence time in which each SILD solution was in contact with the surface was approximately 90 seconds. Note that significant co-precipitation of SILD solutions evidently occurred during this synthesis due to the large particles identified by AFM.

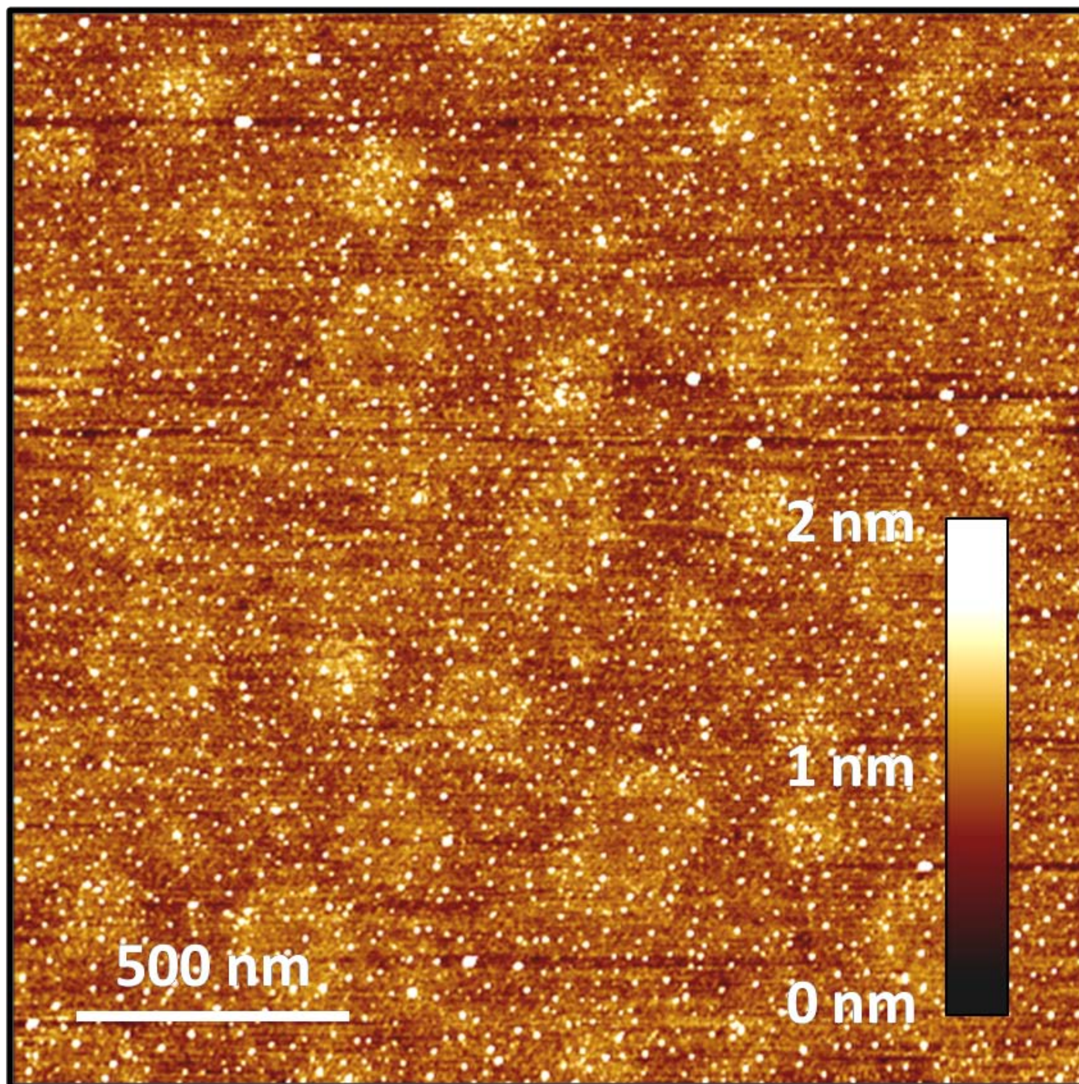

Figure B.5. AFM image of the underlying alumina thin film of Figure B.4 supported on a silicon wafer and dried at 450ºC for 2 hours that was followed by subsequent deposition of barium oxide through 5 SILD cycles of alternating 0.01 M $Ba(NO_3)_2$ and 4.5 wt% NH_4OH solutions in 25% ethanol & 75% DI water according to the SILD procedure described in Sections 3.2 and 3.4. The residence time in which each SILD solution was in contact with the surface was approximately 30 seconds. Following SILD of barium oxide this sample was rinsed with acetone and dried again at 450ºC for 0.5 hours.

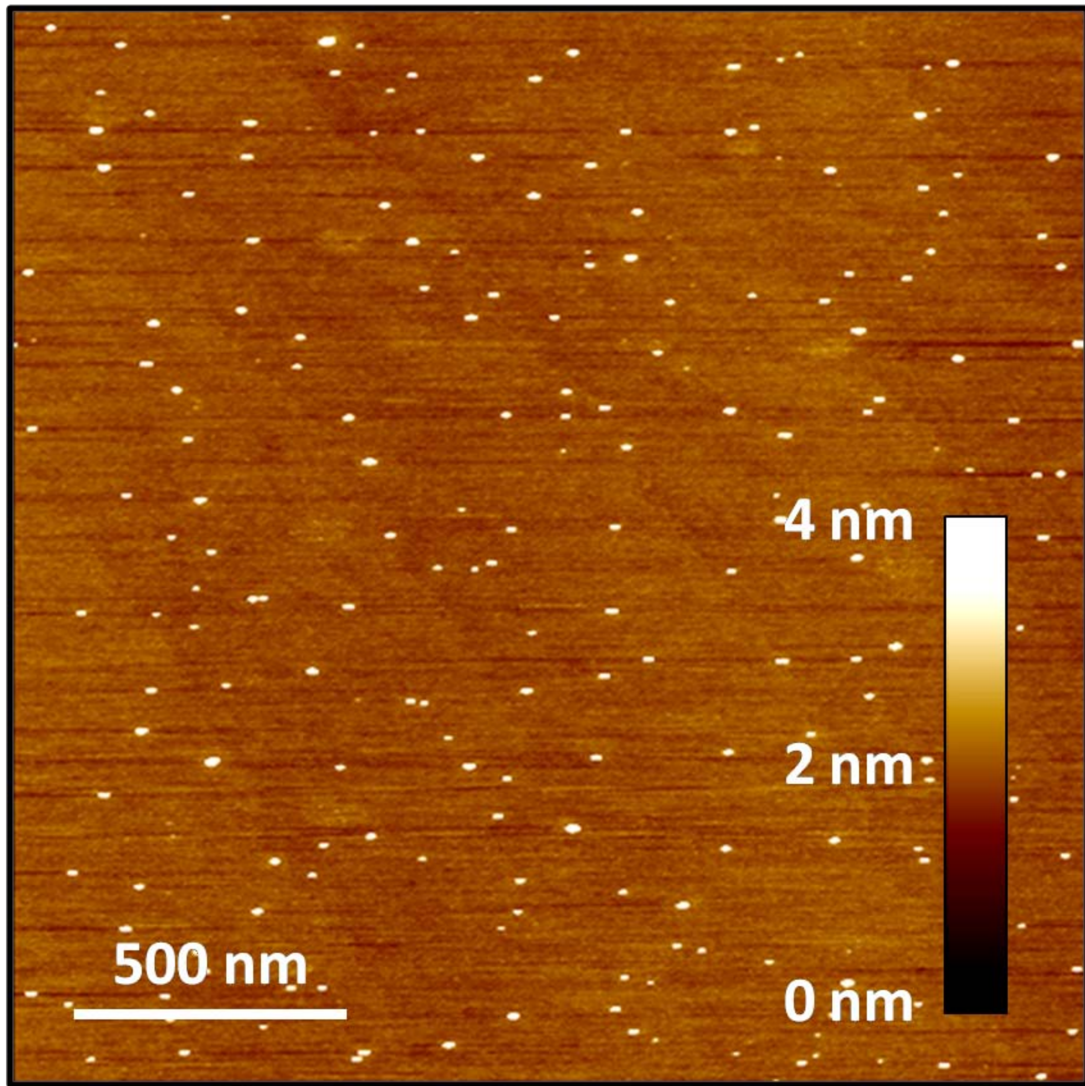

Figure B.6. AFM image of a barium oxide thin film that was synthesized on a silicon wafer through 5 SILD cycles of alternating 0.01 M $Ba(NO_3)_2$ and 4.5 wt% NH_4OH solutions in 25% ethanol & 75% DI water according to the SILD procedure described in Section 3.2. The residence time in which each SILD solution was in contact with the surface was approximately 30 seconds.

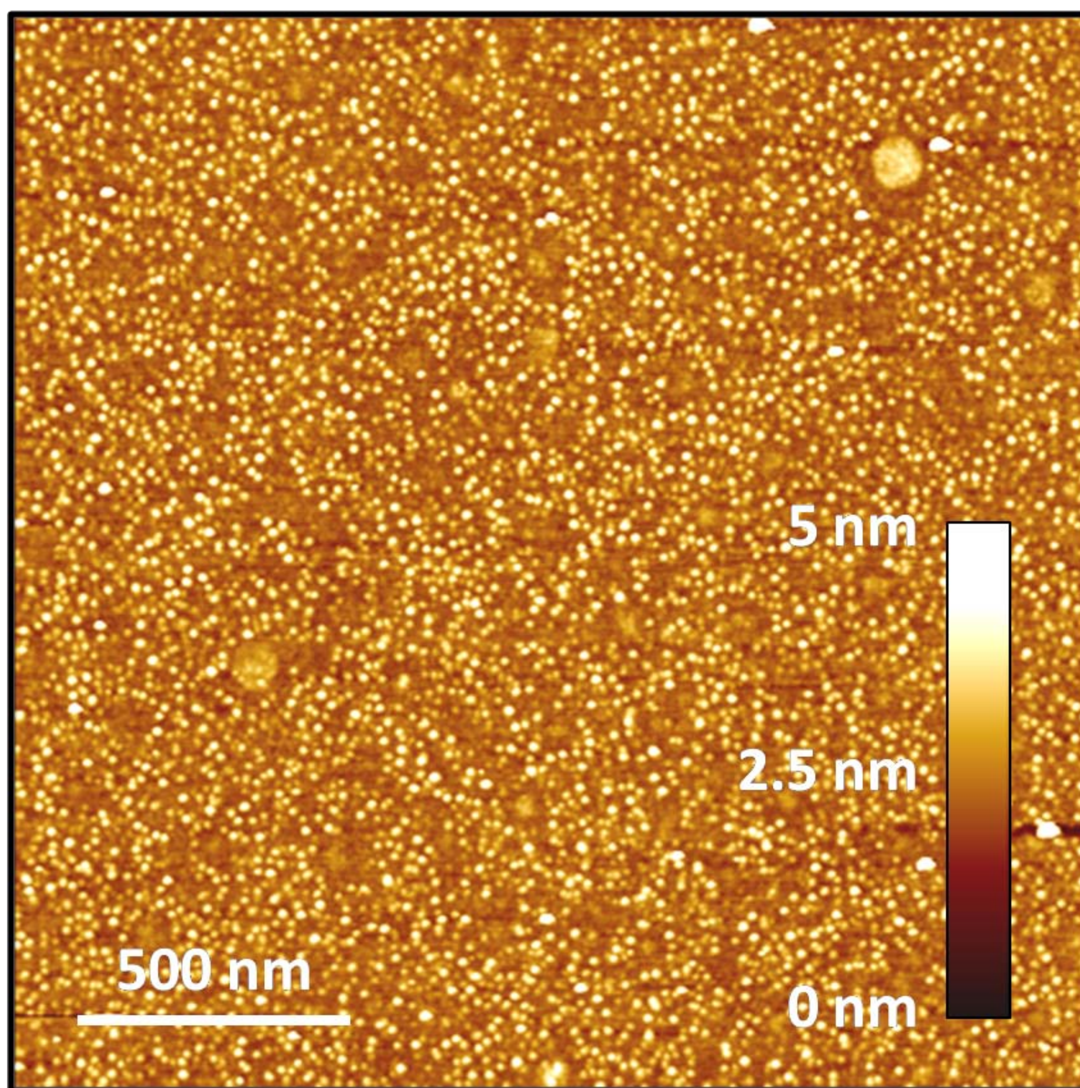

Figure B.7. AFM image of a multilayer alumina and barium oxide thin film that was synthesized on a silicon wafer as follows: (1) 30 SILD cycles of alternating 0.02 M $Al(NO_3)_3$ and 4.2 wt% NH_4OH solutions in 25% ethanol & 75% DI water according to the SILD procedure described in Sections 3.2 and 3.4 with a residence time of approximately 90 seconds. (2) the alumina layer supported on a silicon wafer was dried at 450ºC for 0.5 hours. (3) subsequent deposition of barium oxide through 16 SILD cycles of alternating 0.01 M $Ba(NO_3)_2$ and 0.04 M KOH solutions in 25% ethanol & 75% DI water according to the SILD procedure described in Sections 3.2 and 3.4 with a residence time of approximately 30 seconds. (4) the barium oxide and alumina layers were dried at 450ºC for 0.5 hours. (5) subsequent rinsing with acetone and DI water prior to acquiring this AFM image, may have helped clean the surface of this image.

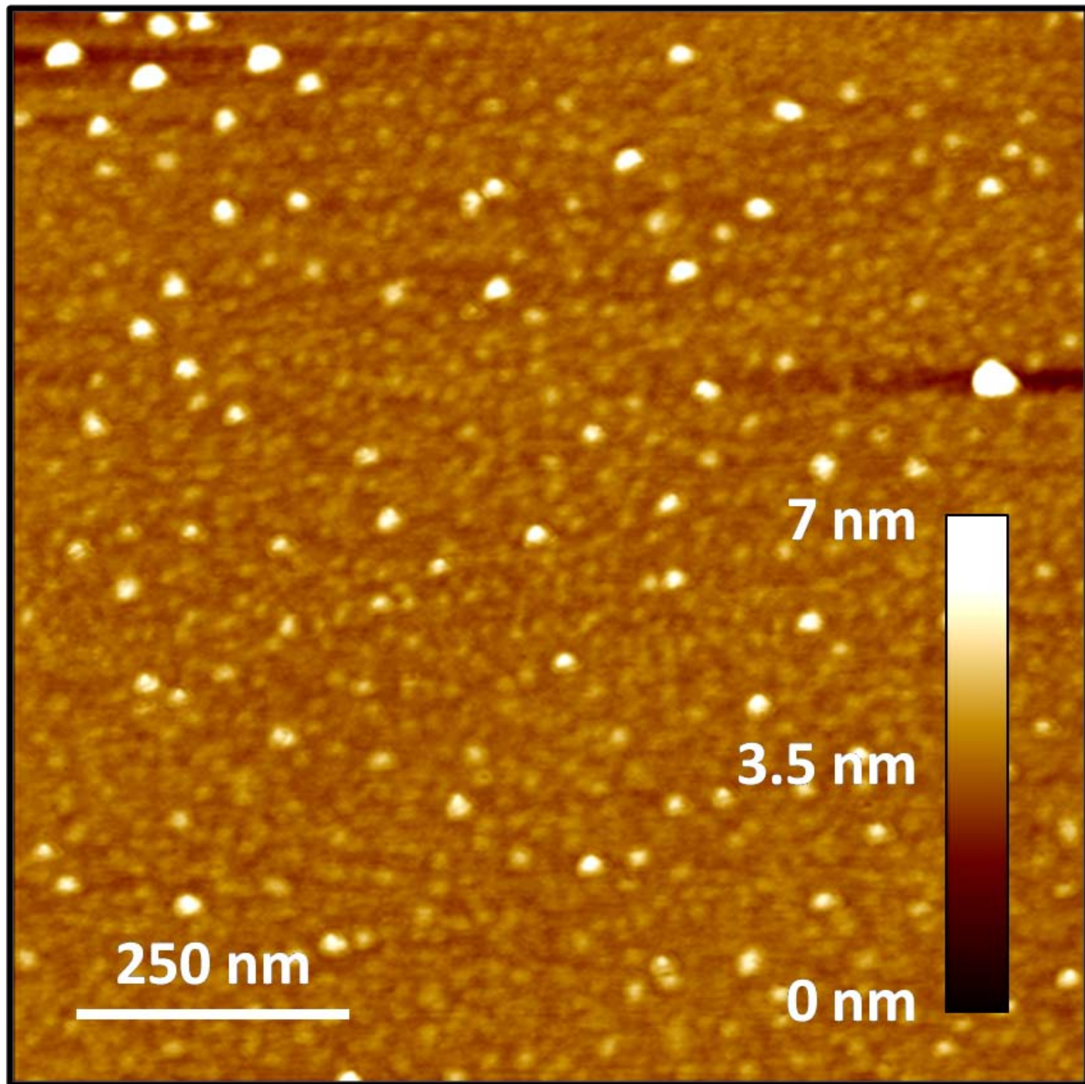

Figure B.8. AFM image of a barium oxide thin film that was synthesized on a silicon wafer through 50 SILD cycles of alternating 0.01 M $Ba(NO_3)_2$ and 0.04 M KOH solutions in 25% ethanol & 75% DI water according to the SILD procedure described in Section 3.2. The residence time in which each SILD solution was in contact with the surface was approximately 30 seconds.

Bibliography

[1] Y.F. Nicolau. Appl. Surf. Sci. 22 (1985) 1061.

[2] J.A. Davis, R.O. James, J.O. Leckie. J. Colloid Interface Sci. 63 (1978) 480.

[3] A. Martínez, C. López, F. Márquez, I. Díaz. J. Catal. 220 (2003) 486.

[4] S. Lambert, C. Cellier, P. Grange, J.-P. Pirard, B. Heinrichs. J. Catal. 221 (2004) 335.

[5] M.L. Breen, J.T. Woodward, D.K. Schwartz, Allen W. Apblett. Chem. Mater. 10 (1998) 710.

[6] T. Niesen, M. R. De Guire. J. Electroceramics 6 (2001) 169-207.

[7] R.K. Iler. J. Colloid Interface Sci. 21 (1966) 569.

[8] Y.F. Nicolau. Fr. Patent 2569427.

[9] V.P. Tolstoy. Russ. Patent 1386600.

[10] Y.F. Nicolau, J.C. Menard. J. Cryst. Growth 92 (1988) 128.

[11] V.P. Tolstoy. Russ. Chem. Rev. 62 (1993) 260.

[12] V.P. Tolstoy, E.V. Molotilkina. Russ. J. Inorg. Chem. 3: 39 (1994) 372.

[13] V.P. Tolstoy. Russ. Chem. Rev. 75 (2006) 161.

[14] G. A. Parks. "The isoelectric points of solid oxides, solid hydroxides, and aqueous hydroxo complex systems" Department of Mineral Engineering, Stanford (1964).

[15] R. Resch, T. Prohaska, G. Friedbacher, et al. Fresenius' J. Anal. Chem. 353 (1995) 772-777.

[16] R. Resch, G. Friedbacher, M. Grasserbauer, et al. Fresenius' J. Anal. Chem. 358 (1997) 80-84.

[17] R. Resch, G. Friedbacher, M. Grasserbauer, et al. Fresenius' J. Anal. Chem. 361 (1998) 613-617.

[18] S. Park, E. DiMasi, Y. Kim, W. Han, P.M. Woodward, T. Vogt. Thin Solid Films 515 (2006) 1250-1254.

[19] G. Korotcenkov, V. Macsanov, V. Brinzari, V. Tolstoy, J. Schwank, A Cornet, J. Morante. Thin Solid Films 467 (2004) 209-214.

[20] S. Park, B. L. Clark, D. A. Keszler, et al. Science 297 (2002) 65.

[21] V. P. Tolstoy, I. V. Murin, A. Reller. App. Surf. Sci. 112 (1997) 255.

[22] S. Park, G. S. Herman, D. A. Keszler. J. Solid State Chem. 175 (2003) 84–87.

[23] V. P. Tolstoi. Russ. J. Appl. Chem. 72 (1999) 1326.

[24] E. V. Tolstobrov, V. P. Tolstoi. Russ. J. General Chem. 69 (1999) 856.

[25] M. Ristov, G. J. Sinadinovski, I. Grozdanov, M. Mitreski. Thin Solid Films 149 (1987) 65-71.

[26] A. E. Jimenez-Gonzalez, P. K. Nair. Semiconductor Sci. Tech. 10 (1995) 1277.

[27] A. Jimenez-Gonzalez, R. Suarez-Parra. J. Crystal Growth 167 (1996) 649-655.

[28] P. Mitra, A. P. Chatterjee, H.S. Maiti. Mater. Letters 35 (1998) 33.

[29] A. P. Chatterjee, P. Mitra, A. K. Mukhopadhyay. J. Mater. Sci. 34 (1999) 4225.

[30] E. V. Tolstobrov, V. P. Tolstoi. Russ. J. Appl. Chem. 68 (1995) 899.

[31] S. Lindroos, M. Leskela. Inter. J. Inorg. Mater. 2 (2000) 197-201.

[32] A. E. Jimenez-Gonzalez. J. Solid State Chem. 128 (1997) 176.

[33] V. P. Tolstoi. Russ. J. Inorg. Chem. 40 (1995) 208.

[34] V.P. Tolstoy. Thin Solid Films 307 (1997) 10.

[35] M. Boulouz, A. Boulouz, A. Giani, A. Boyer. Thin Solid Films 323 (1998) 85.

[36] K. Yasuda, S. Suenaga, H. Inagaki, Y. Goto, H. Takeda, K. Wada. J. Mater. Sci. 35 (2000) 317.

[37] K. Koski, J. Holsa, P. Juliet. Surf. Coat. Technol. 121 (1999) 303.

[38] N. Miura, H. Kurosawa, M. Hasei, G.Y. Lu, N. Yamazoe. Solid State Ionics 86–88 (1996) 1069.

[39] D. Galbarra, F.J. Arregui, I.R. Matias, R.O. Claus. Smart Mater. Struct. 14 (2005) 739.

[40] T.F. Chao, K.J. Walsh, P.S. Fedkiw. Solid State Ionics 47 (1991) 277.

[41] K. Wang, M.A. Morris, J.D. Holmes, J. Yu, R. Xu. Microporous Mesoporous Mater. 117 (2009) 161.

[42] E. Nikolla, J. Schwank, S. Linic. J. Catal. 250 (2007) 85.

[43] E. Nikolla, J. Schwank, S. Linic. Catal. Today 136 (2008) 243.

[44] A.R. Tadd, B.D. Gould, J. Schwank. Catal. Today 110 (2005) 68.

[45] B.D. Gould, A.R. Tadd, J. Schwank. J. Power Sources 164 (2007) 344-350.

[46] M. Aberg. Acta Chem. Scand. A 31 (1977) 171.

[47] A. Singhal, L.M. Toth, J.S. Lin, K. Affholter. J. Am. Chem. Soc. 118 (1996) 11529-11534.

[48] X. Chen, J. Schwank, J. Li, W.F. Schneider, C.T. Goralski, P.J. Schmitz. Appl. Catal., B 61 (2005) 164.

[49] X. Chen, J. Schwank, J. Li, W.F. Schneider, C.T. Goralski, P.J. Schmitz. J. Mater. Chem. 15 (2005) 366.

[50] J. Szanyi, J.H. Kwak, D.H. Kim, S.D. Burton, C.H.F. Peden. J. Phys. Chem. B 109 (2005) 27.

[51] J.H. Kwak, D. Mei, C.W. Yi, D.H. Kim, C.H.F. Peden, L. Allard, J. Szanyi. J. Catal. 261 (2009) 17.

[52] A.Y. Stakheev, L.M. Kustov. Appl. Catal. A 188 (1999) 3-35.

[53] S. Roy, A. Baiker. Chem. Rev. 109 (2009) 4054.

[54] Y. Ji, C. Fisk, V. Easterling, U. Graham, A. Poole, M. Crocker, J.-S. Choi, W. Partridge, K. Wilson, Article in Press Catal. Today (2010), doi:10.1016/j.cattod.2009.12.009.

[55] R.D. Clayton, M.P. Harold, V. Balakotaiah, C.Z. Wan, Appl. Catal. B 90 (2009) 662.

[56] A. Martínez, C. López, F. Márquez, I. Díaz, J. Catal. 220 (2003) 486.

[57] S. Lambert, C. Cellier, P. Grange, J.-P. Pirard, B. Heinrichs, J. Catal. 221 (2004) 335.